Joana Filipa Gingeira Jardim de Azevedo

Bachelor Degree on Chemical and Biochemical Science Engineering

Improvement of the Manufacturing Process of a Novel Microfiltration Ceramic Membrane

Dissertation presented at Faculty of Sciences and Technology of NOVA University of Lisbon to attain the Master degree in Chemical and Biochemical Science Engineering

Supervisor: Prof. Dr. João Paulo Serejo Goulão Crespo, Cathedratic Professor, FCT-UNL

Adviser: Dr. Hugo Miguel Magalhães Macedo, Founder & CEO of Smart Separations Ltd

Judge:

President Examiner: Prof. Dr. Mário Fernando José Eusébio

External Examiner: Dr. Svetlozar Gueorguiev Velizarov

Supervisor: Prof. Dr. João Paulo Serejo Goulão Crespo

September, 2016

FACULDADE DE CIÊNCIAS E TECNOLOGIA
UNIVERSIDADE NOVA DE LISBOA

UNIVERSIDADE NOVA DE LISBOA

Faculdade de Ciências e Tecnologia

Departamento de Engenharia Química e Bioquímica

Melhoramento do Processo de Fabrico de uma Nova Membrana de Microfiltração

Por:

Joana Filipa Gingeira Jardim de Azevedo

Dissertação apresentada na Faculdade de Ciências e Tecnologia da Universidade Nova de Lisboa para a obtenção do grau de Mestre de Engenharia Química e Bioquímica

Orientador: Prof. Dr. João Paulo Serejo Goulão Crespo, Professor Catedrático, FCT-UNL

Co-Orientador: Dr. Hugo Miguel Magalhães Macedo, Fundador & CEO da Smart Separations Ltd

Lisboa, Setembro 2016

NOVA UNIVERSITY OF LISBON

Faculty of Sciences and Technology

Chemical and Biochemical Science Engineering Department

Improvement of the Manufacturing Process of a Novel Microfiltration Membrane

By:

Joana Filipa Gingeira Jardim de Azevedo

Dissertation presented at Faculty of Sciences and Technology of NOVA University of Lisbon to attain the Master degree in Chemical and Biochemical Science Engineering

Supervisor: Prof. Dr. João Paulo Serejo Goulão Crespo, Cathedratic Professor, FCT-UNL

Adviser: Dr. Hugo Miguel Magalhães Macedo, Founder & CEO of Smart Separations Ltd

Lisbon, September 2016

Improvement of the Manufacturing Process of a Novel Microfiltration Membrane

ACKNOWLEDGEMENTS

The completion of this masters dissertation would not have been possible without instrumental support, to which I'll be forever grateful.

To Dr. Hugo Macedo, for making it possible for me to perform this project in Smart Separations and for all the resources provided.

To Dr. Hugo Macedo, once more, for his guidance, total support, availability, knowledge, opinions and criticism , full cooperation solving issues and obstacles that arose during the project and for all his words of incentive. To Professor João Paulo Crespo, for his supervision which despite the long distance, was always available.

To the whole staff at the Department of Chemical and Biochemical Engineering of the Faculty of Science and Technology for the knowledge passed on during my enrolment.

I hereby thank all of my co-workers at Smart Separations, especially to Dr. Hugo Macedo and Dr. Ben Kingsbury for all their help.

To my friends and colleagues, Carlos Sopas and Leandro Parada, and many others which will not be mentioned but know who they are, that had my back through this journey and throughout the last few years, for their companionship, strength and support.

Lastly, I thank my family, in particular to my mother, grandmother and brother, for their unconditional support, incentive, friendship and total help overcoming the obstacles that emerged throughout this venture. I dedicate this work to them!

ABSTRACT

Membranes are highly selective barriers that are used to separate particles and/or molecules from a fluid, purifying it. The selectivity of membranes depends on pore size, composition, electrochemical properties and/or the properties of the media being separated. This technology has been gaining importance over the last few years, particularly for its application in several different industries such as food processing, biotechnology, pharmaceutical and research industries. However, current microfiltration membrane technologies are inefficient and/or too expensive.

Smart Separations Ltd, a startup funded in 2013 in London (England), has developed an innovative patented technology, that allows the production of microfiltration flat ceramic membrane with conically-shaped pores that cross through them. These could address current hurdles, whilst offering a wide range of applications through easy pore size manipulation.

This research project aims at optimising the manufacturing process of Smart Separations's membranes, specifically the lapping operation, which is the critical stage where truly flat and smooth membranes are obtained, in addition to the tight control of the pore sizes. It was also important to characterise the membranes and confirm the reliability of the in-house characterisation techniques.

The manufacturing process of the membranes was optimised by studying the influence of some parameters in the lapping operation, such as time and cut thickness. The studied membranes were then characterised based on different parameters, such as their microstructure (e.g. pore sizes, pore size distribution, pore geometry and connectivity), gas permeability and functionality (dust retention). After the lapping operation, membranes were observed on an optical microscope and SEM, and the results were analysed using Image Pro Premier 9.1. Porometry results along with the in-house permeability tests were compared to data on the same samples provided by a subcontractor company, Porometer, to assess their accuracy.

After interpreting the lapping results, it was concluded that the lapping technique used wasn't yet accurate enough to determine the exact lapping parameters to produce specific pore-sized membranes. In-house permeability tests are accurate according to Porometer's data, although pore size results don't match up due to the lapping not being accurate enough and the limitation of the selected area by imaging analysis.

Smart Separations is currently developing an automated lapping fixture that will improve the lapping accuracy to better analyse the effects of each different parameter in production.

Keywords: ceramic membrane, microfiltration, lapping, microstructure and permeability.

RESUMO

As membranas são barreiras altamente seletivas usadas para separar partículas e/ou moléculas de fluídos, purificando-os. A seletividade das membranas depende do tamanho de poros, composição, propriedades eletroquímicas, e/ou propriedades do meio a ser separado. Esta tecnologia tem ganho importância nos últimos anos, particularmente pela sua aplicação em diversas industrias tais como processamento de comida, biotecnologia, industria farmacêutica e investigação. Contudo, as atuais tecnologias de produção de membranas de microfiltração são ineficientes e/ou demasiado dispendiosas.

A Smart Separations Ltd, uma startup fundada em 2013 em Londres (Reino Unido), desenvolveu uma tecnologia inovadora, patenteada, que permite a produção de membranas cerâmicas de microfiltração com poros cónicos que a atravessam. Estas podem superar alguns destes obstáculos, e ter um vasto alcance de aplicações através da fácil manipulação do tamanho de poros.

Este projeto de investigação ambiciona à otimização do processo de manufatura das membranas da Smart Separations, particularmente a operação de lapping, que é o passo crítico onde membranas verdadeiramente planas e sem irregularidades são obtidas, para além do controlo rigoroso do tamanho de poros. Foi também importante a caracterização das membranas e confirmar que os métodos de caracterização usados pela empresa são fidedignos.

O processo de produção das membranas foi otimizado através do estudo da influência de alguns parâmetros na operação do lapping, tais como tempo e espessura de corte. As membranas estudadas foram então caracterizadas baseadas em diferentes parâmetros, tais como microestrutura (ex. tamanho de poro, distribuição de tamanho de poros, geometria e conectividade dos poros) ,permeabilidade de gás e funcionalidade (retenção de pó). Depois do lapping, as membranas foram observadas através de um microscópio ótico e SEM, e os resultados foram analisados no Image Pro Premier 9.1. Resultados de porometria em conjunto com os testes de permeabilidade efetuados na empresa foram comparados com dados das mesmas membranas obtidos por uma empresa subcontratada, Porometer, para avaliar a sua precisão.

Depois da interpretação dos resultados de lapping, foi concluído que a técnica de lapping usada ainda não se encontra precisa o suficiente de forma a determinar os parâmetros de lapping exatos para produzir membranas com tamanho de poros específicos. Os testes in-house de permeabilidade são fiáveis de acordo com os dados da Porometer, contudo os resultados de tamanho de poro não coincidem devido ao lapping não ser preciso o suficiente e às limitações da seleção de área na análise de imagens.

A Smart Separations está atualmente a desenvolver um acessório de lapping automático que irá melhorar a precisão do lapping para uma melhor análise do efeito de cada parâmetro na produção.

Palavras-chave: membrana cerâmica, microfiltração, lapping, microestrutura e permeabilidade.

CONTENTS

List of Figures

List of Tables

Abbreviations / Nomenclature

Abbreviation	Definition
3D	Three dimensional
AFM	Atomic force microscopy
Al_2O_3	Alumina
CSLM	Confocal scanning laser microscopy
EDS	Energy dispersive x-ray spectroscopy
EM	Electron microscopy
FESEM	Field emission scanning electron microscopy
MF	Microfiltration
MIP	Mercury intrusion porosimetry
MWCO	Molecular weight cut off
NF	Nanofiltration
RO	Reverse osmosis
SEM	Scanning electron microscopy
TEM	Transmission electron microscopy
TMP	Transmembrane pressure
UF	Ultrafiltration
ZrO_2	Zirconia
SS	Smart Separations

Symbol	Definition	Unit
A	Permeation area	m^2
C_f	Solute concentration in the feed	$mol.m^{-3}$
C_p	Solute concentration in the permeate	$mol.m^{-3}$
J	Volumetric permeate flux	$m^3.m^{-2}.s^{-1}$
K	Kozeny constant	
l	Pore length or membrane thickness	m
L_P	Permeability of the membrane	$m^3.m^{-2}.s^{-1}.Pa^{-1}$
M_P	Mass flow rate of the permeate	$kg.s^{-1}$
P_f	Pressure in the feed	Pa
P_p	Pressure in the permeate	Pa
P_r	Pressure in the retentate	Pa
Q	Volumetric permeate flow	$m^3.s^{-1}$
r	Pore radius	m

R	Solute rejection	%
slp	Slope	$m^3.m^{-2}.s^{-1}.Pa$
t	Time	s
V	*V*olume	m^3
$V_{membrane}$	Total volume of the membrane	dm^3
W_{dry}	Dry weight of the membrane	G
W_{wet}	Wet weight of the membrane	G
ΔP	Applied pressure	Pa
ε	Porosity	
θ	Contact angle	o
ρ_p	Permeate density	$kg.m^{-3}$
ρ_{water}	Density of the water	$g.dm^{-3}$
σ	Surface tension	$N.m^{-1}$
τ	Tortuosity	
μ	Viscosity of the fluid	$N.s.m^{-2}$ or Pa.s

1

INTRODUCTION

1.1 Background of This Research Work

Membrane filtration is a separation method commonly known as a physical process, although it can also be used as a chemical process. The selectivity of membranes is highly dependent on the separation method, the properties of the media being separated, the composition of the membrane and its electrochemical properties (e.g. hydrophilic, hydrophobic, pH, charge and coating) in addition to its pore size. This is a common operation used to separate solids from other solids or fluids, where particles bigger than the filters' pore sizes are retained. Filtration can be divided into five different ranges, between 10^{-4}µm and 100µm (or 0.1mm) and they are commonly used in tandem with each other. Increasing in order of particle size, these are classified as: reverse osmosis, nanofiltration (NF), ultrafiltration, microfiltration and clarification. This work focuses on the microfiltration range, which is commonly applied to separate micro-particles sized above 0.1µm and below 30µm, a range that includes, amongst others, human cells.

Several microfiltration industries rely upon inefficient and/or highly expensive methods to separate particles at the cellular range. This is most likely related to the fact that microfiltration is in a challenging technological middle, between the widely developed ultrafiltration technologies and the large pore sizes of clarification. Different approaches have been tried thus far to reach this middle: a) by opening the membrane's micro-pores of ultrafiltration membranes using track-etching technology, which is inefficient because they're usually polymeric membranes, that lose stability and become fragile, making them unsuitable when pores are larger than 1µm; or b) by making the sieves' pores used for clarification smaller, using lithography imprinting technology, but this is a very expensive and commercially limited technology. As far as our literature research goes, none have yet addressed the challenging middle of microfiltration in an effective way (Macedo 2015). There is hence a lack of a defined technology within the range of microfiltration applications that can be easily applied in industrial and large scale processing.

There is also the challenge of producing a versatile membrane with the widest reliable range of filtration possible, and thus the widest range of applications. That is the challenge this project intends to tackle.

1.2 Smart Separations's Technology

The research work that composes this thesis was developed at Smart Separations Ltd. Smart Separations is a start-up company based in London, United Kingdom, which was founded in July 2013. It has established a partnership with the University of Surrey, where some of these experiments were conducted. From its inception, the company has been growing very quickly, developing its patented technology.

The company has developed a new flat filter within the microfiltration range. The targeted particle sizes of the membranes manufactured are in the range of <1 to 30μm, allowing the separation of large suspended solids such as bacteria, yeast, red blood cells, colloids and animal fat. The need to separate particles within this size range is spread throughout several market segments where microfiltration is either already in use or can potentially be used. Smart Separations's patented microfiltration technology offers the possibility for applications in many different industries (e.g. biotechnology, pharmaceutical, environment and dairy industry) with direct impact in our daily life (e.g. dairy products, beverages) and indeed in our health (e.g. water and gas emission treatment, blood processing, etc.). There are currently other microfiltration technologies; however, these are underdeveloped, out-dated and present limited scale-up ability (e.g. large costs, inefficiency, etc).

The technology developed by Smart Separations is innovative. It can overcome most of the problems that other technologies have, through a unique pore structure design that offers anti-clogging and tight control over its adjustable pore sizes. These characteristics make Smart Separations's membranes much more efficient and less expensive than the available technologies, allowing for an easy and widely applicable product.

The key factors of Smart Separations's technology are the materials that it is made of (ceramics) and the design of the pores, which renders excellent properties to the membrane product. The structure of these membranes is unique, with the largest pore sizes in one side, as support, which then gradually decrease towards the other surface, where the actual separation takes place. This particular design reduces the chance of clogging, as every particle that enters the pores will come out through the other side because it has a larger diameter. The pore design also allows for a better control of the pore sizes within the range of microfiltration. Other important advantage of these pores is that while the tighter surface pores control the separation, the larger pores optimize the flux. Furthermore, the conical pores allow low tortuosity factor (≈1) which is a great advantage in comparison to most flat ceramic membranes. Common ceramic membranes present tortuous and interconnected pore morphology. High measurements of the actual fluid path length through the membrane relative to the actual membrane thickness, tortuosity factor, relates to higher pressure drops. As a consequence, the pressure on the inlet

side has to be increased in order to guarantee that the fluid passes through the membrane. Another great advantage is its single separation layer (surface filtration) and the manufacturing process is quite simple in comparison to the commonly and mostly used composite ceramic membranes. Composite membranes can only be achieved through multiple steps. Each step involves a high temperature sintering treatment, making the ceramic membrane fabrication extremely expensive (Li 2007). Clearly, combining the multiple manufacturing steps into a single one, such as Smart Separations's technology, is desirable in cutting production time and costs, and hence membrane price.

Smart Separations's membranes are made of a ceramic substrate (Al_2O_3, alumina) that confers a rigid structure and high temperature tolerance, allowing structure modifications that would not be possible to achieve with polymeric membranes. These membranes can also be sterile cleaned and used in harsh environments due to the highly resistant materials that they are made of. They can also be recycled, reducing the environmental footprint of traditional filtration methods. The surface is flat and uniform. Membranes are also made of a polymer that forms perfectly circular pores with the possibility of controlling the pore sizes. The manufacturing process is quite simple and doesn't require very expensive equipment. Smart Separations´s technology reaches precision of pore sizes almost without any effort, unlike for example the method of "drilling" pores through track-etching. (Macedo 2015)

To widen the scope of applications and the market potential of this technology, it is even possible to render them special, even "smart", characteristics. As an example, coating the membranes with various active molecules could allow the in-line degradation of organic compounds, such as those responsible for strong smells. The possibility of coating with active chemical molecules and/or having electrically-conductive properties could further the scope of this technology as a functionalised effective filter for a number of applications, such as air purification and gas emissions treatment. The main advantages of Smart Separations's membranes are summarised in Figure 1.1.

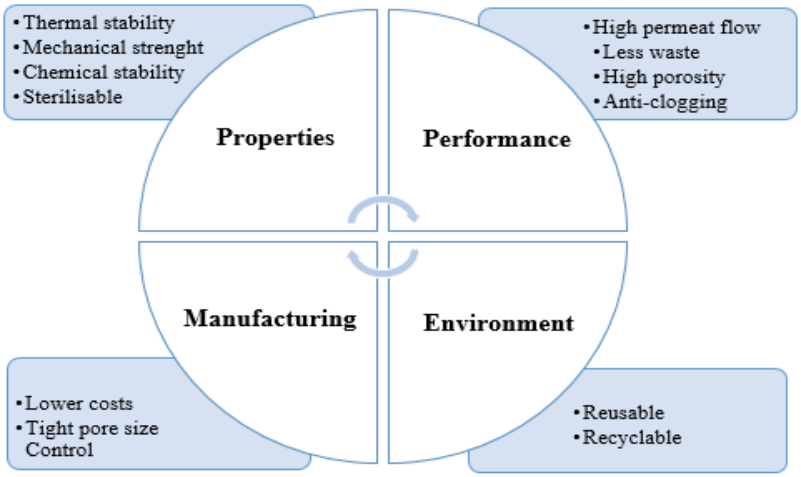

Figure 1.1- Main advantages of Smart Separations's technology (Macedo 2015).

Smart Separations's filters have been improved and tested over the last two years. The manufacturing process is being optimised, and therefore a better quality and low cost membrane should soon be available in the market (Macedo 2015).

1.3 Thesis Research Objectives

The aim of this work is to optimise the manufacturing process of a microfiltration membrane, more specifically the control of the pore sizes by improving and studying the lapping operation. Lapping is a final mechanical finishing operation used to manufacture Smart Separations membranes after sintering and produces surfaces truly flat and smooth in addition to opening and controlling its pore sizes. In order to achieve the main goal of this work, specific objectives were considered, Figure 1.2:

- Create a standard operating procedure for lapping of Smart Separations's membranes.
- Study the effect of time on material removal;
- Determine the conditions of lapping to obtain the maximum porosity with minimum material removal and time, on the bottom surface;
- Study the effect of the cut thickness on material removal;
- Determine the conditions of lapping to obtain a predicted pore size on the top surface;
- Analyse the geometry and connectivity of the pores;
- Confirm that in-house characterisation techniques are reliable and up to standard, by comparing porometry and permeability results obtained by imaging analysis and experimental tests with the results from a certified company, Porometer;
- Comparison of dust retention efficiency between Smart Separations's membranes and a commercially available membrane.

The lapping study is very important as this is the technique used to control pore sizes, one of the most important unique selling points of the company, whilst crucial to cater for different applications. Also, lapping is the least developed operation in the manufacturing workflow of Smart Separations's membranes. Hence, it is important to optimise this operation, while allowing the treatment of more than one membrane simultaneously, always considering the scaling up aspect of the process.

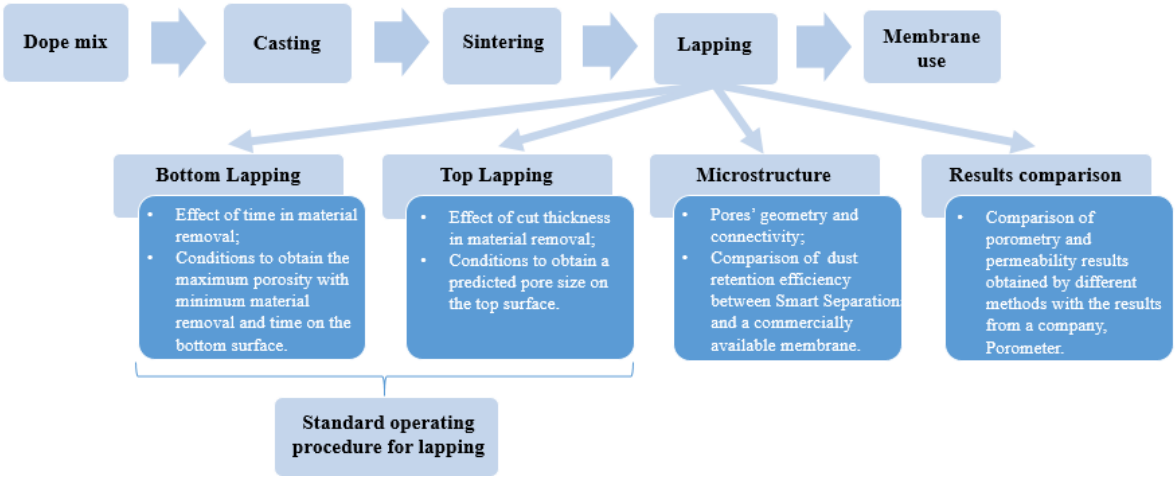

Figure 1.2-Main objectives in each step of the lapping study.

1.4 Thesis Outline

Beyond the present introduction, this thesis includes four other chapters.

In chapter 2 membrane technology is briefly explained, as well as microfiltration applications. The manufacturing process of Smart Separations's membranes is described, with focus on lapping. Finally, techniques for membrane characterisation are explained and assessed.

In chapter 3 the materials used throughout this work for lapping and characterisation of SS's membranes are explained. It also includes the methodology applied for lapping, and an explanation of the tool, Image Pro Premier, used for characterisation of the membranes after lapping.

Chapter 4 has the results obtained in the experiments and their discussion. Additionally, a comparison between the results obtained and results from a subcontractor company is made.

Finally, chapter 5 includes the main conclusions of this study and proposals for future work.

2

FRAMEWORK

In this chapter a revision of membrane technologies is presented, including the different configurations and materials. The main application of microfiltration are also described. The manufacturing process of Smart Separations's is briefly explained, focusing on the lapping step. For last, characterisation techniques used for the characterisation of membranes are presented.

2.1 Membrane Technology

Membrane filtration is a separation technique that allows particles to be removed from a fluid. A contaminated fluid is passed through a special pore-sized membrane to separate microorganisms and/or suspended particles, using its ability to control the permeation rate of a species through them. The separation goal is to divide the feed stream into permeate, the feed part that goes through the membrane, and retentate, the rejected part not able to cross the pores of the membranes. There are various methods to enable substances to penetrate through a membrane. Examples of these are: application of pressure, maintenance of a concentration gradient across both sides of the membrane, introduction of electric potential, hydrophobic or hydrophilic properties, pH or even the possibility of coating membranes with active chemical molecules (Lenntech).

Filtration can be divided into five different separation processes, represented in Figure 2.1.

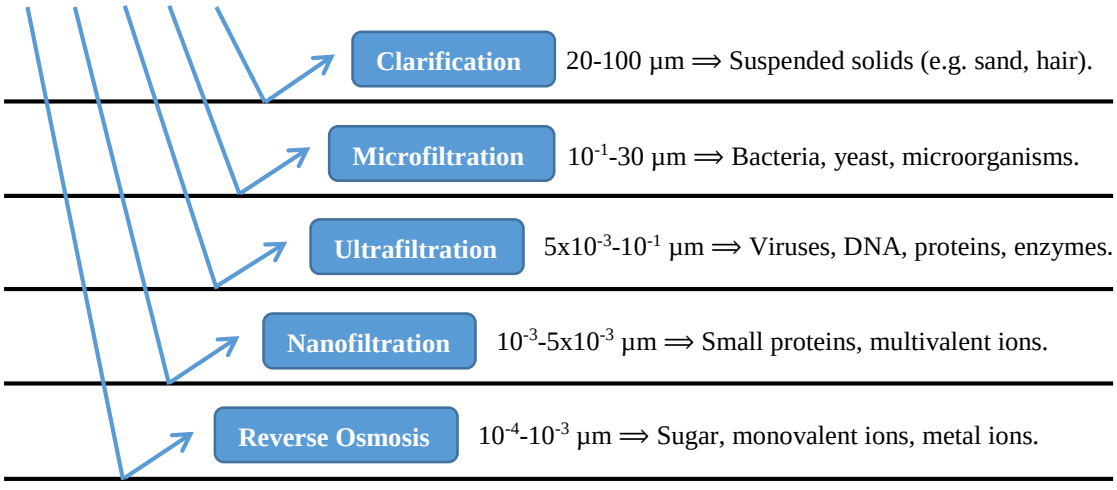

Figure 2.1-The filtration processes, relative particle sizes and substances to be separated (U.S. Environmental Protection Agency 2005, Charcosset 2012).

The target of reverse osmosis is the ionic range, while nanofiltration is used to separate particles at the molecular range. Ultrafiltration membranes target the molecular and macro molecular range, and microfiltration targets are micro molecular and macro particle ranges. Finally, clarification is the filtration process that is used to separate the biggest particles in the macro particles range.

All of the techniques mentioned above can be classified as pressure driven processes. Table 2.1 shows the approximate pressure ranges required for the various membrane filtration processes, typical fluxes and membrane morphology.

Table 2.1- Approximate pressure ranges, flux and morphology for membrane filtration processes (Lieven, Pierre et al. 2005, Foley 2013, Jaffrin 2015).

Filtration Technique	Pressure Range (bar)	Typical Flux ($l.m^{-2}.h^{-1}.bar^{-1}$)	Membrane Morphology
Microfiltration	0.5-3	>50	Porous
Ultrafiltration	1-10	10-50	Porous
Nanofiltration	7-40	1.4-12	Porous/Dense
Reverse Osmosis	25-100	0.05-1.4	Dense

In these pressure-driven membrane processes as the flux range increases with the increment of pore sizes, the applied pressure decreases. Theory tells that smaller pores lead to greater pressure drops across the membrane (Foley 2013). For a given flow rate, an increase in filter area will reduce the pressure drop across the filter, because the amount of fluid flowing per unit of filtration area is decreased (pressure drop is inversely proportional to the filter area). A typical set of curves for the relationship with filter size is given in Figure 2.2.

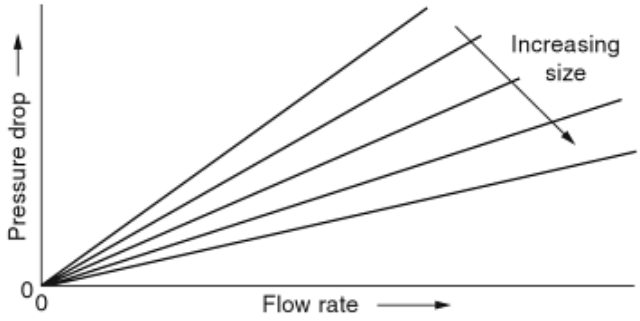

Figure 2.2-Relationship between filter size, pressure drop and flow rate (Sutherland 2008).

2.1.1 Classification of Membranes

A general classification of membranes, based on different aspects such as nature, separation regime, geometry and internal structure is shown in Figure 2.3. All of these have a great impact on membranes properties and consequent application.

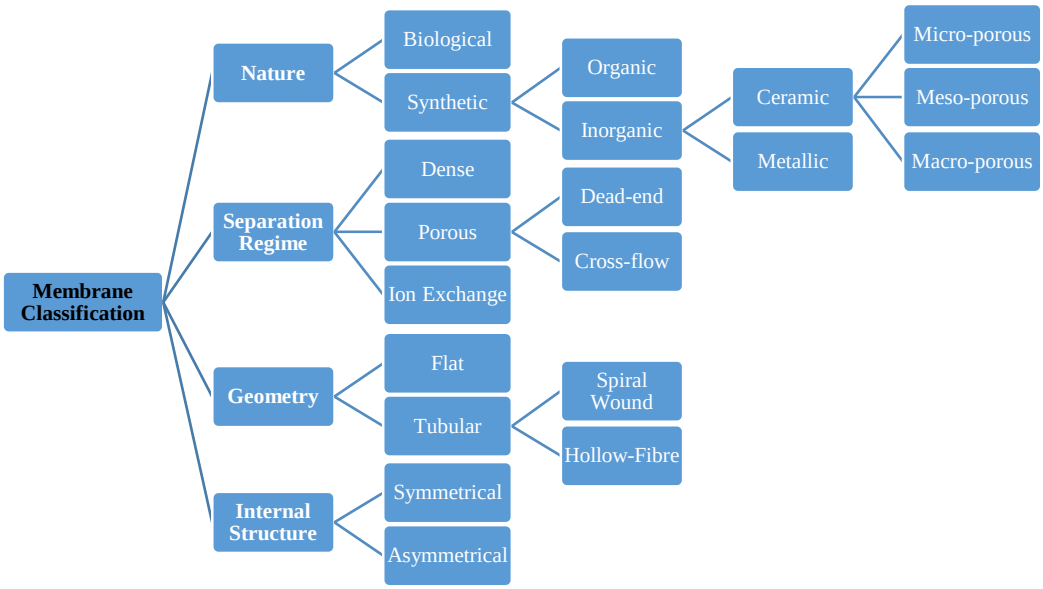

Figure 2.3- Membrane classification diagram (Falco, Salladini et al. 2011).

Biological membranes are easy to fabricate, although they have very limited operating temperatures (<100 ºC) and pH ranges, while also presenting problems with cleaning and susceptibility to microbial attack. Inorganic membranes have a higher temperature stability (>200 ºC) than polymeric (organic) membranes (<300 ºC). For this reason, they are much more interesting for industrial chemical processes. Membranes are considered dense when the transport of components involves a stage of dissolution and diffusion across the membrane. Membranes are classified as porous when permeate transport occurs preferentially in the continuous fluid phase that fills the membrane pores. When separation occurs due to the different charge of the species to be separated it is called electrochemical effect. In porous membranes there are two standard modes of operation: dead-end and cross-flow as it is possible to see in Figure 2.4. In the dead-end mode the fluid is forced through the membrane pores usually by applying pressure on the feed side. Microfiltration is usually operated in the cross flow mode, were the feed flows on the membrane surface to prevent cake formation and hence fouling caused by suspended solids in the feed stream or by deposition or adsorption of small particles inside the membrane's pores. (Falco, Salladini et al. 2011, Charcosset 2012)

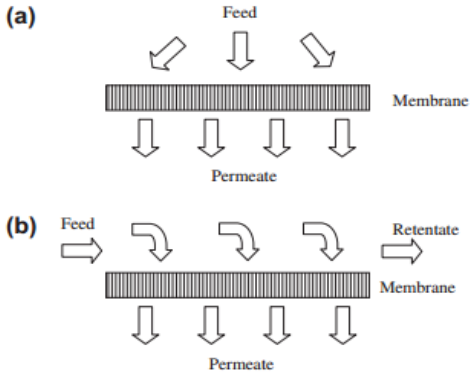

Figure 2.4- Configurations of dead-end (a) and cross-flow (b) operation modes (Charcosset 2012).

Tubular configuration consists of a matrix of randomly oriented bonded fibers that capture particles within the depth of the filter (American water works association 2005, Kumar, Ghoshal et al. 2015, Sterlitech 2015). Flat discs are ideally suited for critical applications requiring maximum particle recovery. Some advantages of this geometry is the possibility of sub-micron pore size ratings, the ability to retain bacteria and other particles depending on the pore sizes, and generally stable structure (Sterlitech 2015). Symmetrical membranes show uniform pore sizes in cross section while asymmetrical ones have usually smaller pore sizes on the membrane's surfaces. Depending on the their composition, membranes can be classified as composite when they combine two different structures (layers) into the same membrane which can be symmetrical or asymmetrical, with distinct pore sizes and thickness. The bottom layer provides mechanical support, while the middle layers bridge the pore size differences between the support layer and the top layer where the actual separation takes place (Kumar, Ghoshal et al. 2015).

2.1.2 Materials of Membranes

Each application requires a different membrane property, which is why it is important to better understand the available materials. Membranes can be divided into two types: organic (polymer-based) and inorganic (ceramic-based). On the membrane market, polymeric membranes dominate, although the potential use of ceramic membranes has been growing because they can be specially applied in a large range of industrial processes and pollution treatment technologies due to their thermal stability and mechanical and chemical resistance (Kumar, Ghoshal et al. 2015).

2.1.2.1 Polymeric Membranes

The vast majority of industrial membranes consist of polymers. They are used for different separation methods such as ultrafiltration, microfiltration and membrane chromatography. Many polymers might be custom-tailored, blended or used in the form of copolymers to improve membrane properties such as higher flux and lower fouling (Parma 2013). Figure 2.5 summarises advantages and disadvantages of polymeric membranes.

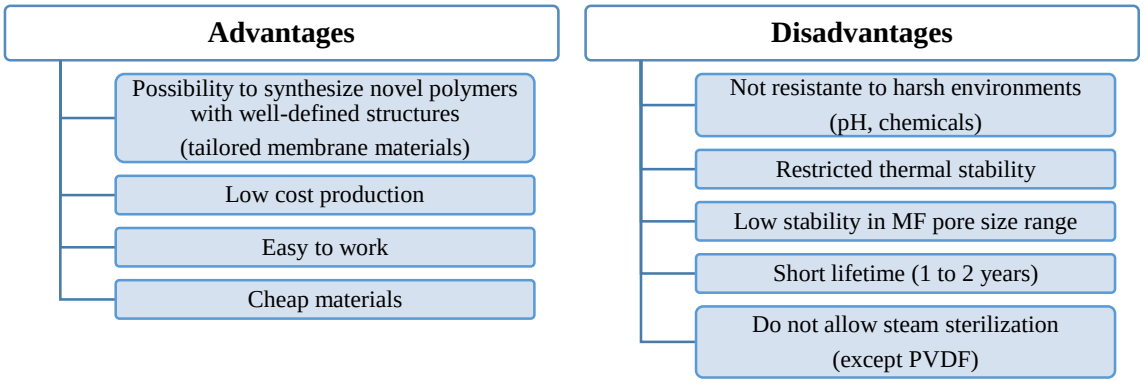

Figure 2.5- Advantages and disadvantages of polymer based membranes (Staszak, Karaś et al. 2013, Jaffrin 2015).

2.1.2.2 Ceramic Membranes

Ceramics are usually made of compounds formed from metallic and non-metallic elements, typically crystalline in nature (ordered structure). Different types of ceramics have also different properties but in general they are heat and corrosion resistant, chemical inert and hard but brittle (Chemistry Explained 2015). In general, most of the commercialised ceramic membranes are produced from advanced ceramics such as metallic oxides (alumina (Al_2O_3), zirconia (ZrO_2), titania), silica (glass), metals and zeolite or a combination of these (Charcosset 2012, Lorente-Ayza, Mestre et al. 2015).

The chemical bonds in ceramics can be covalent, ionic, or polar covalent, depending on the chemical composition of the ceramic. When the components of the ceramic are a metal and a nonmetal, the bonding is primarily ionic, as aluminium oxide (Al^{+3}) (Chemistry Explained 2015). Aluminium oxide is a compound of aluminium and oxygen (Al_2O_3) it commonly occurs in its crystalline polymorphic phase α-alumina, which is the thermodynamically stable form (Almandoz, Pagliero et al. 2015).

Figure 2.6 summarises advantages and disadvantages of ceramic membranes.

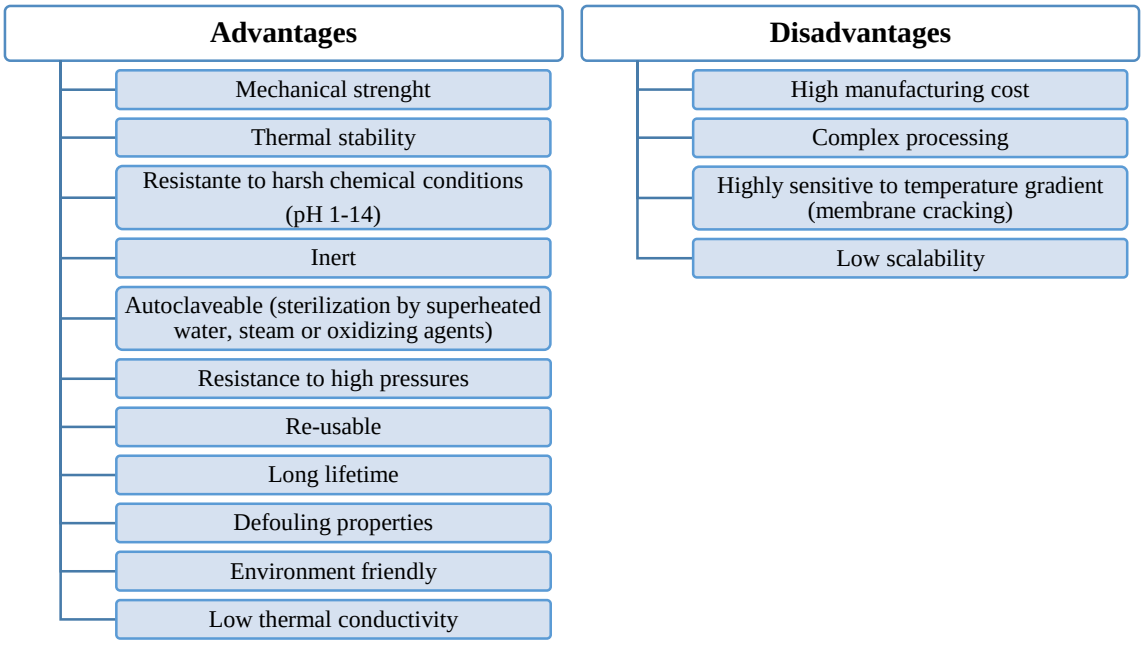

Figure 2.6- Advantages and disadvantages of ceramic based membranes (Staszak, Karaś et al. 2013, Lorente-Ayza, Mestre et al. 2015, Synder Filtration 2015).

2.2 Microfiltration

Microfiltration membranes are specially designed for the separation of large suspended solids such as colloids, particulates, fat, and microorganisms such as large bacteria and red blood cells and leukocytes, while allowing sugars, proteins, salts, and low molecular weight molecules to pass through the membrane (Koch Membrane Systems 2015).

2.2.1 Applications

This membrane process is used for concentration of soluble molecules and suspended solids, purification and clarification by removing suspended solids in diverse fields such as environmental applications, biotechnology and pharmaceutical applications, food and beverage processing, as shown in Figure 2.7.

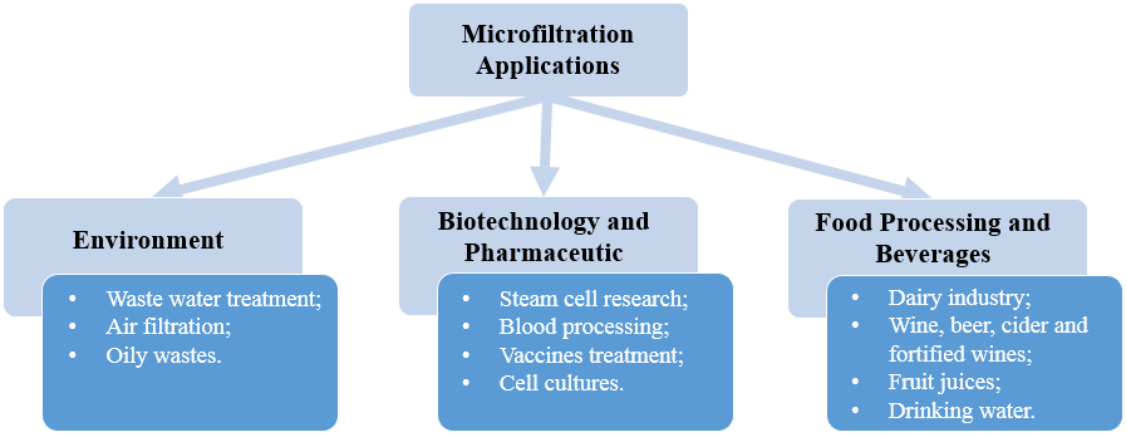

Figure 2.7- Applications of microfiltration membranes.

Increasing environmental concerns and tighter legislation on emissions lead to the applications of micro filters. Wastewater treatment is used to decrease wastewater volumes usually originated from agriculture, or from different industries such as petrochemical, textile, nuclear and paper (Belibi, Nguemtchouin et al. 2015, Government digital service 2015). Gas emissions is a big issue in all chemical industries, which leads to the need for air filtration. Applications in oily waste is increasing, especially where the value of recovered material is high or where the savings from the reduced waste volume are high (Laitinen 2002, Kumar, Ghoshal et al. 2015).

Microfiltration membranes are used in the biotechnology and pharmaceutical industries for primary extraction, purification and concentration of biomass, antibiotics, vitamins, enzymes, amino acids, bio polymers and bio pesticides. There are also applications in the treatment of vaccines, cell cultures, recombinant proteins and continuous fermentation (Laitinen 2002). The bioprocessing industries have a big share in the microfiltration market, as for most applications membranes are single-use and disposable. Health organizations, private blood banks, stem cell research and development groups also use microfiltration techniques (Jaffrin 2015).

The first large scale application of inorganic membranes was on food and beverage industries. Nowadays, the main application of membranes is in the dairy industry with different purposes such as bacterial and fat removal, concentration of milk and milk products. The beverage industry uses microfiltration membranes for the clarification and sterilisation of the

final products, by filtering colloids, precipitates, suspended particles and microorganisms (algae, bacteria, fungi). Membranes are applied for the filtration of wine, beer, sake vinegar, cider and fortified wines, fruit juices. Drinking water is the second largest application of microfiltration (Noble and Stern 1995, Laitinen 2002).

Each application requires different membrane properties, such has materials, designs and more importantly pore size. In Table 2.2 are presented the common applications for each pore size in the microfiltration range, although there are more applications not described here.

Table 2.2- Applications for a given pore size in the microfiltration range (Sterlitech 2015).

0.01 µm	0.03 µm	0.1 µm	0.2 µm
• Chemotaxis • Cytology • Epifluorescence	• Virus filtration • Mycoplasma removal	• Sterilization • Clarification • HPLC sample preparation • Bacteria removal	• Microbiological analysis • Prefiltration • Protein, enzyme filtration
0.4 µm	**0.6 µm**	**0.8 µm**	**1.0 µm**
• Sterility testing • Trace metal analysis	• Particle analysis • Filtration of corrosive solutions	• Removal of RBC from plasma • Toxicity testing	• General microfiltration • Serum Prefiltration
1.2 µm	**2.0 µm**	**5.0 µm**	**8.0 µm**
• Particulate analysis • Medical assays • Immobilizations	• Chemotaxis • Red blood cells • DNA	• Filtration of Corrosive solutions • NIOSH analysis methods	• Cytology
10.0 µm	**12.0 µm**	**14.0 µm**	**20.0 µm**
• Large bacteria filtration • Cancer cell studies	• Metastasis tumor cells • Schistosoma filtration	• Chemical filtration • Alcohol filtration	• General filtration

2.3 Smart Separations's Manufacturing Process

Here is a brief description of the manufacturing process of Smart Separations's membranes, dope mixture, casting, phase-inversion, sintering and lapping, as shown in Figure 2.8. In this work, a larger focus will be dedicated to optimising the lapping process.

Figure 2.8- Manufacturing steps of Smart Separations's membranes (Macedo H. 2015).

2.3.1 Dope mixture and Casting

Dope mixture: The initial "green" powder mixture is mainly composed by α-alumina, the ceramic support material of the membranes, with an organic solvent, a polymer (pore former) and a chemical binder. The polymer used is a thermoplastic polymer, tough and stable at high temperatures (200 ^{O}C) that form conical pores during the phase inversion process. All these compounds are mixed in a rotary mixer until an homogeneous solution is obtained. Then, the degassing process allows the production of membranes with reduced defects, which are usually caused by air bubbles. The equipment used is a rotary shaker for mixing the reagents, a vacuum pump and a degassing chamber. (Macedo H. 2015)

Casting: The following step is casting using an auto-coater with heater for casting the dope under a controlled environment. This method is primarily used for the manufacturing of flat sheet ceramic membranes. The method involves a casting knife and a reservoir for the slurry of ceramic powder. Briefly, the dope mixture is poured into a reservoir behind a casting knife which has a controlled small "gap" (Figure 2.9). The knife is set in motion and the gap between the knife blade and carrier determines the thickness of the sheet formed. (Macedo H. 2016)

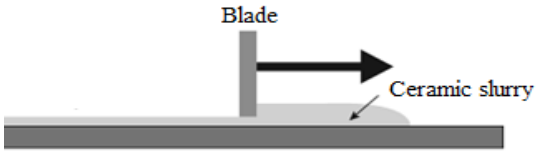

Figure 2.9- Casting method for ceramic membrane preparation (Basile 2013).

2.3.2 Phase-inversion and Sintering

Phase-inversion: After the dope is cast onto an aluminium plate, the system is then immersed into water. This triggers the phase inversion process, by removing the solvent present in the dope mixture through water (non-solvent). The polymer suffers a phase change by becoming solid, this precipitation occurs because of the exchange of solvent and non-solvent. The non-solvent (water) enters the casted dope, pushing the alumina to the side, while convective cells of polymer precipitating start to form. The pore structure is obtained from a combination of mass transfer and phase separation. The large thin film is then cut into the desired shape (circles) and heat treatment follows. (Macedo H. 2015)

Sintering: The heat treatment has two main stages: the burnout and the sintering. The polymer, working as the pore-former, has already completed its goal and its presence in the final membrane does not have a positive effect. Hence, on the first stage the burning of the polymer occurs at a temperature below 1000°C. Afterwards, the temperature is increased to the sintering temperature of alumina to eliminate any remaining binder or solvent and most importantly to interconnect the particles contained in the dope in order to consolidate the membrane ceramic structure through sintering. Fusion of the alumina micro particles is done by approaching its

melting point, decreasing its porosity, while changing grain size and shape and changing pore size and shape during sintering, becoming a lot more resistant afterwards. (Macedo H. 2016)

2.3.3 Lapping

After sintering there are still no open pores at the surfaces of the membranes, although the pores are present. To open these at a determined pore size, lapping is required. This opening is highly controlled, allowing tight control and accuracy of pore size. Lapping allows the manufacturing of membranes in a systematic way in order to produce membranes with lower batch-to-batch variability, while reducing operator errors. Lapping is a final abrasive finishing operation that corrects minor imperfections of shape, refines surface finish and produces close fit between mating surfaces (dimensional flatness). (Macedo H. 2015, Macedo H. 2016)

2.3.3.1 Equipment

Lapping is a five-body process that involves an abrasive, a carrier (paste or liquid) to be applied between the work piece surface, a rotating table called lapping plate and 3 or 4 fixtures (Figure 2.10). These fine-grained loose abrasive particles are often purchased ready mixed and suspended in viscous or liquid carrier often made with an oil soap, mineral oil or grease base. The carrier holds the abrasive in suspension before and during use. The carrier also disperses the heat, allowing the temperature not to increase too much. The abrasives used for lapping may occasionally be as coarse as 100-280mesh, and more often, 320-800mesh are used. Abrasive particles size should be selected based on the target finish and material removal rate. It is possible to use conventional abrasives such as aluminium oxide or super abrasives such as diamond particles. The advantages of lapping with diamonds over aluminium oxide, can be summed up in: faster, cleaner, most cost effective, higher overall productivity. Ceramics are typically processed with water-based slurries containing monocrystalline diamond for greatest economy. To gain the full benefit of the inherent strengths of diamond as an abrasive, the ideal lapping machine design features high down-pressure/down-force (5psi and higher), a robust drive system to tolerate the high down-pressure used and a variable speed drive with high top-end RPM capability. (Schneider 2002, Irvin 2011)

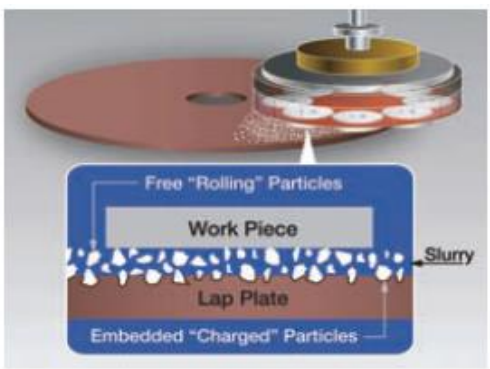

Figure 2.10- Body parts involved in lapping (Irvin 2011).

Proper plate selection is vital. The lapping plate must be kept perfectly flat. The work piece must be at least as hard as the lapping plate, or the abrasive will be charged into the work piece. The plate must be of optimal hardness and malleability to maintain flatness, accept a diamond charge, and accelerate the rolling abrasive action. Lapping ceramics with diamond typically requires a lapping plate made from composite metal iron or cast iron for rough operations. Composite metal copper is needed for general purpose and finishing operations. The use of a composite ceramic plate can eliminate concerns regarding potential metal contamination. After a certain period of use, the lapping plate will become worn and no longer remove material at a consistent rate, which, in turn, introduces undesired production inaccuracy. This requires reconditioning to re-establish plate flatness and meet end-part flatness tolerance and surface finish requirements. (Macedo H. 2016)

2.3.3.2 Method

The work piece that is to be lapped should be previously finished close to the final size. The lapping process works by pushing the points of the diamond grains into the work surface to abrade microchips of the workpiece material. While some of the diamond particles in the carrier can become embedded within the lapping plate to perform a fine grinding action (soft plate lapping), abrasive particles in lapping may also be continuously loose and rolling "free particles" (hard plate lapping). This abrading action on the work surface is repeated millions of times in order to effectively remove material while simultaneously providing a polishing action (especially when using abrasive particles as fine as 50nm). As a result, lapped surfaces do not have directional marks.

The workpiece is held in the fixtures. These fixtures and the lapping plate rotate. This rotation of the fixtures serve two purposes. First it conditions the plate, that is, it distributes the wear so that the lapping plate stays flat for longer and secondly, it holds the work piece in place. The speed at which the plate turns is determined by the work requirements. When precise accuracy is needed, 10-15RPM is applied, and when polishing is performed up to 150RPM is used. A pressure of about 3psi must be applied to the work pieces. Although, sometimes their own weight is sufficient, if not, a round, heavy pressure plate is placed on the fixtures. A consistency of the contact area results in repeatable removal rates and excellent batch-to-batch reproducibility. The reduced contact area provided by a grooved plate increases the load per unit area, therefore increasing removal rates. The grooves also allow air to pass through the workpiece and the plate. The air makes vacuum impossible which facilitates the work piece removal without breaking it. An added benefit is that the groove also aids in clearing away swarf.

Lapping consistency is the key to success, therefore it is important to make an effort to control the contact area, pressure, plate speed, charging process, slurry dispensing and the quality of the diamond slurry. Controlling these process variables leads to desired stock removal, flatness, and uniform surface finish. (Schneider 2002, Irvin 2011, Macedo H. 2016)

2.3.3.3 Reconditioning the plate

Reconditioning a ceramic lapping plate requires cutting away the top surface to restore flatness and retexturing the plate so that it can be charged. This is performed using a facing device that uses a diamond tool bit to remove the top worn layer of the lapping plate, machining it flat to within microns. To produce a controlled surface geometry and texture, the device then makes a second pass, which machines a groove pattern that serves as the basis for structured embedding of abrasive particles. Facing devices provide superior control over the groove pattern (macro texture) and land shape (micro texture) of the plate surface, which allows for greater consistency in removal rates and surface finishes (Irvin 2011).

2.3.3.4 Applications

Almost any material, hard or soft, can be lapped, as well as any shape, as long as the surface is flat (Schneider 2002). The materials that can be lapped include steel, stainless steel, chromium carbide, tungsten carbide, aluminium, copper, bronze, alineo (aluminum-nickelcobalt), ceramics, glass, sapphire and plastic (Irvin 2011).

Diamond lapping is appropriate for ceramic machining or finishing operations that face challenges such as:

- Working with non-oxide advanced ceramics or dense, high purity oxide ceramics (these materials are super-hard, but they are not harder than diamond, which can offer more economical processing);
- Improved sealing;
- Improved cosmetic surfaces;
- Planarising joined dissimilar materials (e.g., laminates, composites);
- Surface deburring, removal of “gummy” materials;
- Thinning/finishing parts with poor aspect ratios;
- Greater planar, spherical or conical surface requirements.

Almost any application of engineered ceramics with high flatness and/or surface finish requirements may benefit from the diamond lapping process (Irvin 2011).

2.4 Characterisation Techniques

Membranes are widely used in very different applications, and the requirements for an optimal membrane might differ strongly. Fundamental knowledge of the membrane characteristics affecting its performance in a specific application is needed to ensure a good

choice of a membranes. Therefore it is necessary to develop methods that allow a quantitative determination of all the vital parameters. These include chemical composition, morphology, mechanical strength, corrosion resistance, permeability and thermal stability. Sophisticated characterisation methods for porous membranes are gaining importance because of the higher complexity of the newest generation of membranes. The most commonly characterisation techniques used for the analyses of membranes' morphology and permeability are now described.

2.4.1 Morphology

An important characteristic of porous membranes is the shape and geometry of the pores. Another factor of interest is the pore size distribution in a porous microfiltration membrane, since pores do not have the same size but exist as a distribution of sizes.

2.4.1.1 Bubble Point Method

The bubble point method has been one of the most widely used methods for determining the membrane pore size and pore-size distribution. It can be used as the basis for a method of testing the integrity of the filter.

It is based on the principle that a porous filter, immersed in and thoroughly wetted by a specific liquid, the pressure required to force a gas bubble through a pore is inversely proportional to the diameter of the pore. A schematic drawing of the test apparatus is given in Figure 2.11.

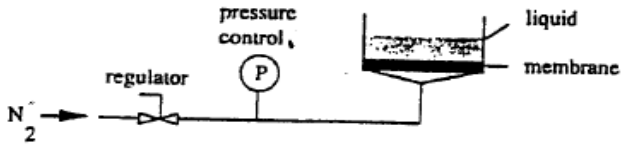

Figure 2.11- Schematic drawing of a bubble-point test apparatus (Mulder 1996).

The relationship between pressure and pore radius is described by the Laplace equation:

$$r = \frac{2 \cdot \sigma}{\Delta P} \cdot cos\theta \qquad (Eq. 2.1)$$

where ΔP is the pressure difference across the membrane (Pa), σ the surface tension at the liquid/air interface ($N.m^{-1}$), r the pore radius (m) and θ the contact angle between the two liquids and the membrane pore wall. During the test the pressure which is necessary to press a certain solution out of the membrane is measured. An air bubble will penetrate through the pore when its radius is equal to the pore. This means that the contact angle is 0º and $cos\theta = 1$. After increasing the pressure over the capillary pressure, the liquid is expelled from the largest pores, allowing air to permeate. By successively increasing the pressure, smaller and smaller pores are opened for air permeation (Figure 2.12).

Figure 2.12- Schematic diagram of the principle of the bubble point method (Li 2007).

The ideal flow versus pressure drop curve obtained is usually S shaped, through which pore size distribution can be calculated (Figure 2.13). Since the surface tension at the water/air interface is relatively high, if small pores are present, it is necessary to apply high pressure or replace water by alcohol for example. At the highest pressure the gas flow of the dry membrane must be equal to the wet membrane. If it is not the case there are still some smaller pores present in the membrane.

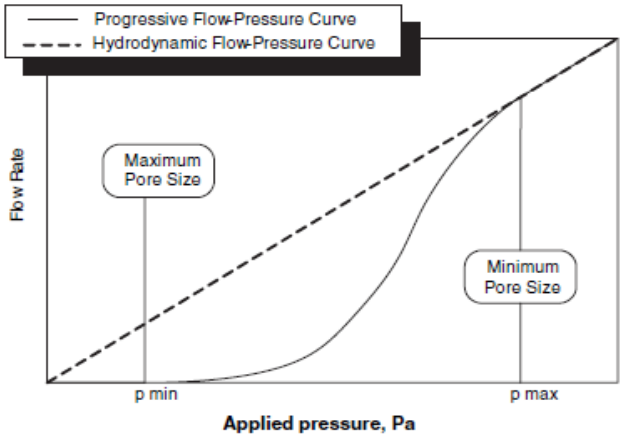

Figure 2.13- Theoretical flow-pressure curve for the bubble point method (Li 2007).

An advantage of this method is that it does not damage nor contaminate the filter, being a non-destructive test. Some disadvantages are that different results are obtained with different liquids and the rate of pressure increase and the pore length may influence the result (Mulder 1996, Li 2007, Sutherland 2008, Reingruber, Zankel et al. 2011, Charcosset 2012).

2.4.1.2 Mercury Intrusion Porosimetry (MIP)

Mercury porosimetry is one of the most popular methods for determining pore size, pore size distribution, surface area and total volume of pores in ceramic membranes. The pore sizes covered by this technique range from 5nm to 10µm.

The method is based on the fact that mercury is a strongly non-wetting liquid on most materials (since its contact angle is greater than 90º and consequently $cos\theta < 0$). When mercury is forced into a dry membrane with the volume of mercury being determined at each pressure, a cumulative volume of mercury as a function of the applied pressure is established, from which the pore-size distribution is deduced because every pressure is related to one specific pore size by Laplace equation. During the experiment, the largest pores are filled with

mercury at a certain minimum pressure. As the pressure increases further, smaller pores are filled until a maximum intrusion value is reached, that is all pores are filled.

The main advantage of this method is that surface area and volume of pores can be determined, but it has some disadvantages. It's a destructive technique, as once the pores are filled with mercury it is very difficult to remove and the contamination is more or less permanent. Small pore sizes require high pressures, which may damage the membrane pore structure and lead to an erroneous pore size distribution. This makes mercury porosimetry more suitable for characterisation of inorganic membranes with very stable structures. This method determines all the pores presented in the membrane including dead end pores, this may result in overestimation of the membrane permeation characteristics. Mercury is extremely toxic and must be handled with care. The apparatus is rather expensive and membranes must be characterised dry (Mulder 1996, Li 2007, Charcosset 2012, Basile 2013, Parma 2013, Ghouil, Harabi et al. 2015, Lorente-Ayza, Sánchez et al. 2015).

2.4.1.3 Permeability Method

If capillary pores are assumed, the pore size can be obtained by measuring the flux through a membrane at a constant pressure using the Hagen-Poiseuille equation:

$$J = \frac{\varepsilon \cdot r^2 \cdot \Delta P}{8 \cdot \mu \cdot \tau \cdot l} \qquad (Eq. 2.2)$$

where, J is the volumetric flux through the membrane ($m^3.m^{-2}.s^{-1}$), ε is the porosity of the membrane, r is the average pore radius of the membrane (m), ΔP is the applied pressures across the membrane (Pa), l is the pore length (m), τ is the tortuosity factor, and μ is the liquid viscosity (Pa.s) (Mulder 1996).

Or Kozeny-Carman, equation 2.3, can be used if pores are assumed to be voids between close-packed spheres of equal diameter;

$$J = \frac{\varepsilon^3 \cdot \Delta P}{K \cdot \mu \cdot l \cdot A^2 \cdot (1-\varepsilon)^2} \qquad (Eq. 2.3)$$

where K is the Kozeny constant, which is dependent on the pore shape and tortuosity and A the permeation area (Mulder 1996, Lorente-Ayza, Sánchez et al. 2015).

The water flux through the membrane is measured as function of the applied pressure. At a certain minimum pressure the largest pores become permeable, while the smaller pores still remain impermeable. Finally, when the maximum pressure is reached the smallest pores become permeable. This minimum pressure depends mainly on the type of membrane material present (contact angle), type of permeate (surface tension) and pore size, Laplace equation.

Experimental simplicity is the main advantage of this method, while one of the problems encountered is the assumption of pore geometry and experimental results are often difficult to interpret (Mulder 1996).

2.4.1.4 Rejection Measurements

Rejection coefficient define the efficiency of the filtration process, and is calculated by:

$$R(\%) = 100 \cdot \left(1 - \frac{C_p}{C_f}\right) \qquad (Eq. 2.4)$$

where C_p and C_f are the solute concentration in the permeate and in the feed solution, respectively (Mulder 1996, Li 2007, Charcosset 2012, Lorente-Ayza, Mestre et al. 2015).

2.4.1.5 Water Uptake

What information does it give:

The weight difference between wet and dry membranes is measured by immersion of distilled water or boiling water immersion method, allowing the determination of membrane volume porosity. The porosity of the membrane is measured by:

$$Porosity(\%) = \frac{W_{wet} - W_{dry}}{\rho_{water} \cdot V_{membrane}} \cdot 100 \qquad (Eq. 2.5)$$

where, W_{wet} is the wet weight of the membrane (placed in distilled water for overnight), W_{dry} is the dry weight of the membrane, $V_{membrane}$ is the total volume of the membrane and ρ_{water} is the density of the water (Kumar, Ghoshal et al. 2015, Lorente-Ayza, Sánchez et al. 2015).

2.4.1.6 Summary

Table 2.3- Summary of membrane morphology characterisation methods (Mulder 1996, Li 2007, Charcosset 2012, Lorente-Ayza, Mestre et al. 2015).

	Bubble Point Method	**Mercury Intrusion Porosimetry (MIP)**	**Permeability Method**	**Rejection Measurements**	**Water Uptake**
Microporous Range	✓	✓	✓	-	-
Specific surface area	×	✓	×	×	×
Pore size	✓	✓	✓	×	×
Pore size distribution	✓	✓	✓	×	×
Total volume porosity	×	✓	×	×	✓
Rejection coefficient	×	×	×	✓	×
Only active pores determined	✓	×	✓	-	×
Safety	✓	×	✓	✓	✓
Non-destructive test	✓	×	✓	✓	✓
Available at University of Surrey	✓	×	✓	Calc (Concentration)	Calc (Weight)

2.4.2 Microscopy Methods

Microscopy methods allow the visualisation of the membrane surfaces and cross-sections. These images provide a good impression of the membrane structure and are analysed by image processing software. Image processing software is used to calculate quantitative parameters such as pore diameters, mean pore size, pore size distribution, the porous fraction and so on.

2.4.2.1 Electron Microscopy (EM)

The morphology of membranes surfaces and their cross sections is routinely analysed via electron microscopy. The follow techniques allow information about surface roughness and grain size or shape of ceramics at the membrane surface, as well as layer continuity and thickness of the membrane. It is also possible to estimate pore size and shape using electron microscopy. In general electron microscopy is a high-vacuum technique, which gives images of only dry membranes and also requires extensive preparation of the samples (Somasundaran 2006, Basile 2013). Figure 2.14 is a schematic drawing of the two electron microscopy methods most used, SEM and TEM, and the optical microscopy method.

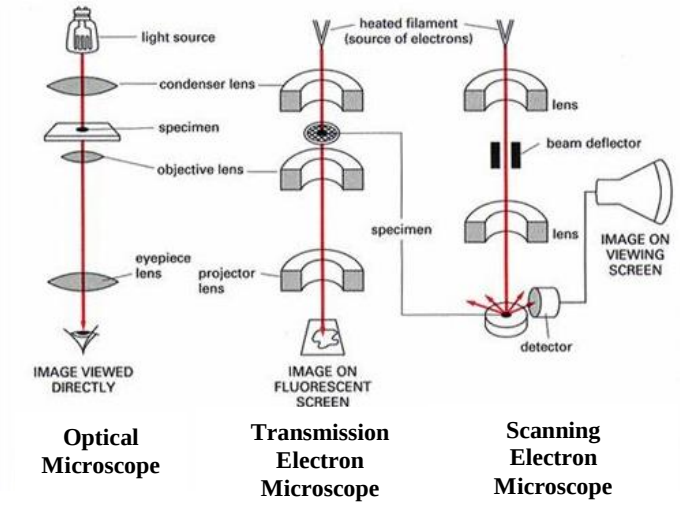

Figure 2.14- Principal features of an optical microscope, a transmission electron microscope (TEM), and a scanning electron microscope (SEM) (University of Edinburgh 2010).

- **Scanning Electron Microscopy (SEM)**

SEM has been used for many years to characterise the porous structure of microfiltration membranes. It allows a clear view of the overall structure by the photographs obtained.

In SEM, a beam of electrons is produced at the top of the microscope by heating a metallic filament. The incident electrons are called primary (high-energy) electrons, and those reflected are called secondary electrons (low-energy). The primary electron beam passes through electromagnetic lenses, which focus and direct it down towards the sample. The

electron beam interact with the atoms that make up the sample surface, and produce secondary electrons. The back scattered electrons produce characteristic x-rays, light, specimen current and transmitted electrons that detectors collect and convert them to a signal that is sent to a viewing screen. To observe cross sections of flat-sheet membranes, the samples are usually briefly frozen in liquid nitrogen and then broken manually.

Some advantages of this technique is its resolution of around 10-50nm, a depth resolution of 1–10nm, and due to the large depth of field, the SEM images visualise the membrane surface morphology three-dimensionally. However, vacuum conditions are required in conventional SEM, which means that the sample has to be analysed in its dry state. When a membrane is placed in the electron beam, the sample can be burned or damaged depending on the type of material and accelerating voltage employed. This can be prevented by coating the samples with a charge conducting (carbon, gold, platinum, or palladium by low vacuum sputter coating) layer. The coating is needed to prevent charging up of the membrane, and to increase the conductivity of the sample to obtain superior image quality. The main difficulty in characterising porous structure using software for image analysis by SEM image is the projection-type distortion, which complicates measurements of the "throat-type" pores, making then smaller than the actual ones (Mulder 1996, Kallioinen and Nystro¨m 2008, Charcosset 2012, Parma 2013).

- **Transmission Electron Microscopy (TEM)**

In TEM, primary high-energy electrons are transmitted and diffracted through a thin specimen. Therefore, before TEM, the dry membrane is embedded in a resin. A very thin slice (less than 50nm) is cut for electron to penetrate.

The maximum resolution of TEM is 0.3–0.5nm, and therefore, it can be used even in the characterisation of NF and RO membranes. It is useful in the characterisation of multiphase morphologies because it provides information on the inner structure of the particles and gives the possibility to show the differences in chemical structure in the sample as contrasts in the image. Due to the limitations in sample preparation, such as small cracks in samples caused by the cutting procedure, and the influence of the embedding resin on the membrane structure, resolution at 10nm is often used to interpret the images obtained (Kallioinen and Nystro¨m 2008, Charcosset 2012).

- **Field Emission Scanning Electron Microscopy (FESEM)**

FESEM give the same information as SEM but with a better resolution 1-5nm. While SEM has a thermionic emitter, FESEM has a field emitter. Thermionic emitters use electrical current to heat up a filament. When the heat is enough to overcome the work function of the filament material, the electrons can escape from the material itself. Thermionic sources have

relative low brightness, evaporation of cathode material and thermal drift during operation. Field emission is one way of generating electrons that avoids these problems. A field emission does not heat the filament. The emission is reached by placing the filament in a huge electrical potential gradient. The charging problem and beam damage to the sample can be diminished by applying the FESEM technique rather than SEM, which uses a lower accelerating voltage compared to conventional electron microscopy (Polytechnic of Turin , Mulder 1996, Li 2007, Kallioinen and Nystro¨m 2008).

2.4.2.2 Optical Microscopy

The optical microscope is particularly useful for detection of large (>1mm) membrane defects, macro voids, fouling particles, or ensure successful coating of a surface. In optical microscopy light transmitted through the sample is reflected from the sample surface and forms an image, which is magnified with a lens system. This technique is low-cost and the interactions between a sample and the used radiation cause almost no distortions in the sample. No sample pre-treatment is needed and the samples can be analysed in their wet or dry state because the sample is not exposed to a vacuum during imaging. However, resolution is poor compared to other methods (only 1µm), being limited to the characterisation of surface macrostructure (Li 2007, Kallioinen and Nystro¨m 2008, Charcosset 2012, Basile 2013).

2.4.2.3 Atomic Force Microscopy (AFM)

Atomic force microscopy (AFM) gives topographic images by scanning a sharp tip over a surface. The instrument consists of a sharp tip that is attached to the end of a flexible cantilever. A laser beam is reflected from the cantilever to an optical sensor. During an analysis the tip is translated over the sample and the deflections are detected by the optical sensor via reflectance of the laser beam from the cantilever (Figure 2.15). In the contact mode, the tip is very close to the surface being imaged and is responding to very short range repulsive interactions with the sample. In the non-contact mode, the tip responds to attractive Van der Waals interactions with the sample, the tip being generally at a distance of 5–10nm away from the surface. This mode of operation is suitable for materials, such as polymeric membranes, which are soft or liable to mechanical damage as the forces used for imaging are lower than in the contact mode. AFM measurements give access to the surface roughness, pore size, pore density and pore-size distribution.

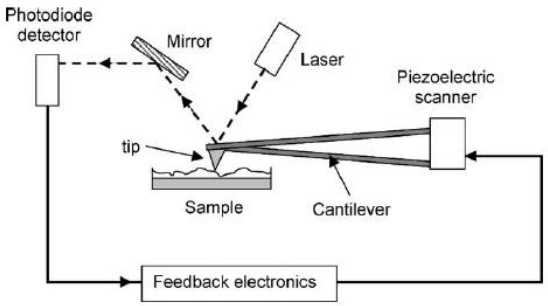

Figure 2.15- Schematic illustrating AFM with feedback (Chan and Chen 2004).

Some advantages of this technique are that both lateral and depth resolution can reach the subnanometer range. It does not require pre-treatment, allowing the analysis of no conducting surfaces in dry and wet environments, since measurements can be carried out under atmospheric conditions avoiding potential samples damage caused by the vacuum conditions required in most other techniques. However, surface roughness may result in images difficult to interpreted, relatively small area that can be scanned, the maximum scan area being approximately 100μm^2. AFM may distort membrane pore size due to rounded corners near pore entrance and if the pores are smaller than the tip AFM underestimates the pore dimensions, and the scanning depth is also limited by the tip size. (Mulder 1996, Chan and Chen 2004, Somasundaran 2006, Kallioinen and Nystro¨m 2008, Charcosset 2012).

2.4.2.4 Confocal Scanning Laser Microscopy (CSLM)

CSLM provides high resolution optical images with depth selectivity, where the incident light source is a laser. The laser beam is focused on a limited spot in the sample and the light reflected, backscattered, or emitted from the spot in focus is detected. A pinhole in front of the detector obstructs the light reflected from the illuminated regions of the sample below and above the in-focus point to reach the detector (Figure 2.16). Thus, only one point of the sample is observed at a time. In order to obtain an image of the sample the laser beam is scanned over the sample surface and the detected signal is recorded point by point to produce the image. Imaging may be performed in the reflective or in the fluorescence mode.

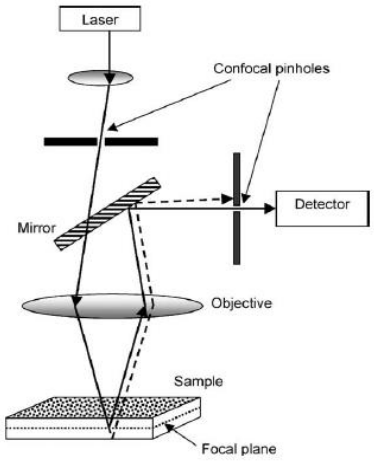

Figure 2.16- Schematic of confocal microscopy (Chan and Chen 2004).

This technique allows accurate and non-destructive optical sectioning in a plane perpendicular or parallel to the optical axis of the microscope. A series of images can be recorded at different depths by changing the position of the focalisation plane. The images can be computer processed to present the information as a complete three-dimensional reconstruction, allowing 3D morphology characterisation. CSLM requires only minimal specimen preparation and wet samples can be studied. On the other hand, is has low resolution, 180 nm in the focal plane (x, y) and 500–800nm along the optical axis (z), being only applicable to MF membranes (Chan and Chen 2004, Kallioinen and Nystro¨m 2008, Charcosset 2012).

2.4.2.5 Summary

Table 2.4-Summary of microscopical methods to characterise morphology of membranes (Chan and Chen 2004, Kallioinen and Nystro¨m 2008).

	Scanning Electron Microscopy (SEM)	Transmission Electron Microscopy (TEM)	Field Emission Scanning Electron Microscopy (FESEM)	Optical Microscopy	Atomic Force Microscopy (AFM)	Confocal Scanning Laser Microscopy (CSLM)
High resolution	✓	✓	✓	×	✓	×
Analysis of MF membranes (pore size, fine structure)	✓	✓	✓	✓	✓	✓
Vacuum required	✓	✓	✓	×	×	×
Sample pretreatment required	✓	✓	✓	×	×	×
Wet samples can be analysed	×	×	×	✓	✓	✓
Sample destructive technique	✓	✓	✓/×	×	✓/×	×
3D image obtained	×	×	×	×	✓	✓
Depth profiling possibility	×	×	×	×	×	✓
Examination of porous structure	✓	✓	✓	✓	✓	✓
Examination of roughness	×	×	×	×	✓	×
Available at University of Surrey	✓	✓	✓	✓	✓	×

2.4.3 Transmembrane Pressure and Permeability

The production rate is referred to as the permeability of a membrane. The permeability is the reciprocal of the resistance to flow offered by the filter thus, high permeability represents a low resistance and vice versa. Permeation measurements can be made with either a liquid or a gas and can consist of a single component or a mixture.

2.4.3.1 Transmembrane Pressure

The pressure that is needed to push a liquid through a membrane is called the transmembrane pressure. For dead-end configuration, the transmembrane pressure can be calculated by the difference between the pressure on the feed side and on the permeate side (ΔP).

$$\Delta P = P_f - P_p \qquad (Eq. 2.6)$$

For a cross-flow device, the pressure on the feed side is evaluated as the mean of the pressures at the inlet and outlet of the device:

$$\Delta P = \frac{(P_f + P_r)}{2} - P_p \qquad (Eq. 2.7)$$

where P_f and P_r are the pressure of the flowing bulk solution at the inlet (feed) and outlet (retentate) of the device. The pressure on the filtrate side, P_p, is usually negligible. Transmembrane pressure for MF systems usually range from 0.15 to 3 bar and applied pressures from 0.7 to 2 bar (American water works association 2005, Charcosset 2012).

2.4.3.2 Permeability

The permeability characterises the quantity of fluid per unit time and area that crosses the membrane at a given pressure.

First it is necessary to know the volumetric permeate flux through the membrane, J ($m^3.s^{-1}.m^{-2}$), which is an essential parameter in the efficiency of the membrane process It is evaluated from experimental data by:

$$J = \frac{M_P}{\rho_P \cdot A} = \frac{V}{t \cdot A} \qquad (Eq. 2.8)$$

where M_P is the mass flow rate of the permeate ($kg.s^{-1}$), A the permeation area (m^2) and ρ_P the permeate density ($kg.m^{-3}$), V the volume of permeate (m^3) and t the time (s) (Charcosset 2012).

The flow of a fluid through a porous medium can be described by Darcy's law. Darcy's law relates the permeability constant L_p (m^2) with the slope of the straight line. If the flow values obtained are represented against the applied pressure, a straight line may be obtained and the corresponding slope calculated.

$$L_p = \frac{slp \cdot l \cdot \mu \cdot \tau}{A} = \frac{Q \cdot l \cdot \mu \cdot \tau}{\Delta P \cdot A} = \frac{J \cdot l \cdot \mu \cdot \tau}{\Delta P} \qquad (Eq. 2.9)$$

where *slp* the value of the slope ($m^3.s^{-1}.Pa^{-1}$), *l* membrane's thickness (m), μ is viscosity (Pa.s), τ tortuosity and Q volumetric flow rate ($m^3.s^{-1}$) (Glover , Lorente-Ayza, Sánchez et al. 2015). Since darcy's law as given in Eq.2.9 may be written as:

$$J = \frac{L_p \cdot \Delta P}{\mu \cdot l \cdot \tau} \qquad (Eq. 2.10)$$

Equating Hagen-Poisseuille equation (Eq. 2.2), and Darcy's law (Eq 2.10) leads to:

$$Lp = \frac{\varepsilon \cdot r^2}{8} \qquad (Eq. 2.11)$$

It is then possible to obtain the relation between permeability, porosity and mean pore radius of the membrane (Marshall, Holmes et al. 1996).

Permeability of a membrane, L_p, can also be related to the TMP and volumetric permeate flux, J:

$$J = L_p \cdot \Delta P \qquad (Eq. 2.12)$$

Increasing ΔP increases permeate flux through the membrane (Charcosset 2012, Staszak, Karaś et al. 2013, Ghouil, Harabi et al. 2015).

Water and gas permeameters:

The most accurate way of determining membrane performance is to test the membrane in a permeation set-up, as this minimises the real-life operation of the membrane. Water permeability measurements can be carried out by means of a water permeameter specifically designed for disc configuration samples, Figure 2.17.

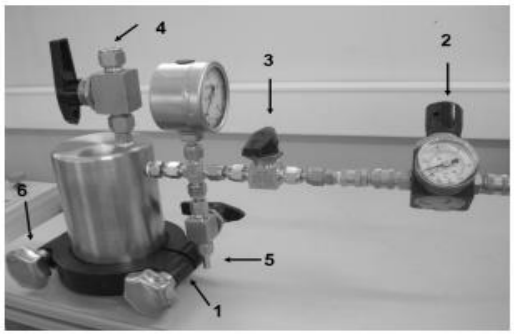

Figure 2.17- Water permeameter for permeability measurements of flat membranes. 1-membrane holder; 2-pressure gauge; 3,4-valves; 5-feed inlet duct; 6-permeate outlet duct (Lorente-Ayza, Mestre et al. 2015).

The water pressure applied to the membrane is varied while water flow through the membrane disc is determinate for a given time. For a direct application of Darcy's law (Eq.2.9) the permeability constant, L_p, can be calculated (Lorente-Ayza, Mestre et al. 2015). The same method can be applied to determine gas permeability using a chosen pressurized gas instead of water and a gas permeameter, as shown in Figure 2.18 (Momeni and Pakizeh 2013).

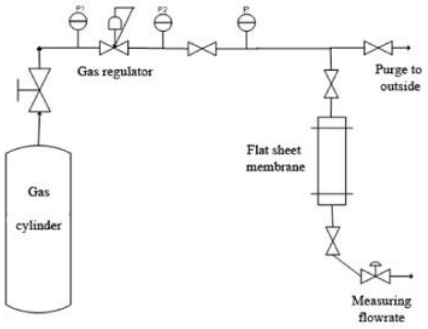

Figure 2.18- Schematic of experimental set-up for gas permeation tests (Momeni and Pakizeh 2013).

2.5 Assessment on Analytical Techniques

Morphology:

Membranes' morphology, more specifically medium pore size and pore size distribution are the key parameters to analyse after lapping.

The bubble point method uses the Laplace equation, which assumes capillary pores; this is not a bad assumption in this study since the pores have a conical design and supposedly aren't connected. One great advantage is that only active pores are characterised. This method does not destroy or contaminate the sample. For these reasons, the bubble point method is an appropriate and complete method to characterise Smart Separations's membranes.

To verify if there are any other pores or fissures that do not cross the membrane, it is possible to measure the water uptake. Water uptake determines the total volume porosity, although it's not a very accurate method. A comparison between the pores volume determined by the bubble point method and total volume porosity would give information about be the dead-end pores.

Permeability method is also a good technique that can be applied to determine the permeability coefficient of the membrane, but it can also give information about the pore size and pore size distribution, just like bubble point method.

Microscopy methods:

To characterise membrane morphology with microscopy techniques, it is important to obtain a good quality image. From the techniques available at the University of Surrey, FESEM would be the best technique to characterise the morphology of membranes. FESEM provides a better quality image than SEM and then the images can be analysed by an imaging software that outputs all the data required. Using FESEM it is even possible to determine the chemical composition by EDS, which is coupled to FESEM. The other techniques available at the University have a few crucial drawbacks that don't make them as suitable as FESEM. The optical microscope has a low resolution, being only able to detect large membrane defects or

pores bigger than 1µm. TEM only analises thin films therefore sample preparation is quite difficult and AFM requires really flat samples.

Permeability:

The most accurate way to determine the permeability of membranes would be using a permeameter. This is so because it determines the flow through the membrane and the variation of pressure applied minimises the human error, while it also mimics the actual live operation. It is then possible to plot these parameters and obtain the corresponding slope. Eq.2.9 is then used to calculate water permeability. This technique is the most accurate because it considers the most parameters and their variations.

Conclusion:

Characterisation of membranes is going to be performed after lapping. It is important to study the influence and change on the main parameters. These parameters are pore size, pore size distribution and their effect on permeability. The easiest and fastest way to determine the vital parameters of this study would be to combine the best techniques for each characteristic.

Initially optical microscope and FESEM analysis would give clear images of the membranes. The images will then be analysed by the Image Pro Premier 9.1 software. The imaging software would provide data about pore size and pore size distribution and results will be compared. To corroborate the results, bubble point method will also be used. Permeability tests would give information about the influence of lapping on the membranes and consequently pore sizes.

3

MATERIALS AND METHODS

In this chapter, materials and equipment used during the lapping process and membrane characterisation processes are described. The method used for the lapping process, as well as the tool used for the evaluation of the results, Image Pro Premiere, are also explained. The methodology used for the permeability tests and the study of pores geometry are detailed in this section, as well as the methods used by Porometer to perform their porometry and permeability tests.

3.1 Materials

The materials and equipment used for the lapping process will now be explained and their purpose indicated. Important definitions used throughout this work will be elucidated. A brief description of the equipment used for characterisation of samples after lapping, such as optical microscope, FESEM and the setup for permeability tests will follow.

3.1.1 Equipment for the Lapping Process

3.1.1.1 Smart Separations's membranes

For this project, Smart Separations's membranes were used and studied. The samples are sintered ceramic membranes, with about 23mm of diameter, about 750µm thick and have closed pores on both sides, according to the company's patent. These pores are in the microfiltration range and have a conical structure. Therefore, after lapping, one surface has smaller pores, while the other has bigger ones. Smart Separations's membranes are represented in Figure 3.1, before and after lapping, as well as different perspectives of the same. For convention, it is called "top surface" to the surface with smaller pores, and "bottom surface" to the one with larger pores. In the lapping process, material is removed from the samples, hence their thickness decreases. The definition for the difference between the initial thickness of the samples and the thickness after lapping is called material removal. (Macedo H. 2015, Macedo H. 2016)

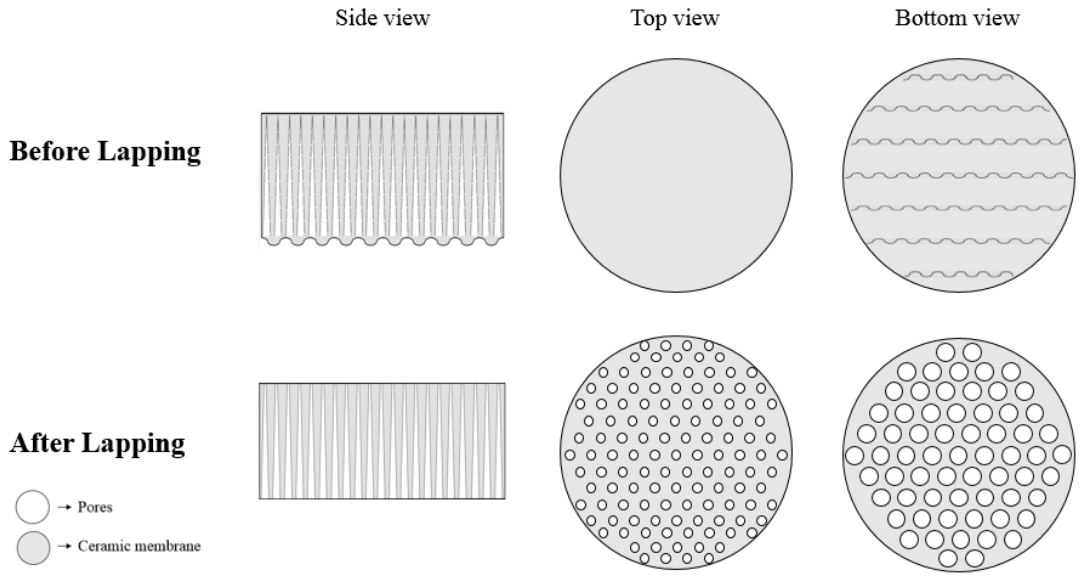

Figure 3.1- Smart Separations's membranes' structure, before and after lapping in different perspectives.

3.1.1.2 Lapping plate

The lapping equipment used was LamPlam M.M. 380 (Figure 3.2). This lapping plate was used to remove a control amount of material from the samples, while smoothing them. It consists of a flat ceramic surface with grooves, in order to prevent samples from breaking and accumulate removed material. It has a diameter of about 38cm. The plate rotates anti-clockwise and has three stoppers in order to maintain the holder of the SS's fixtures in place. Each of the three stoppers has two rubber wheels, allowing the holder to also rotate anti-clockwise, while the plate is rotating. The lapping plate must be flat, and so, a flatness gauge must be used to ensure it. This equipment has a control panel (Figure 3.3), where the first button is to initiate or stop the rotation of the lapping plate. The second button controls the rotation speed. The third control sets the time, in seconds, where each button is assigned to a digit (thousands, hundreds, tens and units, respectively). The fourth control is the time counter of the lapping plate's operation, and the fifth turns the equipment on and off. (Macedo H. 2016)

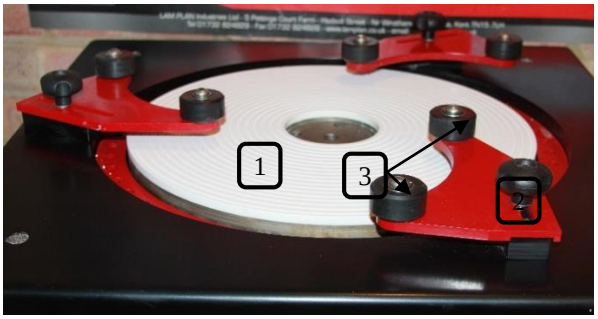

Figure 3.2- Lapping plate and its components. 1- Lapping plate; 2- Stopper; 3- Rubber wheels.

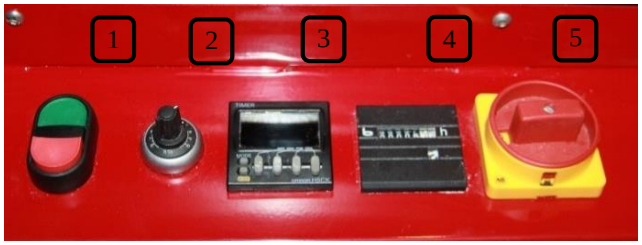

Figure 3.3- Lapping equipment control panel. 1- ON/OFF switch of the lapping plate's rotation; 2- Rotation speed of the lapping plate controller; 3- Time controller; 4- Time counter; 5- ON/OFF switch of the equipment.

3.1.1.3 Flatness gauge

To verify the flatness calibration of the lapping plate, a flatness gauge is used. The equipment has about the same size as the lapping plate, in order to measure the unevenness over the entire plate. It has an accuracy of ± 5µm. The flatness gauge has four supports, two at one end, one at the other and the fourth in the middle. This last support does the flatness readings. First, it is needed to measure the flatness of the metal piece that is inside the box of the flatness gauge (Figure 3.4).

Figure 3.4- Flatness gauge measuring the metal piece.

This metal piece is perfectly flat, and by measuring it, the zero point is known. Then, the flatness of the plate is measured by placing the gauge on top of it (Figure 3.5).

Figure 3.5- Flatness gauge on top of the lapping plate.

If the lapping plate is flat, the reading of the flatness gauge will be the zero point. If the lapping plate is concave, the arrow will go to the left relative to the zero point, having a negative reading. If the plate is convex, the arrow will go to the right, having a positive reading (Figure 3.6). The plate's shapes are a consequence of lapping in preferred zones of the plate. The

concave shape is due to the most usage of the plate at its inner part, and the convex shape is due to the most usage at its outer part. If the plate does not meet the calibration requirements, the conditioning ring is used.

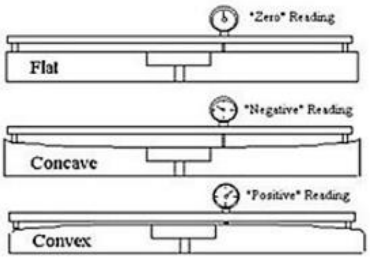

Figure 3.6- Flatness gauge readings (Engis Corporation 2016).

3.1.1.4 Conditioning ring

To calibrate the lapping plate's flatness the conditioning ring is used. The flatness correction is done by removing material from the less used part of the plate. Hereupon, to correct a convex plate the conditioning ring has to be moved to the inner part of the lapping plate. To correct a concave plate the conditioning ring has to be moved to the outside of the lapping plate (Figure 3.7).

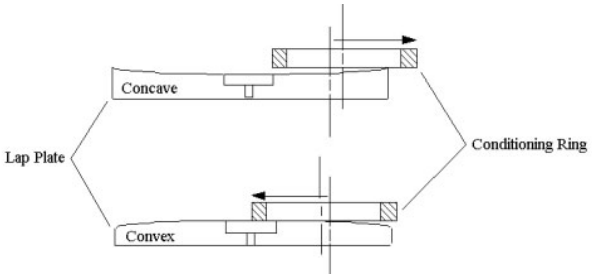

Figure 3.7- Conditioning ring calibrating the lapping plate with concave and convex shapes (Engis Corporation 2016).

3.1.1.5 Diamond liquid and cleaning fluid

A diamond liquid was applied to the lapping plate (Figure 3.8). This liquid is composed of loose abrasive particles of diamond with 9μm and a liquid carrier. The carrier holds the abrasive particles in suspension, while the abrasives remove material from the samples' surface. Before using the lapping plate and the SS's fixtures, it is needed to clean their ceramic surface with a cleaning solvent. Both liquids are harmful, being quite volatile, therefore, special care must be had when using them.

Figure 3.8- Diamond liquid.

3.1.1.6 Smart Separations's fixtures

The present patent pending fixtures were designed by Smart Separations (Figure 3.9). Each of these are composed by a manual micrometer on the top (Figure 3.10), a ceramic surface and a ceramic ring at the bottom (Figure 3.11). The three fixtures are placed on top of the lapping plate with samples between the plate and each fixture. (Macedo H. 2016)

Figure 3.9-The three Smart Separations's fixtures (Macedo H. 2016).

The micrometer (Figure 3.10) has the sleeve and thimble scales in inches. Each unit of the sleeve scale equals 0.1in. Each unit has 4 splits. Each split of the sleeve scale equals one turn of the thimble. The thimble scale has 25 splits, which means that each split is 0.001in that is about 25.4µm.

Figure 3.10- The micrometer of the SS's fixtures and it's scales. 1- Thimble scale; 2- Sleeve scale.

The ceramic surface, on the bottom, has about 5.1cm of diameter, and has grooves in order to avoid samples from getting attached to it, and to accumulate removed material. There is

also a ceramic ring that keeps the samples under the ceramic surface of the fixture while lapping (Figure 3.11).

Figure 3.11- Ceramic surface and ceramic ring on the bottom of the Smart Separations's fixture (fixture upside down). 1- Ceramic surface; 2- Ceramic ring; 3- Groove.

The height of the ceramic surface is controlled by the micrometer with a accuracy of ± 12.5µm. Lower micrometer measurements result in lower heights of the ceramic surface. The calibration point of the ceramic surface of the SS's fixture is the micrometer reading when the ceramic surface is aligned with the ceramic ring (Figure 3.12). The calibration point of the fixtures' ceramic surface does not correspond to the zero reading of the micrometer. If the micrometer reading is reduced one split from the ceramic surface's calibration point, the ceramic surface will be below the alignment of the ceramic ring.

Figure 3.12- Calibration point of the ceramic surface of the Smart Separations's fixture (fixture upside down).

The micrometer measurement when the sample surface is aligned with the ceramic ring is called the calibration point of the sample (Figure 3.13). If the micrometer reading is reduced one split from the sample's calibration point, the sample will be below the alignment of the ceramic ring.

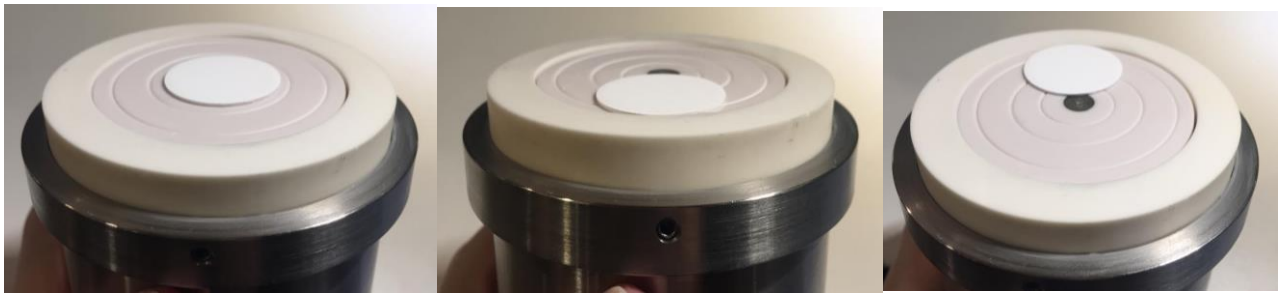

Figure 3.13-Calibration point of the sample (fixtures upside down).

Cut thickness, an important definition, will now be explained. When the micrometer pushes the ceramic surface to a lower height than the sample's calibration point, a certain amount of sample will come out of the ring alignment. This amount is quantified as a thickness measurement. The thickness of the sample out of the ring's alignment is called cut thickness. The calibration point of the sample has 0µm of cut thickness. If the micrometer is reduced 1 split from the sample's calibration point, 25µm of the membrane will come out of the ring's alignment, which means 25µm of cut thickness. Only the samples' surface touches the lapping plate while lapping, except when the cut thickness is 0µm, in which case, the ceramic ring also touches it. The relation between cut thickness, micrometer readings and calibration point of the sample is represented in Figure 3.14.

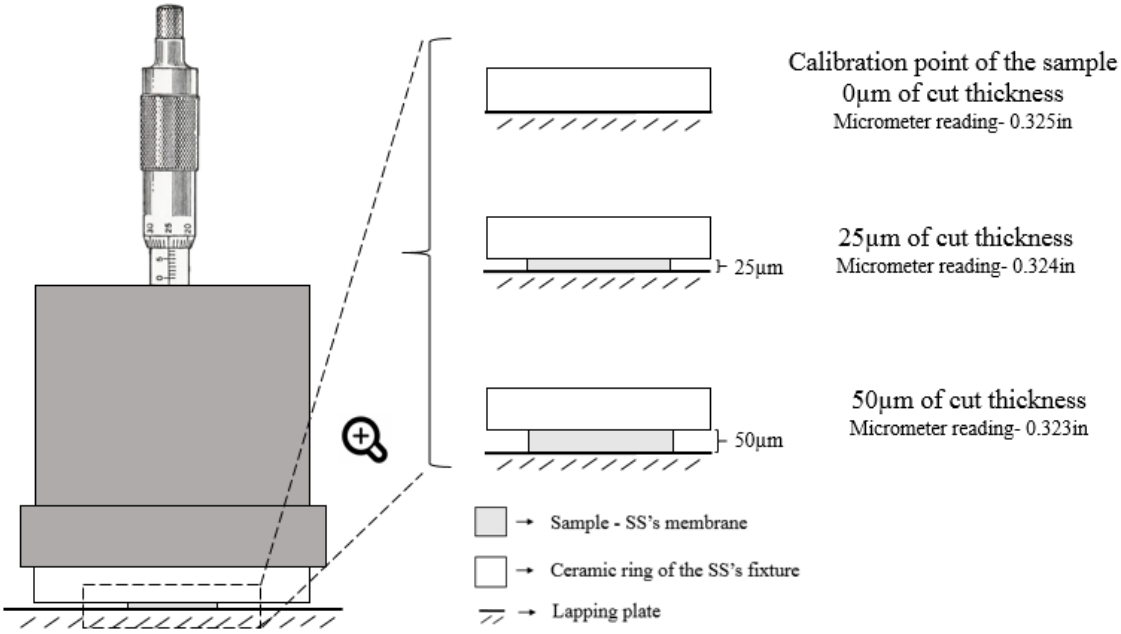

Figure 3.14- Micrometer readings leading to cut thickness variations.

3.1.1.7 Smart Separations's fixtures holders

To maintain fixtures in place while the lapping plate is rotating, a holder is used. The holder is placed on top of the three fixtures (Figure 3.15).

Figure 3.15- Side view of the holder embedded in the three fixtures.

The weight of the holders is supported by the fixtures, because of their metal edges on the bottom (Figure 3.16).

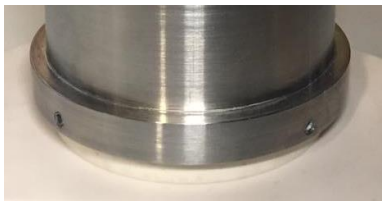

Figure 3.16- Metal edge on the bottom of the SS's fixtures to support the holder.

The holder was designed with three equal sized holes, one for each fixture, in a equilateral triangular shape. This is due to the fact that the weight of the holder has to be equally distributed by the fixtures. The rotation of the lapping plate causes the rotation of the aggregate holder-fixtures, due to friction. This aggregate rotates around the holder's rotation axis (Figure 3.17).

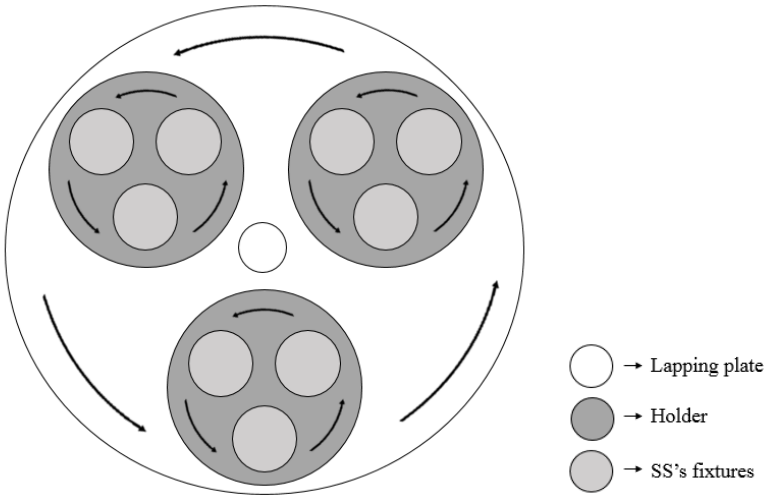

Figure 3.17- Rotation of the SS's fixtures and lapping plate.

The holder used for bottom surface lapping is made of massive metal. In addition to the three holes for the fixtures, it also has three other holes in order to reduce its weight (Figure 3.18).

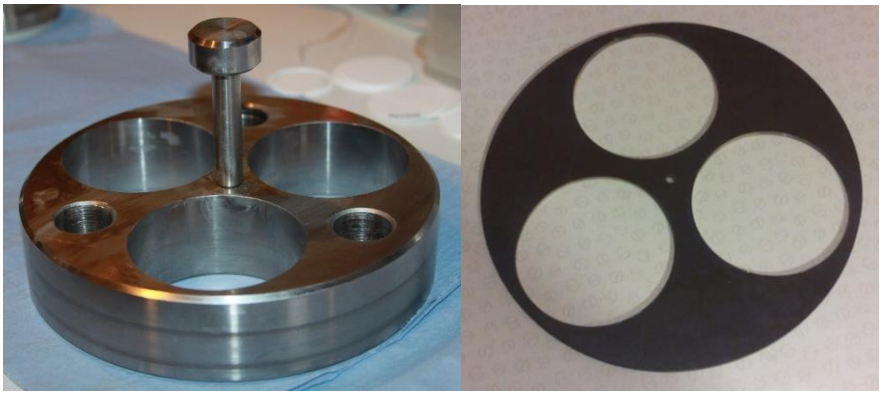

Figure 3.18- SS's fixtures holders used for bottom (left) and top (right) surface lapping.

For top lapping, a lighter and thinner holder is used (Figure 3.18). Three sponge pieces are also used together with the holder, in order to prevent the SS's fixtures from shaking. The weight of the holder is related to the pressure applied on the fixtures and, consequently, on the samples. Lighter holder, applies less pressure on the samples.

3.1.1.8 Micrometer and depth micrometer

To measure the thickness of the samples before and after lapping, a digital micrometer was used (Figure 3.19). The equipment has a spherical tip with a diameter of 6mm. Its range is 0-25mm and an accuracy of ± 0.001mm.

Figure 3.19- Micrometer measuring the thickness of a sample.

A digital depth micrometer was used to measure the depth of the ceramic surface of the SS's fixtures (Figure 3.20), in order to be possible to calculate the error associated with each fixture. Its range is 0-150mm and has an accuracy of ± 0.001mm.

Figure 3.20- Depth micrometer.

3.1.1.9 Ultrasonic bath

Ultrasonic bath (Figure 3.21) is used to clean the membranes after lapping, in order to wash material removed and remaining diamond liquid. This way, when the samples are observed in the microscope, all of its pores are clean. The ultrasonic bath is filled with water just above the middle, and has a time regulator to control how long the membranes are cleaned. It also has a stopper, in order to prevent water from splashing out.

Figure 3.21- Ultrasonic bath.

3.1.2 Equipment for Membrane Characterisation

3.1.2.1 Optical microscope

An optical microscope, AmScope, was used to observe samples after lapping (Figure 3.22). This equipment has a camera attached to its eyepiece, in order to see the sample image on the computer and to take pictures. The computer software used was AmScope 3.7.

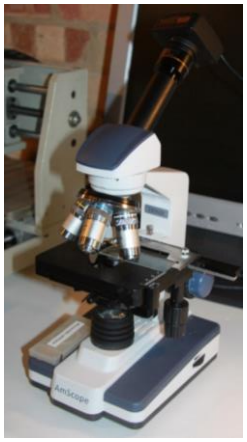

Figure 3.22- Optical microscope with a camera attached.

3.1.2.2 Field Emission Scanning Electron Microscope (FESEM)

Field Emission Scanning Electron Microscope, JSM-7100F (Figure 3.23), was used to collect pictures of the samples. In section 2.4.3.1 is described the operating mode of this equipment, as well as its advantages and disadvantages. There were pictures taken at varying magnifications before and after lapping in order to characterise the membranes. Before the

samples can be observed at FESEM, first they have to be prepared. They're initially dried, on the next day they are golden coated under vacuum and then observed, in order to take pictures and evaluate their structure.

Figure 3.23- Field Emission Scanning Electron Microscope.

3.1.2.3 Permeability tests

The in-house experimental setup used for the permeability tests is depicted in Figure 3.24. The range of the flow meter present in the setup was too high for the flow of the tested membranes. Due to this, in order to calculate the flows, a bucket with water was used with the air outlet underwater and on the bottom of the 2L cylinder. A stop watch was also used.

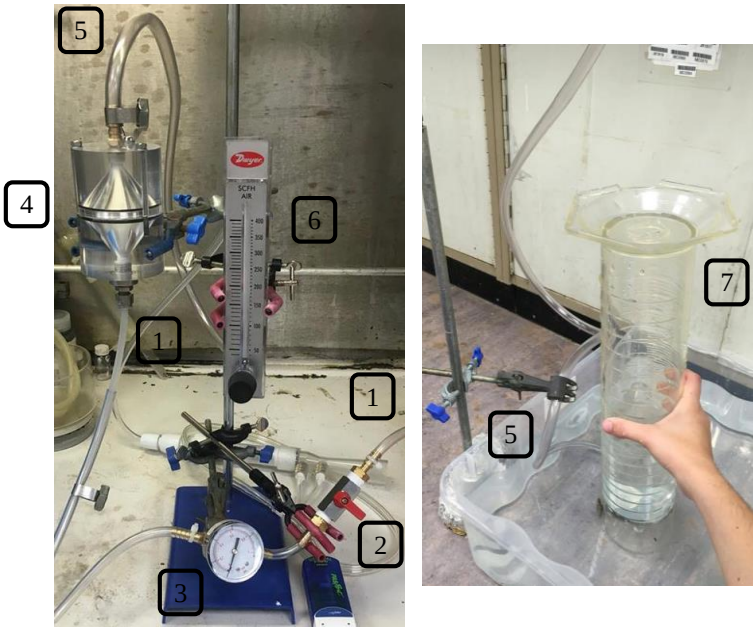

Figure 3.24- Experimental setup for the permeability tests. 1-Air inlet; 2- Valve; 3- Pressure sensor; 4- Permeability rig; 5- Air outlet; 6- Flow meter; 7- 2L cylinder.

A subcontractor company, Porometer, carried out three capillary flow porometry tests and three gas permeability tests for each one of the samples by using a POROLUX$_{TM}$ 1000 porometer.

3.1.2.4 Dust-Load tests

The test equipment was set up as shown in the schematic below.

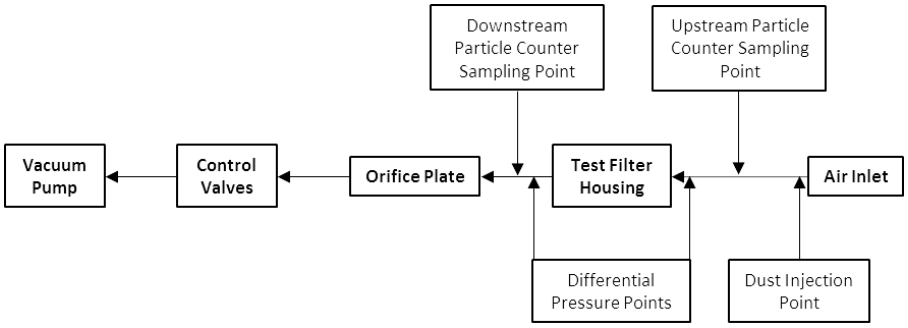

Figure 3.25- Schematic of test setup.

The test equipment was set up as shown in Figures 3.25 and 3.26. The airflow was measured at the orifice plate and moderated by control valves connected to the vacuum pump to produce the required flowrate for the testing.

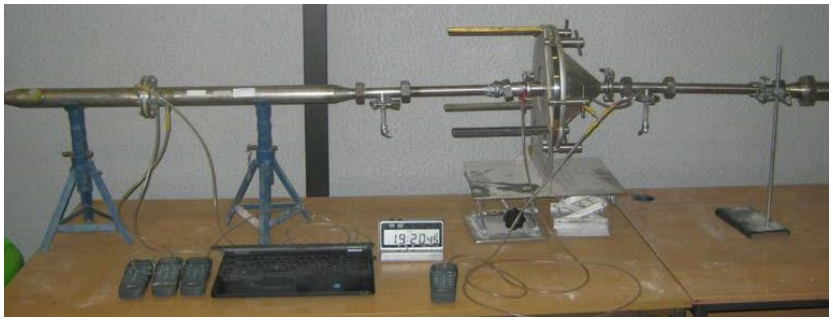

Figure 3.26- Photograph of test setup.

The challenge aerosol selected for testing was ISO 12103-1 A2 Fine. To achieve the chosen concentration of 0.5g/m^3, the Rotating Brush Generator dust feeder was selected, Figure 3.27 and 3.28. The Welas RBG injector allows dust feed rates in the range of approximately 50–2000 mg.min^{-1} (this varies with dust density). The RBG uses a rotating brush to liberate particles from a packed cylinder of dust. The packed cylinder of dust is pushed into the brush using a piston, the speed of the piston determines the rate of dust injection. Compressed air is used to convey the particles that have been aerosolised by the brush into the test rig, the compressed air is regulated allowing the flow rate of air to be controlled.

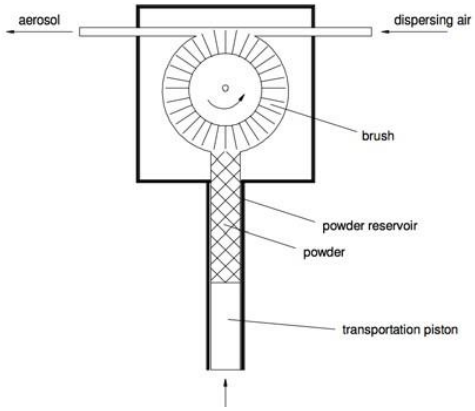

Figure 3.27- Schematic of rotating brush generator.

Figure 3.28- Palas rotating brush generator.

Particle counting and sizing will be performed using the Welas digital 3000 light scattering spectrometer system, manufactured by Palas GmbH, Figure 3.29. The Welas system comprises of the main detector coupled with remote sensors, the sensors are connected by fibre optic cables. The detection principle of the Welas 3000 is white light scatter, the Welas 3000 is compatible with a selection of detectors; each detector is suitable for a specific concentration range.

Figure 3.29- Welas digital 2000 (bottom) with detector (top).

3.2 Methods

The methodology used throughout this work is described in this section. First there is an explanation of the procedure used for lapping and a presentation of the experimental protocols for bottom and top lapping. Secondly, an outline of two methods for imaging analysis, using the Image Pro Premier software. Then, methods for permeability tests and study of pore geometry are described. Finally, the way that the company, Porometer, conducted their experimental tests are explained.

3.2.1 How to do Lapping

The experimental procedure for the lapping process will now be detailed. There were made 3 replicas for each experiment. The lapping procedure was divided into three steps: preparation for lapping, lapping, and characterisation of the samples. Figure 3.30 is a flowchart summarising the three stages of the lapping procedure conducted in this work.

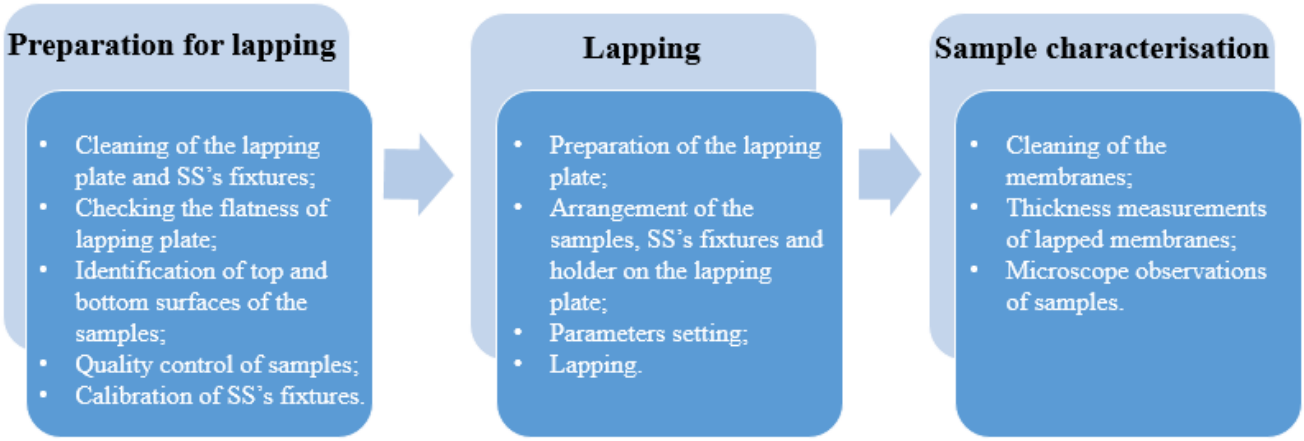

Figure 3.30- Summary of the experimental procedure for lapping, divided into three steps.

- **Preparation for lapping**

In order to make sure the lapping results are reliable, there is the need to prepare all the devices used before lapping. The cleaning, calibration and quality control of some equipments and materials used during this process will now be described.

Cleaning of the lapping plate and SS's fixtures:

Initially the top protection is taken out and the equipment switched ON. To clean the lapping plate, jets of the cleaning fluid are applied to its surface. A speed level of 7 and time of 60s are set. Then, the rotation of the plate is initiated and paper tissue is pressed onto the plate whilst it rotates, as shown in Figure 3.31. The ceramic surfaces of the three SS's fixtures are also cleaned with paper tissue and cleaning fluid.

Figure 3.31- Cleaning of the lapping plate.

Checking the flatness of lapping plate:

The flatness gauge is placed on top of the metal piece inside the device's box. The zero point, explained on section 3.1.1.3, is then known. Two measurements of the lapping plate are taken, by placing the calibration device on top of it in two different positions, but always without any support on the grooves. Both zero point and the measurements of the lapping plate are noted. The plate is considered flat if the gauge's reading is between the zero point and 90 to its left. If the plate is out of calibration, the conditioning ring is used to calibrate the flatness of the plate.

Identification of top and bottom surfaces of the samples:

The top and bottom surfaces of the samples were identified, which are previously defined on section 3.1.1.1, by visual observation in front of a light. In order to be easier to distinguish them, a number is written on the top surface. 1, 2 or 3 is written according to the number of the replica and the SS's fixture used.

Quality control of samples:

Each membrane was seen in front of a light in order to be possible to detect their defects. Membranes with air bubbles, thicker edges, and spots were discarded, even though they had the required measurements. The IDs of the chosen membranes were noted.

Calibration of SS's fixtures:

The components and terms used related to the SS's fixtures are explained in section 3.1.1.6. The ceramic surface of the SS's fixture is raised due to the rotation of the micrometer to higher values. The fixture is then placed on top of a flat surface (Figure 3.32).

Figure 3.32- SS's fixture on top of a flat surface with ceramic surface raised.

It is then discovered the calibration point of the ceramic surface by lowering it until it touches the flat surface. This is done towards a light in order to be possible to see if the ceramic ring rises. If the ceramic ring rises, it means that the ceramic surface's calibration point was passed.

The micrometer is then rotated in order for the ceramic surface of the fixture to rise. Sample is placed on top of flat surface and then the correspondent SS's fixture is placed on top with the sample at the center of the ceramic surface of the fixture (Figure 3.33).

Figure 3.33- Placing the sample and the SS's fixture on top of the flat surface.

Finally, the calibration point of the sample is discovered by lowering the micrometer readings until the ceramic surface touches the sample. The sample calibration point corresponds to 0µm of cut thickness. This is done towards a light in order to see if the ceramic ring rises. If it does, it means that the sample's calibration point was passed. If the calibration point is passed, the ceramic surface is raised all the way up and then lowered again until the calibration point is reached. Once the calibration point of the sample is set, the micrometer is never rotated back, only forwards. Both calibration points are noted. This procedure was replicated for each of the fixtures.

- **Lapping**

Preparation of the lapping plate:

Started the rotation of the lapping plate. Stirred the diamond liquid, making sure there was no sediment in the bottle. Distributed evenly 6 sprays of the 9µm diamond particle liquid on the lapping plate. Placed one SS´s fixture on top of the lapping plate and pushed it to the outside and inside edges of the lapping plate whilst it rotates, in order to spread the diamond liquid evenly. This is only done when the plate is totally dry, which means the first time the lapping plate was used each day.

Arrangement of the samples, SS's fixtures and holder on the lapping plate:

Three samples are placed on the lapping plate in a triangular shape, with their surface to lap down, touching the lapping plate. Then the SS´s fixtures are disposed on top of the corresponding samples carefully, trying to center the samples on the ceramic surface of the fixtures. If lapping less than three samples at a time, all 3 fixtures were placed on the plate without samples. The holder is embedded carefully in the fixtures. For top lapping, three sponges have to be also placed between fixtures. The holder is pushed until it touches two black rubber wheels. Figure 3.34 represents the arrangement for top lapping.

Figure 3.34- SS's fixtures, holder and sponges arrangement for top lapping.

Parameters setting:

In order to set the cut thickness, SS´s fixtures' micrometer is rotated to lower values, reducing the ceramic surface height. The number of splits depends on the desired cut thickness, knowing that one split equals 25µm of cut thickness. Time is set in seconds on the lapping equipment's control panel. Rotation speed is set at seven on the lapping plate control panel. Particle diamond size used was 9µm.

Lapping:

Plate rotation is started. If the holder didn't start to rotate in the same direction as the lapping plate, or stopped, paper is used to clean the outside edge of the plate. The use of diamond liquid was controlled by the dryness of the plate. If light wasn't reflecting on the plate, one spray of liquid would be applied to the inner edge of the plate, making always sure the bottle was stirred before, without sediments.

When the time set is over, and the lapping plate stops rotating, the holder is taken out. Each SS´s fixture at a time is lifted and turned upside down, in order to take out the samples. Ceramic surfaces of the fixtures were cleaned using paper tissue and cleaning liquid.

- **Sample characterisation**

Cleaning of the membranes:

Samples are placed and cleaned in the ultrasonic bath for about 60s. Lapped membranes are then dried on paper towels.

Thickness measurements of lapped membranes:

There were taken 5 thickness measurements of the lapped samples with the ratchet speeder of the micrometer, including 4 edges and the center of the samples. The tip surface of the micrometer was cleaned and calibrated between samples measurements. Notes were taken of the thickness measurements.

Microscope observations of samples:

There were observed lapped surfaces on the optical microscope. For bottom and top surface observations, 10x and 40x lenses were used, respectively with the bottom light of the microscope. 5 pictures of each sample were taken, including 4 edges and the center, having an overall view of the membrane's surface.

3.2.1.1 Experimental Protocols for Lapping of Bottom Surface

Diamond particle size, rotation speed of the lapping plate, time and cut thickness are the parameters considered on this lapping study. Rotation speed, diamond particle size and cut thickness were set at level 7, 9µm and 150µm, respectively, for every experiment on the bottom surface, while time was varied.

While lapping the bottom surface, the influence of time in material removal was studied. In order to do this, bottom lapping was performed, and repeated a number of times, on the same three samples, depending on the duration of lapping. Figure 3.35 represents the

experimental protocol conducted for bottom surface indicating the 3 implemented steps, and a table with lapping parameters and number of repetitions of the last 2 steps.

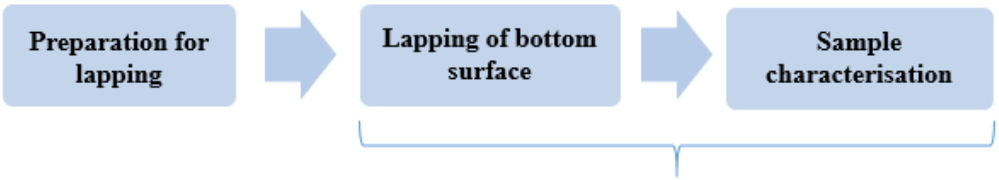

Cut thickness (µm)	Time (s)	N° repeats
150	10	12
	20	10
	30	8
	40	6
	50	5
	60	4

Figure 3.35- The 3 steps and parameters of the experimental protocol for bottom lapping.

Initially, the first step, previously described on section 3.2.1, was conducted. Then, lapping of the bottom surface of three samples with their bottom surface facing down was performed. Cut thickness was set at 150µm on the first run of lapping, and was never changed on the following repetitions. After lapping, the samples are characterised. The lapping and characterisation steps were repeated on the same samples several times, depending on the lapping duration. For example, when lapping is performed for 10s, lapping and sample characterisation steps are repeated 12 times. This means that each of the three samples will be lapped 12 times for 10s making a total of 120s. After each run of lapping, thickness measurements and pictures were taken.

3.2.1.2 Experimental Protocols for Lapping of Top Surface

On this lapping study 4 parameters were considered: diamond particle size, rotation speed of the lapping plate, time and cut thickness. The last two parameters were studied, in order to study their influence on the lapping process. Rotation speed and diamond particle size were set at 7 and 9µm, respectively.

During the lapping of the top surface the influence of cut thickness in material removal and how long it would take to remove a certain amount of material was studied. In order to do this, cut thickness was set at 25 and 50µm and several lapping durations were performed. Figure 3.36 represents the 7 steps and parameters of the experimental protocol for top lapping.

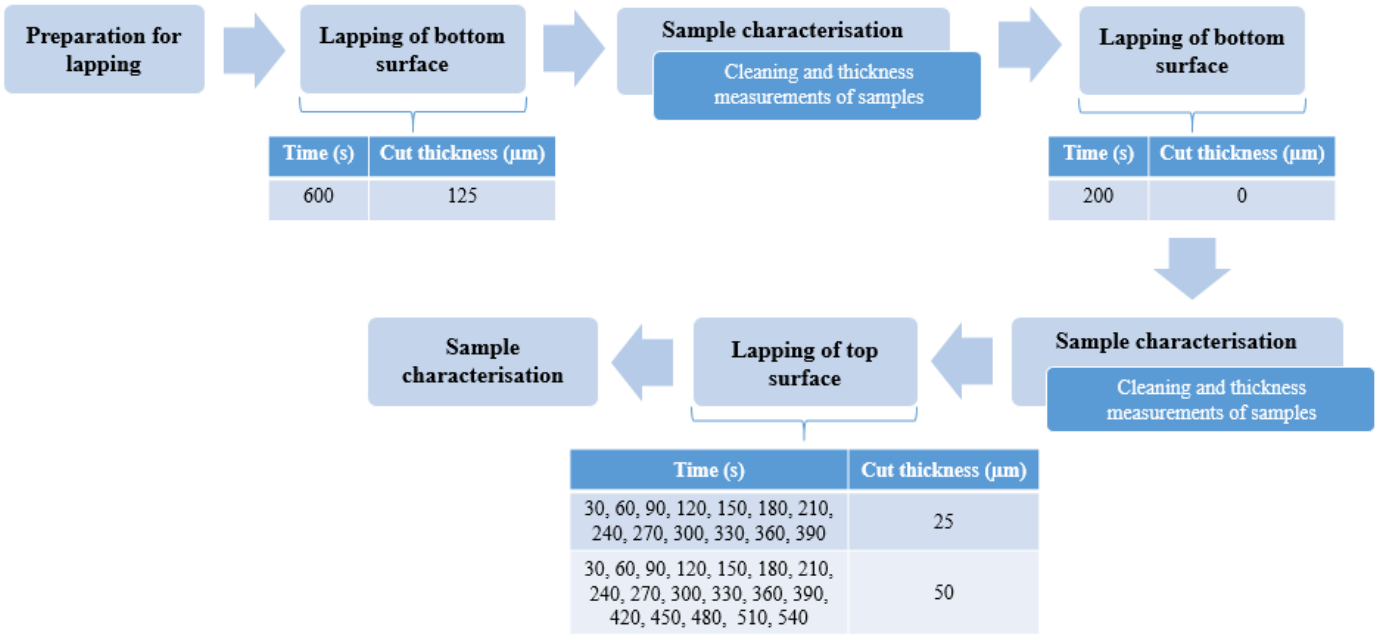

Figure 3.36- The 7 steps and parameters of the experimental protocol for top lapping.

Preparation for lapping is the first step of top lapping. Before lapping of the top surface can be done, 125µm of material is removed from the bottom surface. Therefore, bottom lapping is performed for 600s with 125µm of cut thickness. After that, thickness measurements were taken, in order to see the amount of material removed. Since only the top surface is to be studied, pictures were not taken after bottom lapping. In order to guarantee that all the cut thickness was removed and the sample surface is aligned with the ceramic ring, the bottom surface was again lapped for 200s, without changing the micrometer position. Thickness measurements were again taken in order to guarantee that no more material was removed, proving that the sample is perfectly aligned with the ceramic ring of the fixture. After the 2 steps of bottom lapping and their characterisation, top lapping was performed with different parameters for each set of three samples. After top lapping, samples were characterised, the thicknesses were measured and pictures were taken.

3.2.2 How to use Image Pro Premier

The effect of lapping on Smart Separations's membranes was studied by analysing the photos taken of each sample after bottom and top lapping. Photos were analysed by Image Pro Premier 9.1, allowing the collection of pores' results such as area, circularity, percent area, and minimum, maximum and mean diameter.

The analysis of the pores is done by the selection of the grey levels of the image. The contrast between the pores and the membrane is important in order to select only the pores and therefore obtain accurate results. The results given by the software are calculated by the number

of pixels of each pore. Individual results of each pore, as well as statistic results are collected, although only mean values of each results were used for this study.

A standard operating procedure for the use of Image Pro Premier was completed.

3.2.2.1 Bottom Surface Analysis

After bottom lapping, 5 pictures were taken with an optical microscope using lens 10x of each sample in order to have results of the overall surface. The 5 images of the same sample are opened as a sequence and analysed. A macro was performed to analyse the sequences of images.

The first step on the macro is to improve the background of the images by subtracting the bright background. Follows the calibration of the images and the selection of the threshold from 225 to 255. Results of each image are collected in an excel spreadsheet and then an average of the results of each image is calculated.

Only pores with an area bigger than 10 pixels were considered, in order to avoid misleading results.

3.2.2.2 Top Surface Analysis

Pictures were taken of the top surface of the samples after top lapping with an optical microscope using lens 40x. Only results from one image of each sample were analysed. Since the pores on the top surface are smaller, only pores bigger than 3 pixels were considered. The selection of the grey levels was done manually due to the grey variations of the images, and the low contrast between pores and membrane.

3.2.3 Permeability Tests

Permeability tests of Smart Separations's membranes were conducted. The experimental setup was previously explain in section 3.1.2.3. The method used for these tests is based on what is explained in section 2.4.3.2.

The membrane outlet pressure is atmospheric while the inlet was increased 0,1 bar at a time from 1 to 2 bar creating a pressure difference. The valve is opened until the sensor measures the desired pressure, air goes through the membranes, while the cylinder full of water is placed on top of the air outlet and the time it takes to empty the 2L cylinder is counted with a stop watch. It's then possible to calculate flow and flux values. The volumetric permeate flux ($m^3.m^{-2}.s^{-1}$) is the volume of permeate (m^3), that goes through the membrane with a certain area (m^2) for a period of time (s) (Charcosset 2012).

3.2.4 Pore Geometry

It is possible to study the geometry of the pores through the values of mean pore size, material removal and thickness of the membranes. To determine the angle of the conical pores, the following methodology was employed (Figure 3.37).

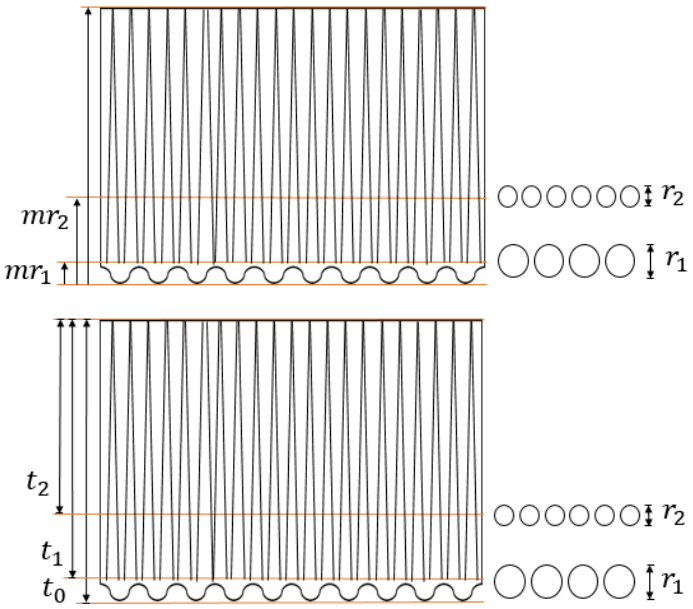

Figure 3.37- Representation of the conical pores of the Smart Separations's membranes. mr-material removal; t-thickness of the membrane; r- pore size.

In order to do this, values of mean pore size were plotted against material removal and thickness. A linear regression is then applied to these results (Figure 3.38).

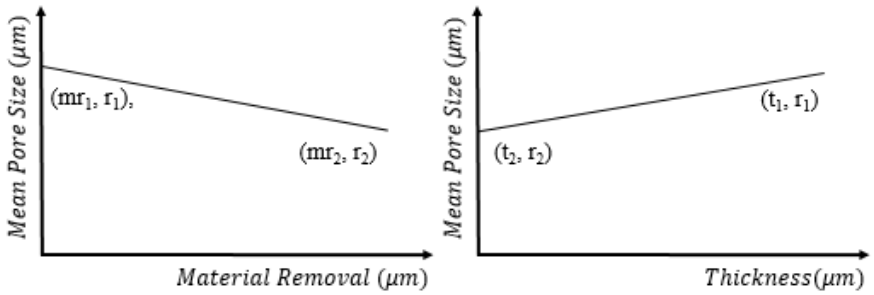

Figure 3.38- Linear regression of the values of mean pore size against material removal and thickness.

With the linear regression equation, it is possible to calculate two points, which correspond to the values (mr_1, r_1), (mr_2, r_2) or (t_1, r_1), (t_2, r_2), where *mr* is the material removal, *t* is the thickness of the membrane and *r* is the mean pore size in Figures 3.37, 3.38 and 3.39. The angle is calculated by:

$$\alpha = \tan^{-1} \frac{mr_2 - mr_1}{\frac{r_1 - r_2}{2}} \qquad (Eq.\,3.1)$$

$$\alpha = \tan^{-1} \frac{t_2 - t_1}{\frac{r_1 - r_2}{2}} \qquad (Eq.\,3.2)$$

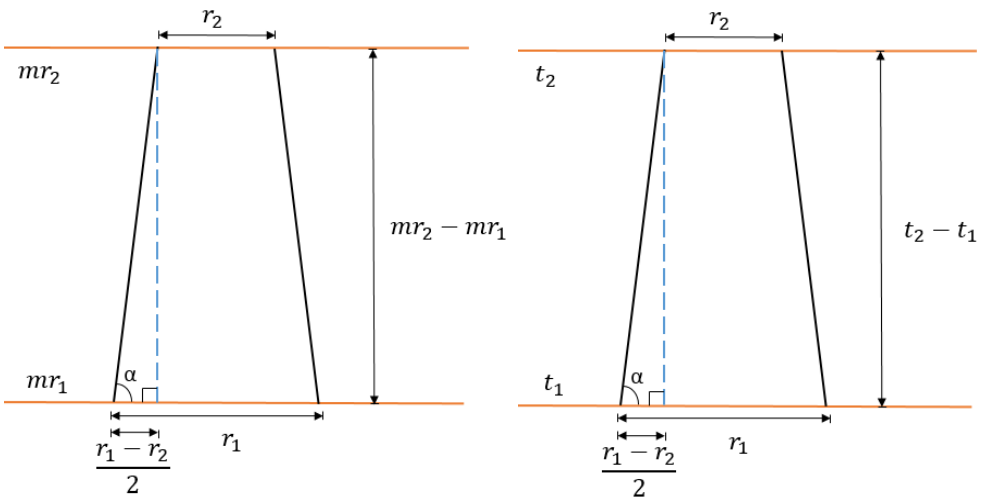

Figure 3.39- Schematic of the pore's angle, and the measurements to its calculation.

3.2.5 Porometer

Three bubble point porometry tests were carried out for each supplied sample based on the pressure step/stability method. First bubble point was measured by using a flow rate of 7 ml/min and a deviation of 30%. The wetting liquid was porefil, with a surface tension of 16 dyn/cm. Three gas permeability tests were also carried out for each sample, using air and a target pressure of 0.5 bar. The samples were tested first gas permeability and then porometry measurements.

Bubble point method measures pore size and pore size distribution information of through pores with good accuracy and reproducibility in one individual and fast measurement. The technique is based on the displacement of an inert and non-toxic wetting liquid embedded in the porous network of a material by applying an inert pressurised gas (e.g. nitrogen), wet run. The "wet curve" represents the measured gas flow against the applied pressure. The gas flow against the applied pressure on the dry sample ("dry run") is also measured. The "half-dry curve" is obtained by dividing the flow values of the dry curve by 2 and it is also plotted against the applied pressure in the same graphic. Information about the porous network can be obtained from data these three curves (Figure 3.40).

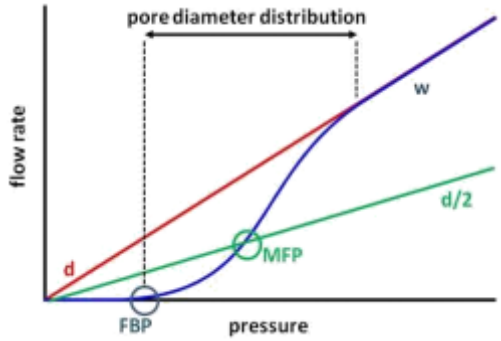

Figure 3.40- Measuring curves and resulting parameters in CFP, where d = dry curve; w = wet curve; d/2 = half-dry curve; FBP = largest pore and MFP = mean flow pore.

The mean flow pore is calculated at the pressure where the wet and the half-dry curves meet and it is the pore size at which 50% of the total gas flow can be accounted. The minimum pore size is calculated at the pressure at which the wet and the dry curve meet, from this point onwards the flow will be the same because all the pores have been emptied.

As explained in section 2.4.1.1 pore sizes can be obtained using the Laplace equation (Eq. 2.1). Furthermore, it is possible to obtain the cumulative filter flow distribution against the pore size and the corrected differential filter flow, which shows the pore size distribution.

The pressure/step stability method was used to take the measurements. A data point is only recorded when the stability algorithms are met for both pressure and flow, which means that the porometer detects when a pore empties at a certain pressure and waits until all pores of the same diameter have been completely emptied before accepting a data point. This is confirmed by measuring a stable gas flow before increasing the pressure to the next value, Figure 3.41.

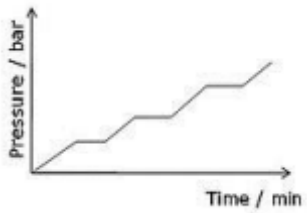

Figure 3.41- Graph of the pressure/step stability method.

3.2.6 Particle Technology dust-load test

A dust rejection efficiency test was performed according to the following method:

1. RBG dust feeder and particle counting detectors are calibrated prior to use;
2. All elements of the feeding system that come into contact with dust are cleaned and weighed;
3. The mass of dust loaded into the cylinder is measured and recorded;
4. The RBG dust feeder accurately reports the volume of the cylinder that has been loaded (diameter is constant; the length is known by the feeder);
5. The packed dust density is calculated;
6. The piston rate can be set (mm/min) to give required dust feed rate (mg/min).
7. At the conclusion of the test remaining dust is weighed and recorded;
8. The elements of the feeding system that come into contact with the test dust are weighed and compared with starting mass.

The Palas/Welas particle counter system measures the concentration, number and size of particles present. The samplers record data from the upstream (bulk) and downstream (after the inlet) locations, the results of which were compared and a fractional efficiency curve was generated.

The duration of these measurements were dependent on each test, however they typically consisted of 3 minute measurements taken upstream then downstream. The fractional efficiency was determined by the Palas/Welas particle counters, which measured the challenge aerosol and produced live results throughout the testing. The equation used to determine the collection efficiency relied on the comparison between the upstream particle counts against the downstream results, and is given below.

$$Fractional\ Efficiency\ (\%) = 100 - \left(\left(\frac{Downstream\ Particle\ Concentration}{Upstream\ Particle\ Concentration}\right) * 100\right) \quad (Eq. 3.3)$$

For the purpose of comparison, an "off the shelf" filter supplied by Sterlitech (MCE Membrane Filters, 0.8µm pore size) was also tested. The procedure for both tests was consistent throughout.

1. The filter under test is inserted into its housing. The Welas sensors are calibrated and are connected to the upstream / downstream sensor points.
2. The vacuum pump is turned on and the control valves are set to restrict flow to its minimum. As the flow rate is increased to set points, the differential pressure over the test filter is recorded in order to determine the initial pressure drop profile.
3. The selected dust feeder is then calibrated so that the injection rate of the challenge aerosol is correct for the required concentration.
4. Once the flow rate has been determined to be stable the test is then started, with the initiation of the dust feeder.
5. Measurements from the required instrumentation are then taken at 10 minute intervals. The system fan is adjusted accordingly to maintain stable air flow throughout the test.
6. At the conclusion of the test; the dust feeder, particle counters and vacuum pump were stopped.

4

RESULTS AND DISCUSSION

4.1 Lapping

The understanding of the lapping process variables is required, because they independently and collectively control the uniformity and material removal rate. The variables studied are time and cut thickness.

The initial step of lapping is to determine and set the bottom lapping conditions in order to have the maximum percentage of open pores with the minimal material removal possible and minimum time. The next step is to control the top pore size. There is the need to set the conditions for a required pore size.

4.1.1 Lapping of the Bottom Surface

4.1.1.1 Objetive

On the bottom surface the goal is to achieve the maximum percentage of open pores with the minimum material removal possible in minimum time. The influence of time in material removal was studied. Therefore, as explained in section 3.2.1.1, different repetitions of time intervals were conducted. Since the cut thickness had to be set at 150µm for all samples and their thickness varies, the calibration of the ceramic surface of the SS's fixtures was needed.

4.1.1.2 Results

Increasing the percentage of open pores the flux is raised, which is one of the most important factors during filtration. The minimal material removal is due to the fact that as lapping is conducted material is removed and consequently the thickness of the membrane decreases. The thinner the membranes are, weaker they became. Since this is a comparative and not quantitative analysis, open pores percentage was considered in order to minimise the error associated with Image Pro Premier since it doesn't always detect all pores. The percentage of open pores was calculated considering 100% of open pores as the maximum porosity achieved.

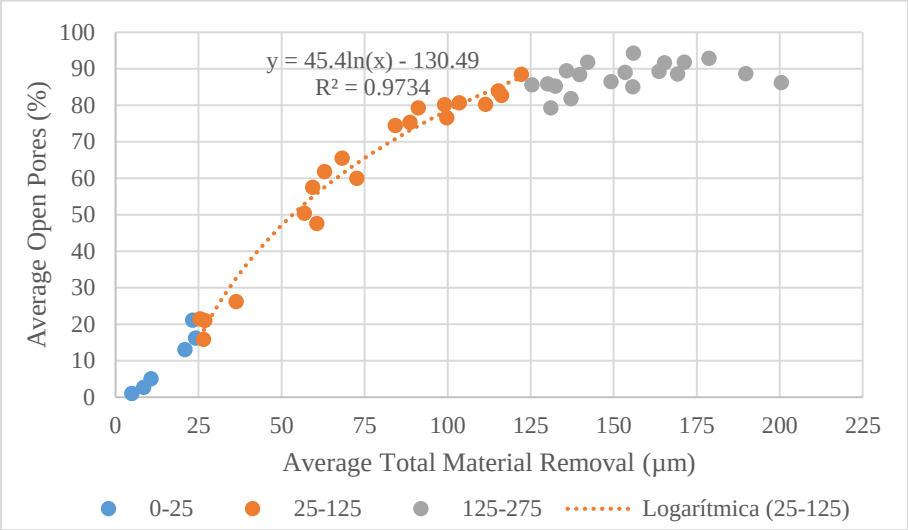

Figure 4.1- Evolution of open pores percentage with material removal.

From Figure 4.1 it is possible to observe that the % of open pores increases with material removal in three phases. From 0 to 25µm of material removal the % of open pores increases drastically from 0 to around 20%, from 25 to 125µm there is a logarithmic increment, and 125µm onwards the % of open pores stabilises. 125µm is the optimal amount of material that has to be removed from the bottom surface to obtain a maximum % of open pores of 89%.

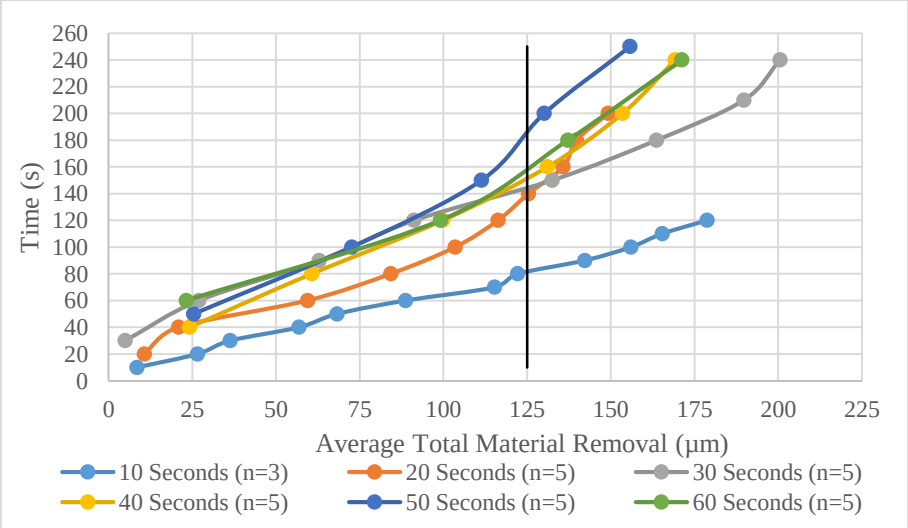

Figure 4.2- Different time intervals to remove 125µm from the bottom surface.

The minimum time required to remove at least 125µm from the bottom surface is 90s, 9 times lapping for 10s, as it is possible to observe in Figure 4.2. It also shows that short time intervals remove material quicker. This is possibly due to the accumulation of removed material on the samples and lapping plate which causes less contact between samples and the diamond particles on the plate. It also shows that the cleaning of the samples, fixtures and plate between each run of lapping has a great impact on material removal.

Table 4.1 summarises the number of repetitions of each lapping duration and times to remove at least 125µm.

Table 4.1- Time to remove at least 125µm from the bottom surface.

Total Material Removal (µm)	142	125	132	131	130	137
Repetition	9·10s	7·20s	5·30s	4·40s	4·50s	3·60s
Time (s)	90	140	150	160	200	180

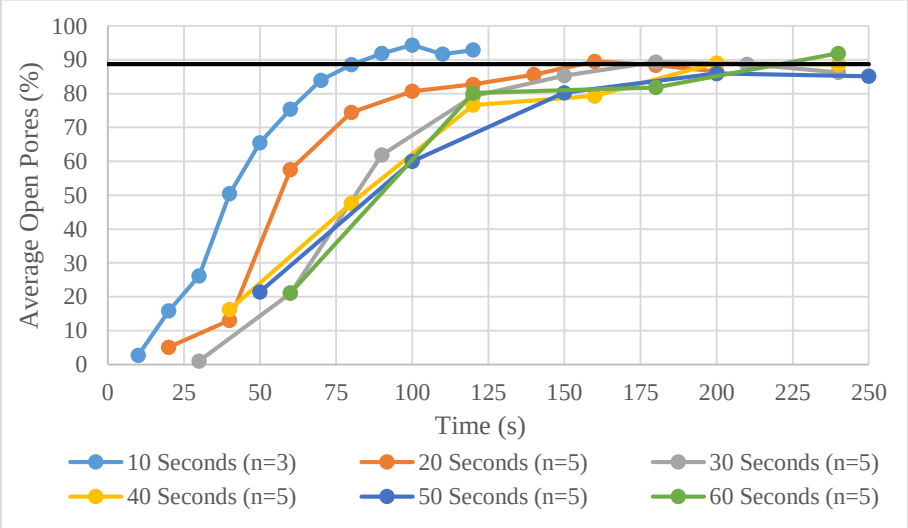

Figure 4.3- Different time intervals to obtain 89% open pores.

Table 4.2- Time to obtain at least 89% open pores.

Open Pores (%)	92	90	89	89	92
Repetition	9·10s	8·20s	6·30s	5·40s	4·60s
Time (s)	90	160	180	200	240

9 repetitions of bottom lapping for 10s produce the required percentage of open pores and, Figure 4.3, and as seen before, removes more than the required amount of material. However to obtain the required percentage of open pores for the other time intervals, one more run of lapping is needed to achieve the requires % of open pores. The time interval of 50s overreaches the required percentage of open pores, which means that probably more material was removed than the optimal thickness for % of open pores. And as the pores are conical once this point is passed, the porosity decreases.

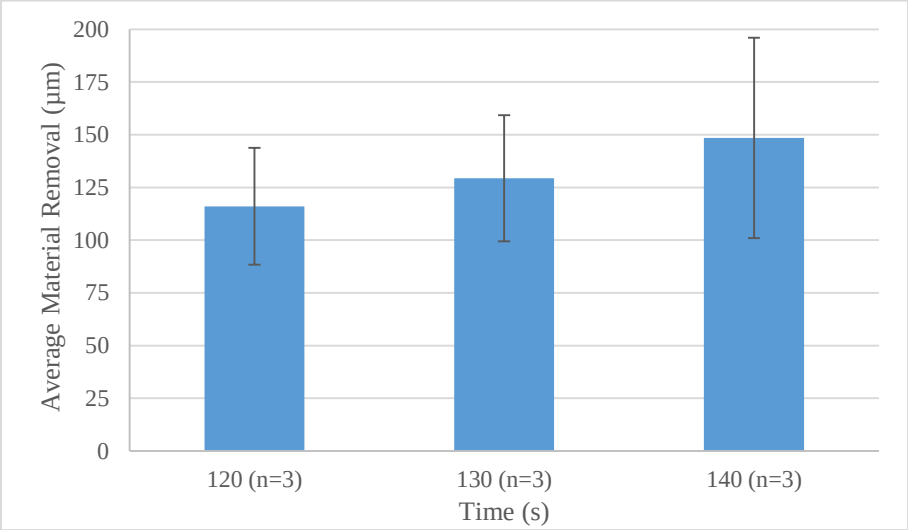

Figure 4.4- Time to remove 125µm in one run of lapping with the heavy holder.

Since lapping is a manufacturing step of Smart Separations's membranes, it is need to determine the time to remove 125µm in one run. Figure 4.4 shows that 130s is the optimum time to remove 125µm with the heavy/metal holder. If the time to remove 125µm wanted to be reduced using lapping variables, it would be expected that it could be achieved by increasing the diamond particle size or increasing the plate's rotation speed. The rate of material removal also depends on the amount of diamond slurry on the plate, if too much slurry if applied the membranes will aquaplane and therefore no material will be removed. Although if too little slurry is applied the material will be removed faster, and if the plate gets too dry the friction increases and membranes may break.

All of the above results are an average of 3 or 5 samples, the plots with the error bars are present in Appendix A. These experiments have some errors associated. The non-uniform material removal on each membrane is due to the error associated with the flatness of the lapping plate and the ceramic surface of the three SS's fixtures. As present in Appendix B the flatness of the plate reaches a maximum error of 5µm per membrane, and the measurements of the ceramic surface's depth has a maximum standard deviation of 4.6µm. Another factor that could be related to the non-systematic material removal is the weight of the holder and the fixtures in conjunction with the rotation of the lapping plate. The weight of the holder and the friction between the plate and the fixtures/membranes whilst the plate rotates can make the fixtures slightly tilt and consequently remove more material in one side of the membrane than the other.

The variation of material removals between membranes with the same lapping conditions is afflicted to the position of the fixtures' micrometer that has a resolution of 25µm. With the help of the depth micrometer is was also detected that sometimes the ceramic surface of the fixtures after lapping was lower than it was set before lapping, which means that the cut

thickness was higher than it was set. This justifies the material removal reaching 200µm when it was expected to only reach a maximum of 150µm since that was the set cut thickness in Figure 4.2.

4.1.2 Lapping of the Top Surface

4.1.2.1 Objetive

Since filtration takes place on the top surface, it's very important to control top pore sizes. Therefore, the aim of the top lapping experiments is to determine the lapping conditions to obtain a required pore size.

During lapping of the top surface the influence of cut thickness in material removal was studied. The time to remove a certain amount of material and the respective pore size was also studied. Therefore, as explained in section 3.2.1.2, the cut thickness was set at 25 or 50µm and several lapping durations were performed.

In order to minimise the error associated with of the bottom surface roughness, thicker edges, and the cut thickness applied to the top surface, a calibration of the bottom surface is required. As it was before concluded, 125µm have to be removed from the bottom in order to have 89% of open pores. 125µm of cut thickness is applied in order to remove them, and then another run with the same cut thickness to make sure that no more material was removed, and therefore the bottom surface of the sample is aligned with the ceramic ring of the fixture. The sample is then flipped and the top surface is aligned with the ceramic ring.

4.1.2.2 Trial

In order to be possible to have a better control of the material removal, a lighter holder was used, since the weight of the holder is on the fixtures, and consequently on the samples. With the lighter holder less pressure is applied on the samples, and consequently slower material removal.

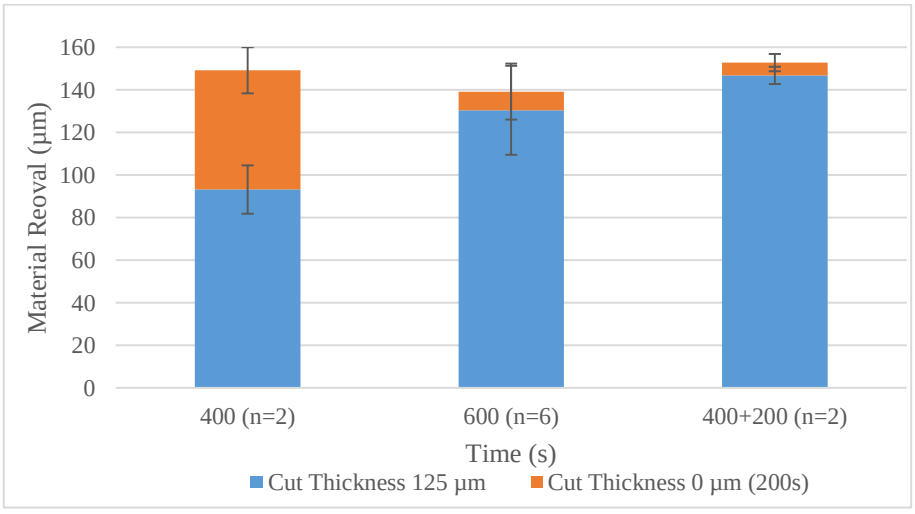

Figure 4.5- Determination of time to remove 125µm in one run using lighter holder.

Top lapping for 400s only removes 90µm and therefore a second lapping run still removes a significant amount of material. As expected, Figure 4.2, 400+200s removes material quicker than 600s, although it removes more than 125µm even with the same cut thickness. This shows that material is still removed even if the cut thickness is achieved, although the removal is slow. As shown in Figure 4.5 the ideal time to remove 125µm from the bottom surface with the lighter holder is 600s.

Lapping was conducted on 12 samples for 600s with a cut thickness of 125µm, Figure 4.6. The material removed was between 101-155µm. Then lapping was again conducted for 200s without changing the micrometer, in order to see if when the sample is aligned with the ceramic ring, no material would be removed. The material removed with 0 cut thickness was between 0 and 23µm.

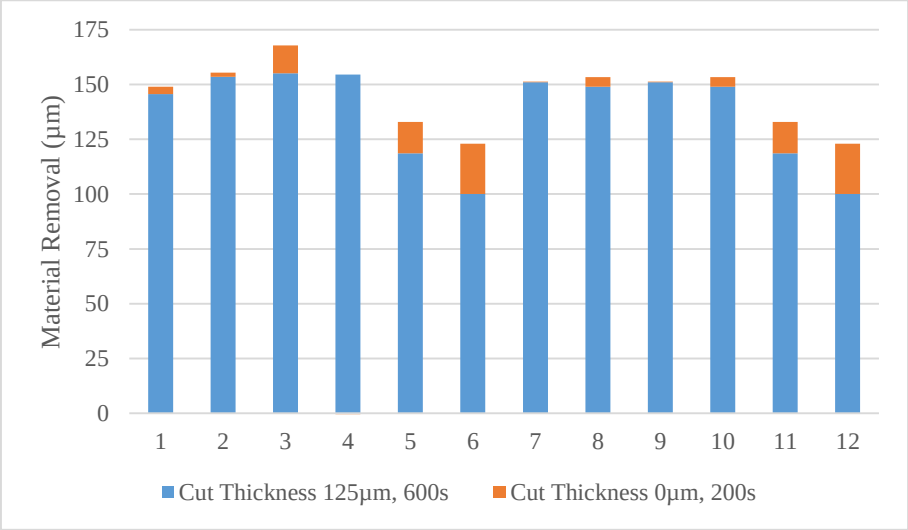

Figure 4.6- Influence of a cut thickness of 125µm on material removal.

For a more accurate study a cut thickness of 25µm was applied. As shown in Figure 4.7, material removal was always below 35µm and in the second lapping run with 0 cut thickness the material removal was below 12 and negative values (strips bars).

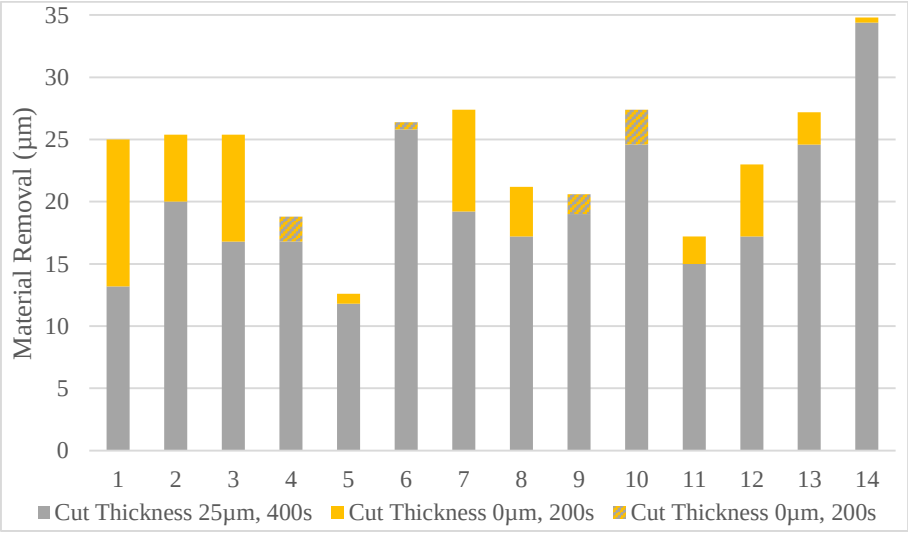

Figure 4.7- Influence of a cut thickness of 25µm on material removal.

These two experiments show that the cut thickness controls material removal, and the variability between the cut thickness and material removal is related to the errors associated with these experiments. Since the fixtures' micrometers are set manually some errors are associated with it. Figure 4.6 shows the error associated with the micrometer is ±25µm, which would be expected since that's its resolution. There is also an error associated with the thickness measurements, since membranes don't have the same thickness through the whole surface and an average of 5 measurements were used, justifying the negative values. In conclusion, when part of the samples is out of the ring's alignment (cut thickness), there is a fast stock removal, and when the membrane is on the edge or below the ceramic ring of the fixture there is slow stock removal. However, after the desired cut thickness has been reached, stock removal should be even slower than it presently is. This can be explained due to the lapping plate being harder than the membrane, and therefore, diamond particles don't become embedded in the lapping plate, not performing fine grinding, only hard plate lapping by the loose rolling free particles on the plate also causing the abrasive to charge the work piece.

4.1.2.1 Results

Figure 4.8 shows the material removed with a cut thickness of 25 and 50µm for different periods of time. It is observed that material is removed quicker with higher cut thickness. Due to the variance of the results it is difficult to determine the exact correlation between time and material removal. However the purposes of the lapping SOP it was considered that to remove around 20µm, lapping has to be conducted for 390s with 25µm of cut thickness, and to remove 50µm, membranes have to be lapped for 540s with 50µm of cut thickness. In order to collect data with less variability, the accuracy of the fixtures' micrometer has to be improved, as well as a systematic control of amount of slurry applied to the plate.

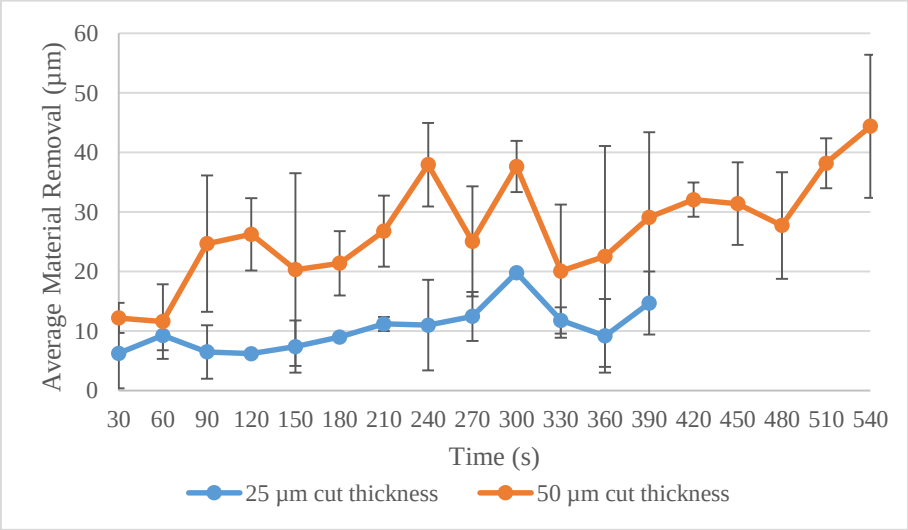

Figure 4.8- Time to remove a certain amount of material from the top surface with cut thickness of 25 or 50µm.

One image from each sample was analysed by Image Pro Premier and the results were plotted against material removal, Figure 4.9. These results aren't very accurate because only one image per sample was studied, and since the taken photos are hard to analyse due to bad image quality (low contrast between the pores and membrane), the program can't detect small pores. Therefore photos with the biggest pores were selected. Furthermore, pore sizes may vary across the sample's surface. Figure 4.9 also shows the mean pore size results from Porometer, using the bubble point method. It is possible to conclude that as the material removal increases also does the mean pore size, as expected. However, this relation is not linear. Comparing the two results is possible to observe that the mean pore sizes given by Porometer are smaller. It is important to notice that Porometer results assume cylindrical pores and pore sizes results are given even if there's only few pores opened.

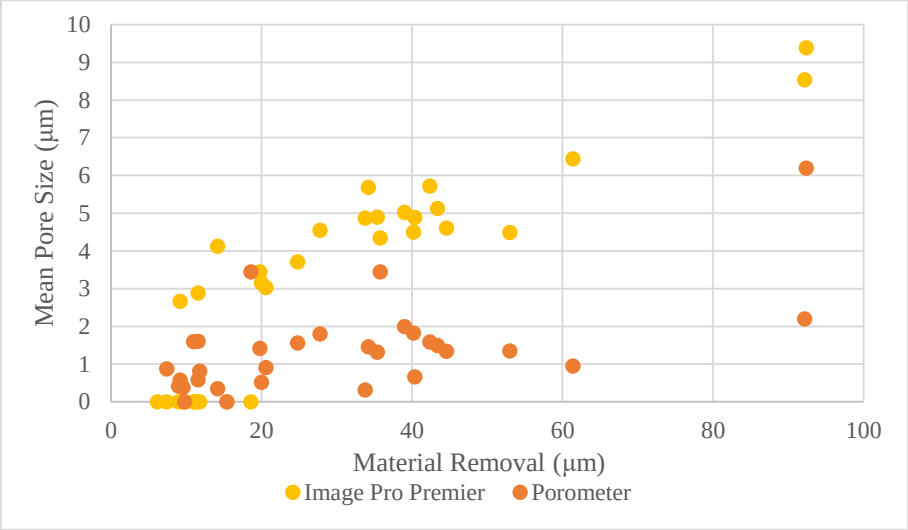

Figure 4.9- Relation between material removal and mean pore size using Image Pro Premier and Porometer results.

With the results from the bottom and top lapping was possible to create a standard operating procedure for lapping. The SOP includes the lapping procedure and the lapping conditions to obtain the highest porosity possible in the bottom surface and the conditions to obtain a certain pore size on the top surface.

A further study on the pose sizes was conducted using SEM pictures of some of the studied samples. The following table 4.3 presents the different pore sizes calculated, Porometer's results, and the correspondent material removal from both surfaces.

Table 4.3- Mean pore sizes calculated by different methods and lapping removals.

	Lapping		Optical Microscope	SEM	Porometer
	Material Removal Top (µm)	Material Removal Bottom (µm)	Mean Pore Size (µm)	Mean Pore Size (µm)	Mean Pore Size (µm)
D17B03S18	6	175	0	Pattern	-
D17B03S21	12	175	0	Pattern	0.8
D17B03S30	19	135	0	Anomaly	3.5
D17B03S32	14	155	4.1	Pattern	0.4
D18B02S06	10	137	0	0	0.4
D18B02S10	15	140	0	1.8	-
D18B02S22	9	108	2.7	1.9	0.6
D18B02S34	28	119	4.6	1.5	1.8
D18B02S48	36	129	4.4	2.5	3.5
D18B03S04	34	124	4.9	3.0	0.3
D18B03S07	39	133	5.0	2.1	2.0

The above table shows that results differ from method to method. While Porometer analyses the whole membrane, microscopic methods only study one photo per membrane, selecting and limiting the considered area. The results variance is due to non-uniform lapping and consequently different pore sizes in different area of the membranes, as it possible to observe in the following SEM photos and consequently in Figure 4.21 with pore sizes distributions. Membrane D18B3S4 and D18B3S7 have the best and worst pore size distribution, with more than 90% of flow at 0.3µm and 9% at 0.6 µm, respectively, although this results were not confirmed by SEM, most likely because of the area selected to analyse. D17B03S18, S21 and S32 only have a few pores opened, therefore for the optical microscope analysis it was considered that there were no pores opened. As it's possible to confirm in SEM pictures, only a few pores are opened and present a certain pattern, however Porometer still calculated a pore size. D17B3S30 presents big random pores (3.5µm) which may be air bubbles.

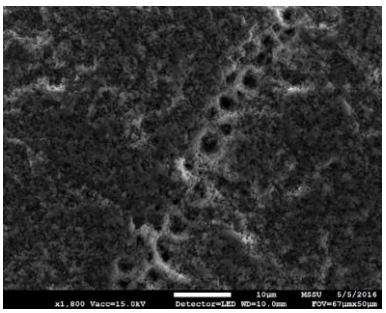

Figure 4.10- D17B03S18- Pattern.

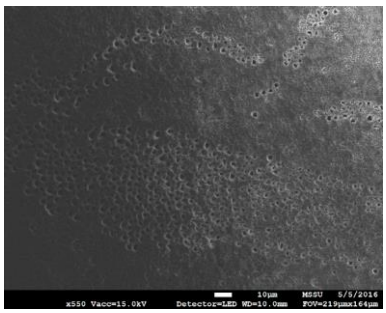

Figure 4.11- D17B03S21- Pattern.

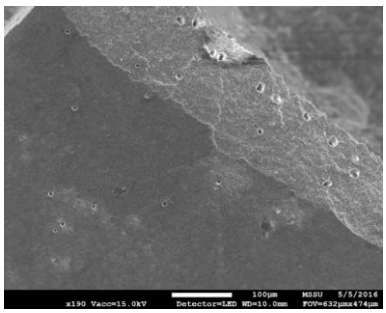

Figure 4.12- D17B03S30- Anomaly.

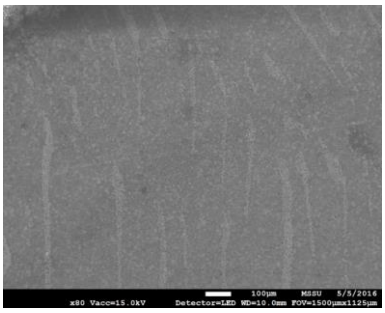

Figure 4.13- D17B03S32- Pattern.

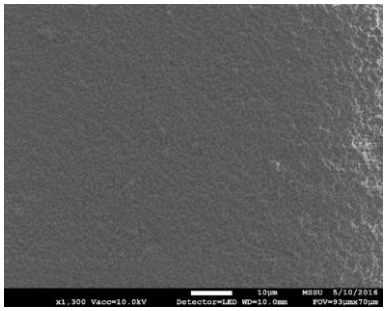

Figure 4.14- D18B02S06- No pores.

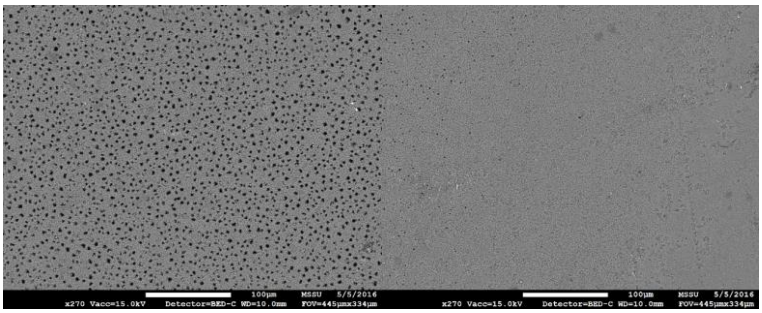

Figure 4.15- D18B02S10- 1.8µm not uniformly lapped.

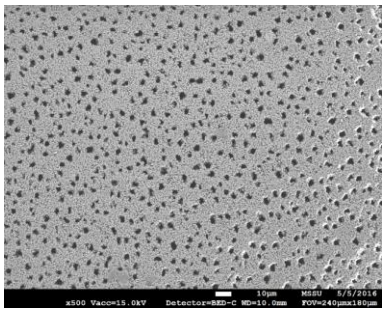

Figure 4.16- D18B02S22- 1.9µm.

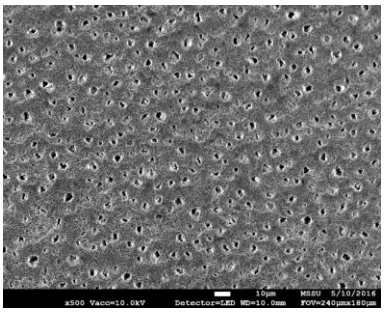

Figure 4.17- D18B02S34- 1.5µm.

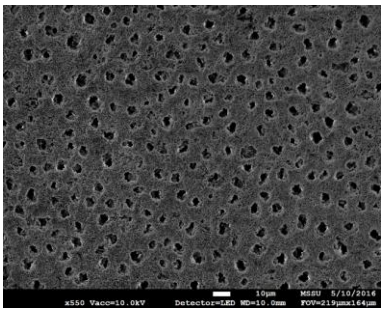

Figure 4.18- D18B02S48- 2.5µm.

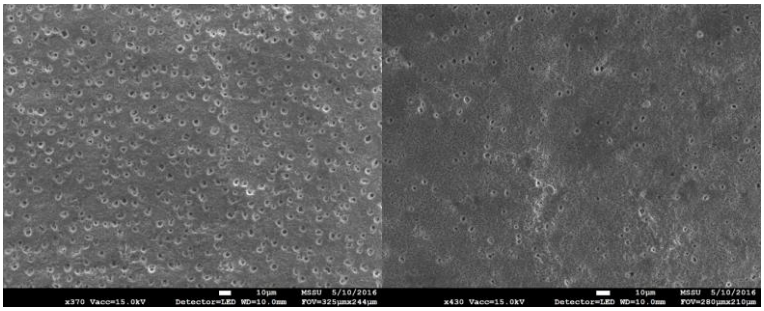

Figure 4.19- D18B03S04- 3.0µm Not uniformly lapped.

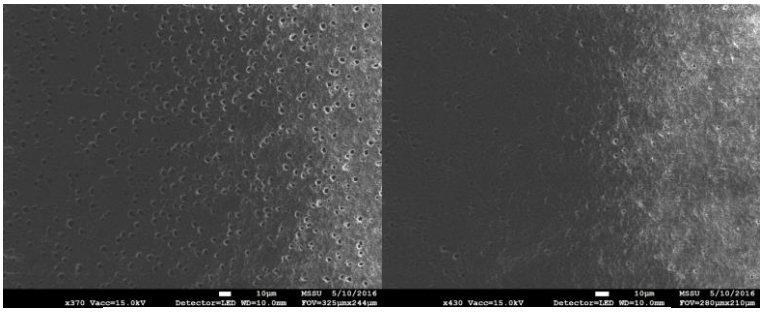

Figure 4.20- D18B03S07- 2.1µm Not uniformly lapped.

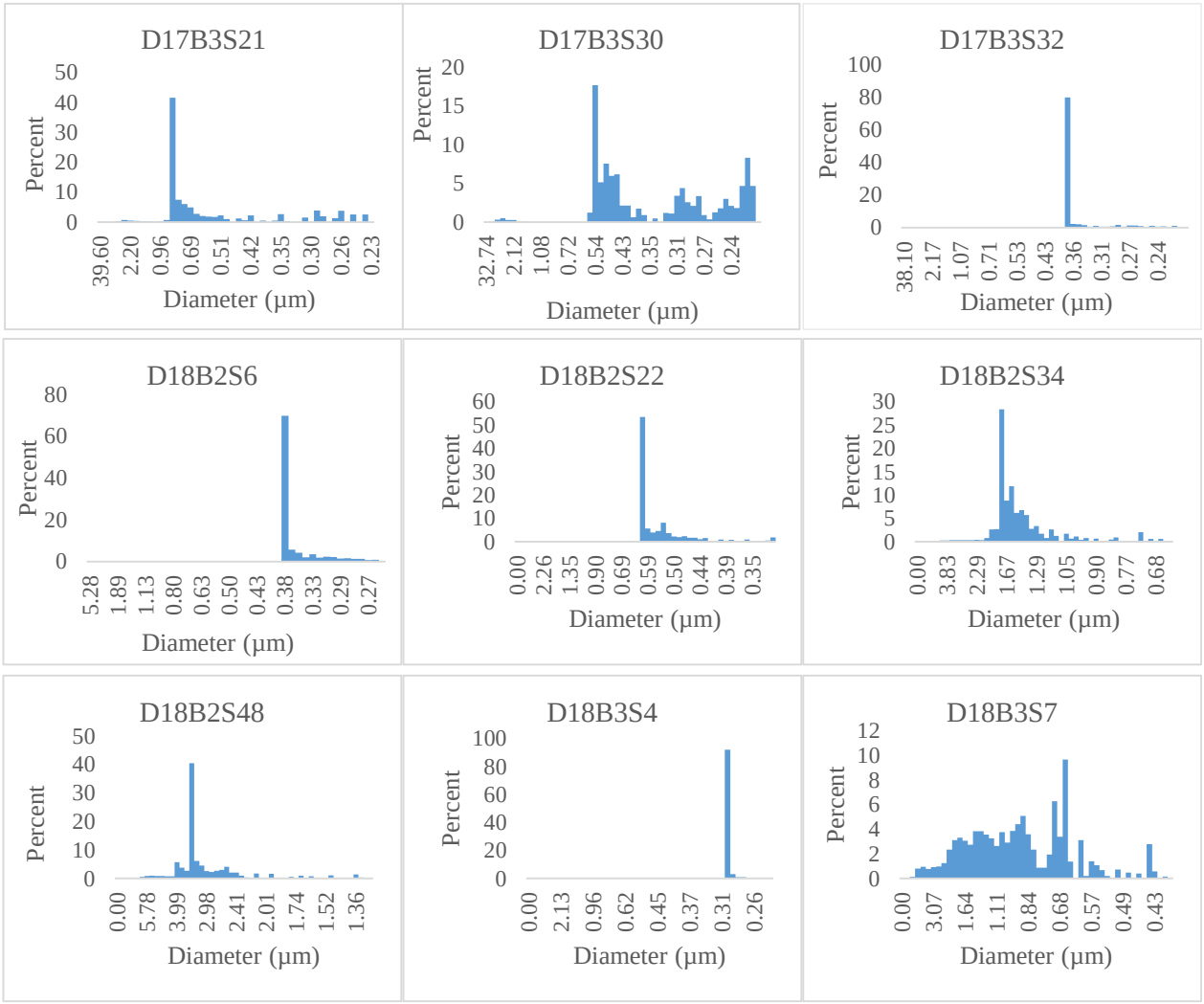

Figure 4.21- Porometer's results of pore size distribution.

These results show that it is needed to keep improving the machinery used for surface engineering of the membranes. This was successfully achieved through the commissioning of a new fixture design of the lapping process (patent-pending), Figure 4.22, with sub-contractor Lam Plan Industries. With their specialized experience in lapping ceramics, it was designed and constructed an improvement of our patent-protected tool to achieve this important goal. This also allowed moving one step closer to achieving a fully automated method.

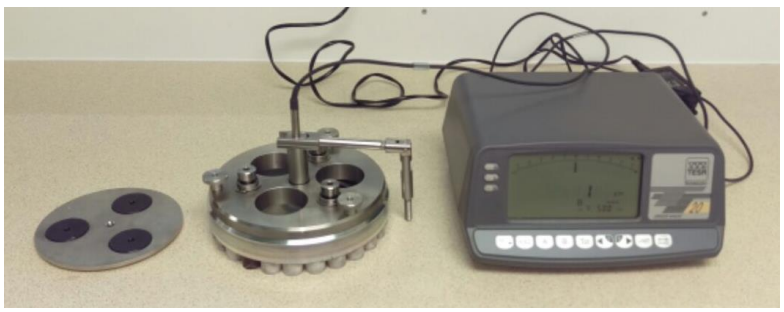

Figure 4.22- New lapping tool to control material removal.

This device will be tested in the future to deploy it as a tool to finely control the amount of stock removal from the surface of our membranes.

Another improvement needed is the implementation of a slurry dispenser to maintain the lapping plate equally wet throughout the entire experiment, since it affects material removal.

Figure 4.23 shows the thickness of membranes before lapping and the quality control limits for each sheet of membranes. To guarantee reproducible results all membranes should have the same initial thickness.

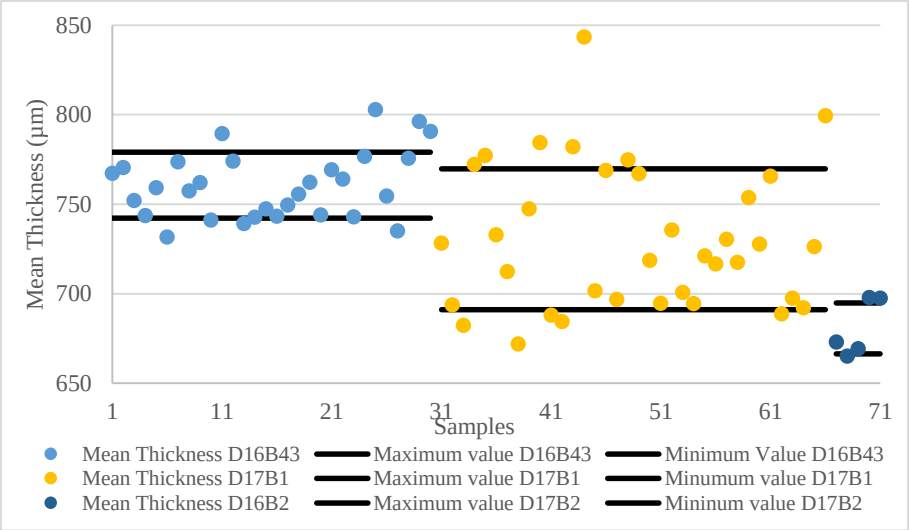

Figure 4.23- Quality control of initial membrane thickness.

4.2 Study on the Membrane Characteristics

4.2.1 Pore Geometry

In this section, pore geometry will be studied. In Figure 4.24 is possible to observe that pores start to open at around 10µm where their circularity increases and reaches its maximum of around 0.8 at 700µm and from 700-800µm of thickness pores start to close. When pores are opening or closing their circularity decreases, although for this study the horizontal cross section of the pores is considered circular. Pores don't open at the same thickness, as it is possible to observe in Figure C.2 in Appendix C. Due to this, on the bottom surface, pores are only considered open when they achieve their highest size, and on the top when there are enough open pores.

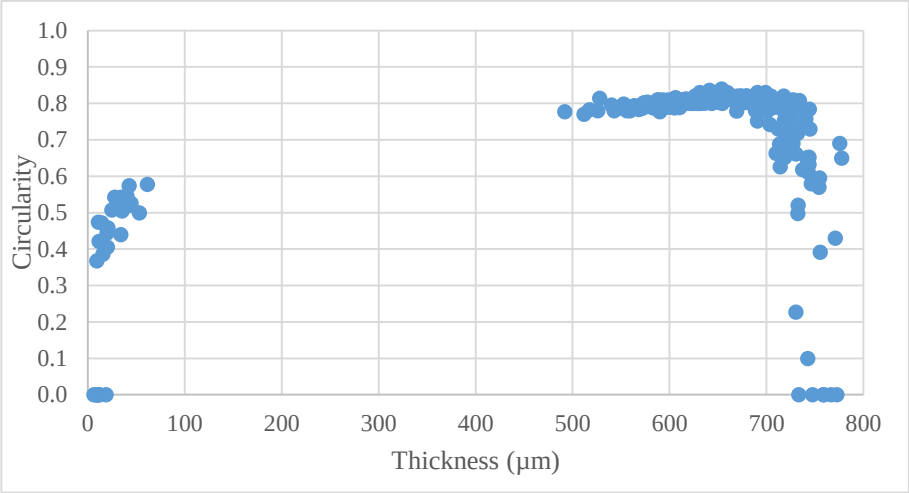

Figure 4.24- Pores' circularity results of bottom and top lapping experiments.

Figure 4.25 depicts the vertical cross section of a membrane, where one can observe its pore geometry. It is possible to observe a conical structure, where the vertex is located on the top surface of the membrane. The follow assumption of top surface pore size valued at 0µm, is due to the results of top lapping which were validated by Porometer. The results show that pores are closed at the top surface of the membrane. Assuming a top pore size of 0µm, means that the pores close at the top surface, although pores close at a lower height.

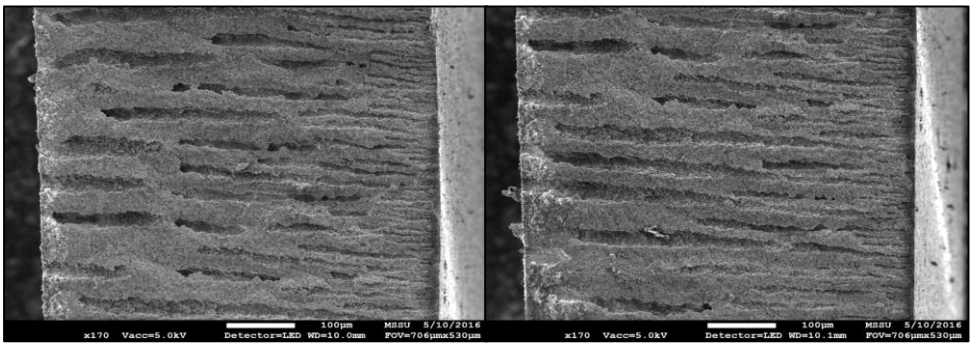

Figure 4.25- Vertical cross section of a membrane, detailing pore geometry.

The data used for this study are bottom and top lapping results, more specifically thickness measurements and correspondent material removals. It is also used the pore sizes (diameter), given by the analysis of photos taken after lapping using Image Pro Premier. In order to study the pores' geometry, the relationship between these parameters were considered. The method used for this study is explained in section 3.2.4.

Follows three cases of study, one for each lapping experiment (bottom, top) and the other using both lapping experiments (bottom and top). In the first two cases the pore size is calculated by a linear regression, and then fixed on the studied surface, varying only the pore size on the opposite surface. When using bottom and top lapping results, the top pore size was fixed at 0µm, and then thickness, pore size at the bottom and the angle were calculated.

4.2.1.1 Bottom Lapping

Lapping was performed on the bottom surface of several membranes with 757µm of mean initial thickness. In order to analyse pores' geometry, the results of the bottom lapping experiments, specifically material removal (50-265µm) and corresponding pore sizes, were studied. Only material removal values over 50µm were considered, because until that point pores are still being opened, therefore did not reach their highest mean pore size, as it is possible to observe in the Figures C.2 and C.3 on Appendix C.

In Figure 4.26 the relationship between pore size and material removal, as well as the corresponding linear regression is shown. It is then concluded that between 50-265µm of material removal the pores present a conical structure.

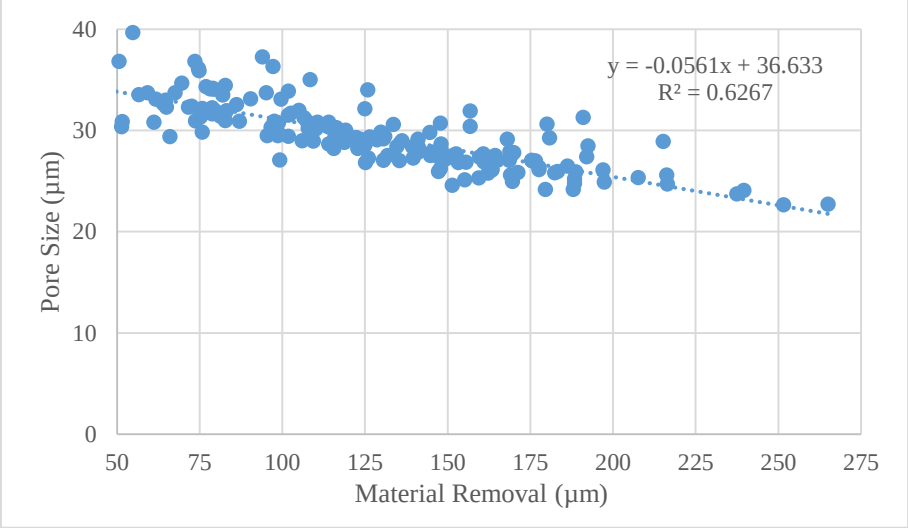

Figure 4.26- Variation of the pore size with the material removal from the bottom surface and its linear regression.

Using the linear regression from the Figure 4.26, two points, (50,34) and (265,22), were considered in order to obtain the angle of the pores (Figure 4.27A). The obtained result is $\alpha_1 = 88.4^{o}$ shown in Table 4.4., case A. Assuming top pore size of 0µm, the following analysis, outlined in Figure 4.27, was performed.

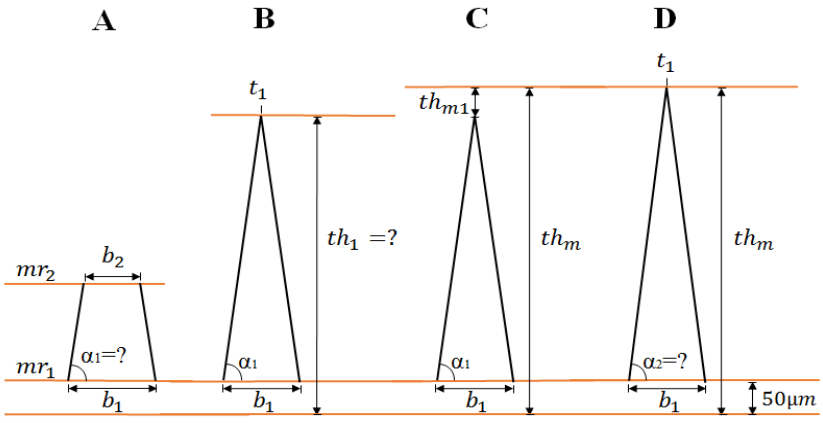

Figure 4.27- Pores' measurements using bottom lapping results. α_i- angles; bi- bottom pore size; mr_i-material removal; t_1-top pore size; th_1- calculated membrane thickness; th_m- mean membrane thickness; th_{m1}- difference between the mean and calculated membrane thickness.

The results from table 4.4 show that according to the linear regression the bottom surface has a pore size of 34µm (case A). Assuming bottom pore size of 34µm and 0µm on the top, according to the linear regression the thickness of the membrane is 653µm (case B). This thickness should correspond to the mean value of the membranes, 757µm, representing a 15.9% increase. Which means that the pores close at 103µm from the top surface of the mean membrane thickness (Figure 4.27C). As it was seen in section 4.1.2, at 103µm from the top surface the pores are already opened. This means that the angle should be higher than the one calculated by the linear regression, which will now be calculated. According to the linear regression the bottom pore size is 34µm and considering the mean thickness of the membrane, 757µm, the angle should be 88.6º, corresponding to an increment of 0.3%, case D.

Table 4.4- Result of pores' measurements using bottom lapping results.

		A	B	C	D	Error (%)
Angle (º)	**α_1**	88.4	88.4	88.4	-	0.3
	α_2	-	-	-	88.6	
Thickness (µm)	**th_1**	-	653	-	-	15.9
	th_m	-	-	757	757	
	th_{m1}	-	-	103	-	-
Pore Size (µm)	**b_1**	34	34	34	34	-
	b_2	22	-	-	-	
	t_1	-	0	-	0	
Material Removal (µm)	**mr_1**	50	-	-	-	-
	mr_2	265	-	-	-	

Figure 4.28 shows the variation of pore size with material removal, considering the 2 obtained angles.

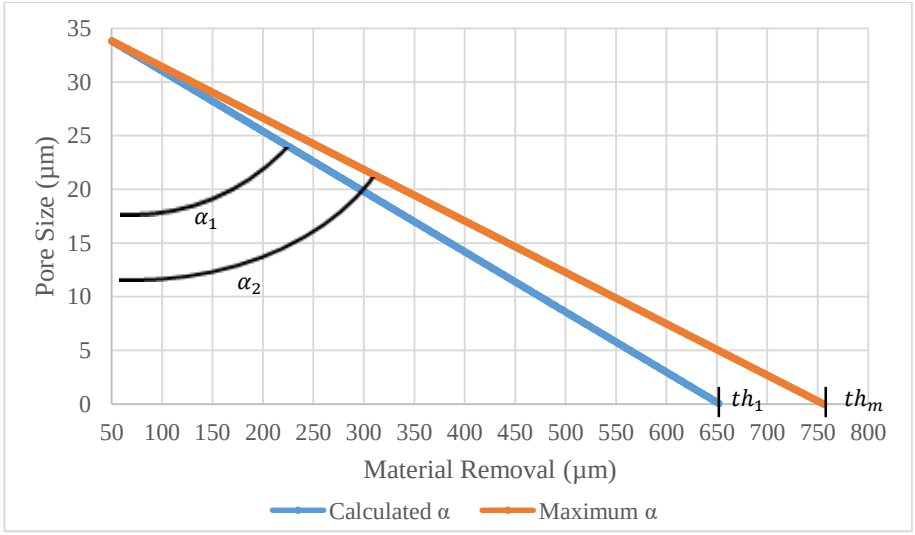

Figure 4.28- Variation of the pore size throughout material removal, for the calculated angle by the linear regression from bottom lapping results, α_1, and the maximum angle, α_2. th_1-calculated thickness; th_m- membranes' mean thickness.

This study was also performed using thickness values, instead of material removal. The results from both values are very similar. It is possible to find this study on Appendix D.

- **Angle comparison of three membranes**

The membranes selected for this study were the three samples in which bottom lapping was conducted 12 times for 10s, in order to have the maximum points possible, Figure 4.29. Total material removal on the three membranes is 160, 169 and 208 for each membrane respectively.

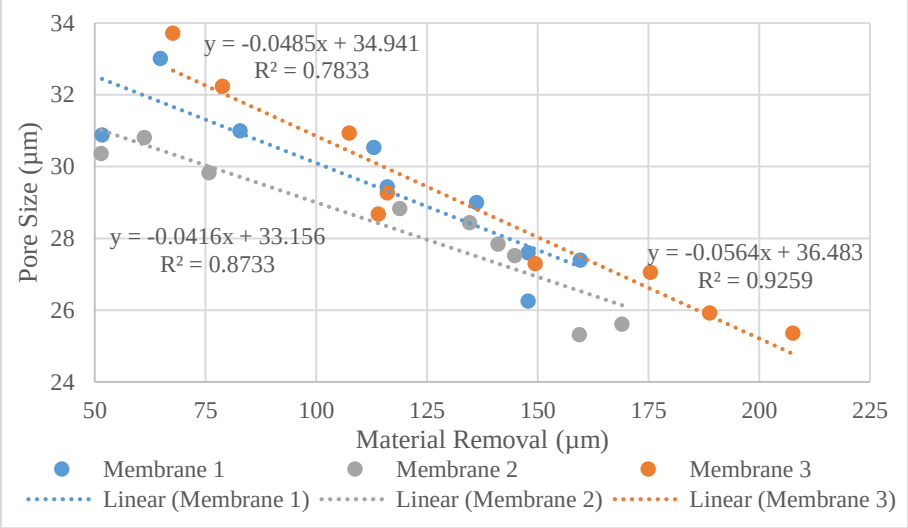

Figure 4.29- Variation of the pore size with the material removal from the bottom surface and corresponding linear regression for three membranes.

It is possible to observe that the values for each membrane validate the conical pore structure, having a mean calculated angle of 88.6º. It is even possible to verify in Table 4.5 that the thinner the membrane, the higher the angle and smaller the bottom pore size.

Table 4.5- Result of pores' measurements using bottom lapping results for three 3 membranes.

	Membrane 1	Membrane 2	Membrane 3
Calculated Thickness (µm)	720	797	647
Initial Thickness (µm)	742	740	750
Error (%)	2.9	7.1	16.0
Calculated α (º)	88.6	88.8	88.4
Maximum α (º)	88.7	88.7	88.6
Error (%)	0.05	0.11	0.27

4.2.1.2 Top Lapping

The membranes used for these experiments have a mean initial thickness of 757µm. In order to analyse pores' geometry, the results of the top lapping experiments, specifically material removal (7-92µm) and corresponding pore sizes, represented in Figure 4.30, were

studied. It is possible to observe that membranes start to open at around 10µm of material removal. The relation between pore size and material removal, as well as the corresponding linear regression is shown in Figure 4.30. It is then concluded that between 7-92µm of material removal pores present a conic structure. In order for the linear regression to have a better adjust pore sizes should be smaller than the ones calculated by Image Pro Premier from 10 to 50µm of material removal.

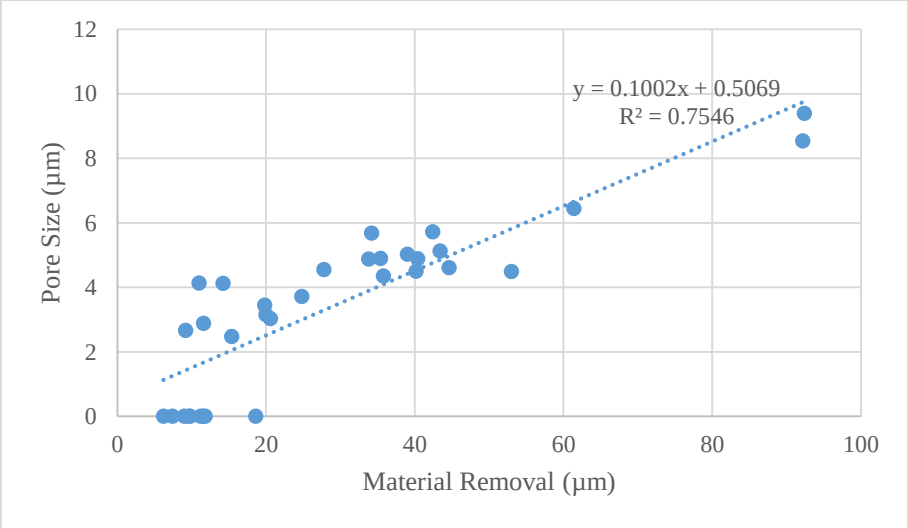

Figure 4.30- Variation of the pore size with the material removal from the top surface and its linear regression.

Using the linear regression from the Figure 4.30, two points, ($0{,}5\times10^{-1}$) and (92,10), were considered to calculate the angle (Figure 4.31A). The obtained result is $\alpha_1 = 87.1^{o}$ shown in Table 4.6., case A. Assuming bottom pore size previously calculated in section 4.1.2.1 by the linear regression, 34µm, the following analyses, outlined in Figure 4.31, will be done.

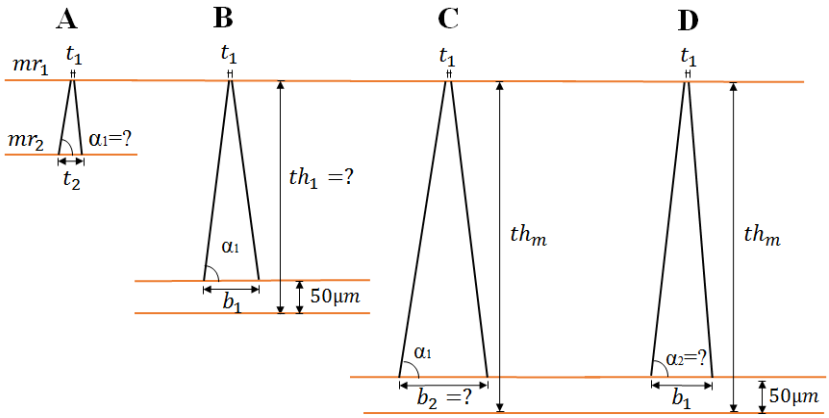

Figure 4.31- Pores measurements using top lapping results, α_i- angles; b_i- bottom pore size; mr_i-material removal; t_i- top surface pore size; th_1- calculated membrane thickness; th_m- mean membrane thickness.

The results from Table 4.6 show that according to the linear regression the pores at the top surface are opened and have 0.5µm (case A), which was seen that it not correct since pores are closed on the top surface. Assuming bottom pore size of 34µm, according to the linear regression the thickness of the membrane is 383µm (case B). The thickness of the membranes

should correspond to the mean value of the membrane, 757µm, representing 97.7% increase. This means that either the pores at the bottom should be bigger or that the angles should be higher than the one calculated by the linear regression. According to the linear regression considering the mean thickness of the membrane, 757µm, the bottom pore size should be 71µm, case C, corresponding to 108.6% increment. Or the angle should be 88.6º, corresponding to an increase of 1.7%, case D.

Table 4.6- Result of pores' measurements using top lapping results.

		A	B	C	D	Error (%)
Angle (º)	α_1	87.1	87.1	87.1	-	1.7
	α_2	-	-	-	88.6	
Thickness (µm)	th_1	-	383	-	-	97.7
	th_m	-	-	757	757	
Pore Size (µm)	b_1	-	34	-	34	108.6
	b_2	-	-	71	-	
	t_1	5×10^{-1}	5×10^{-1}	5×10^{-1}	5×10^{-1}	-
	t_2	10	-	-	-	
Material Removal (µm)	mr_1	0	-	-	-	-
	mr_2	92	-	-	-	

Figure 4.32 shows the variation of pore size in relation to the material removal, considering the 2 obtained angles.

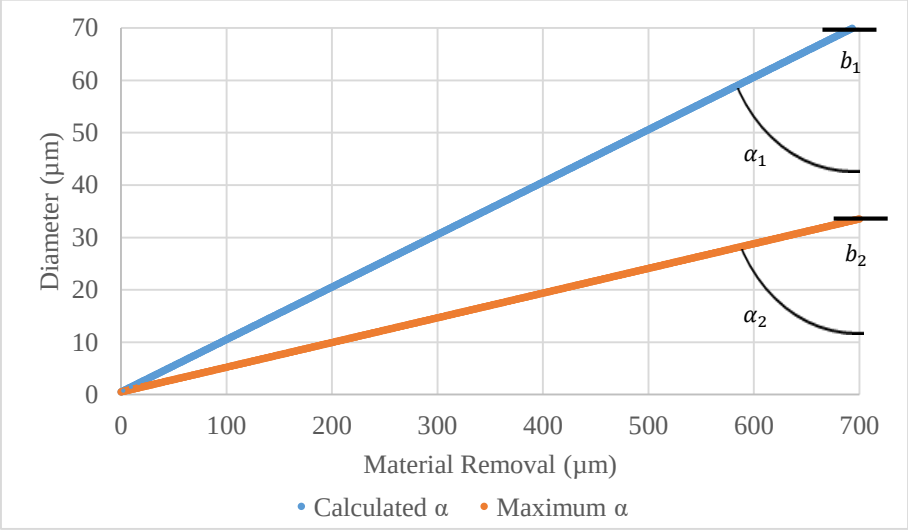

Figure 4.32- Variation of the pore size throughout material removal, for the calculated angle by the linear regression from top lapping results, α_1, and the maximum angle, α_2. b_i- bottom pore size.

4.2.1.3 Bottom and Top Lapping

Pores' geometry was studied using the results of the top and bottom lapping experiments, more specifically thickness (7-700µm) and corresponding pore sizes, represented

in Figure 4.33. In order to place both lapping results in one plot, the material removal values were used for the top, and thickness for the bottom. Only thickness values under 700µm were considered because above that pores start to close. Since membranes' mean thickness used for both bottom and top experiments are the same, the error of using material removal and thickness values for each surface is minimum.

The relationship between pore size and thickness, as well as the corresponding linear regression is shown in Figure 4.33. As seen before, it can be observed that the pores at the top should be smaller in order to have a better fitting between top and bottom results. Despite the lack of results between 92-492µm of thickness can be concluded that the pores present a conic structure from 0-700µm of thickness.

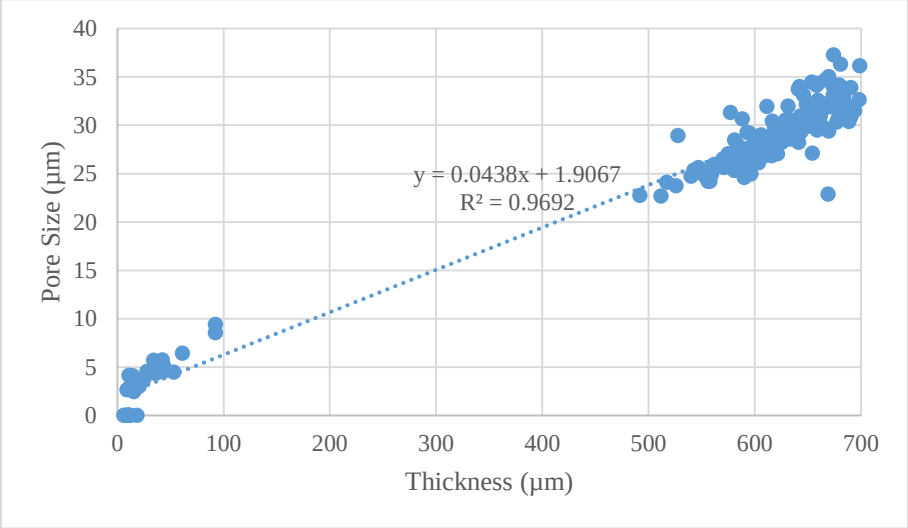

Figure 4.33- Variation of the pore size with the thickness of bottom and top lapping experiments and corresponding linear regression.

Using the linear regression from the Figure 4.33, two points, (0,2) and (700,33), were considered in order to obtain the angle of the pores (Figure 34A). The obtained result is $\alpha_1 = 88.7^o$ shown in Table 4.7, case A. Assuming closed pores at the top surface, 0µm, the following analyses, outlined in Figure 4.34, will be done.

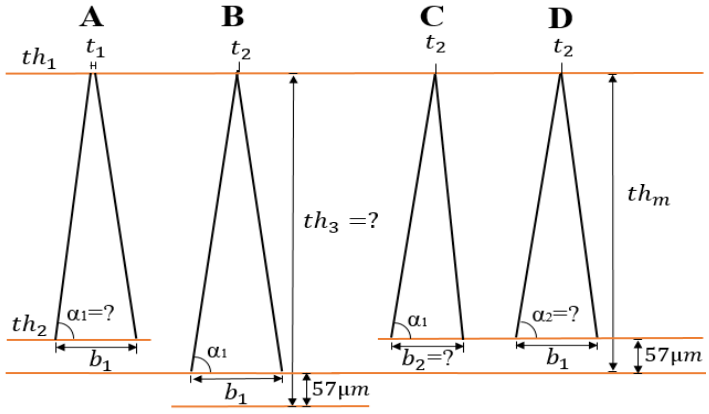

Figure 4.34- Pores measurements using top and bottom lapping results, α_i- angles; b_i- bottom pore size; t_i-top surface pore size; th_1- calculated membrane thickness; th_m- mean membrane thickness.

The results from table 4.7 show that according to the linear regression the pores at the top surface are open and have 2µm (case A). In order to have closed pores at the top and fixing all the parameters, the thickness of the membrane should be 801µm. The difference between the mean membrane thickness and the calculated corresponds to and increment of 5.4%. This means that the pores at the bottom should be smaller or the angles should be inferior to the one calculated. In order to have closed pores at the top surface and considering the mean thickness of the membranes, the pores should have 31µm, corresponding to a decrease of 5.9%, case C. Or the angle should be 88.7, corresponding to a decrease of 0.1%, case D.

Table 4.7- Result of membranes measurements evaluation using bottom and top lapping results.

		A	B	C	D	Error (%)
Angle (º)	α_1	88.7	88.7	88.7	-	-0.1
	α_2	-	-	-	88.7	
Thickness (µm)	th_1	0	-	-	-	-
	th_2	700	-	-	-	
	th_3	-	801	-	-	-5.4
	th_m	-	-	757	757	
Pore Size (µm)	b_1	33	33	-	33	-5.9
	b_2	-	-	31	-	
	t_1	2	-	-	-	-
	t_2	-	0	0	0	

Figure 4.35 shows the variation of pore size in relation to thickness, considering the 2 obtained angles.

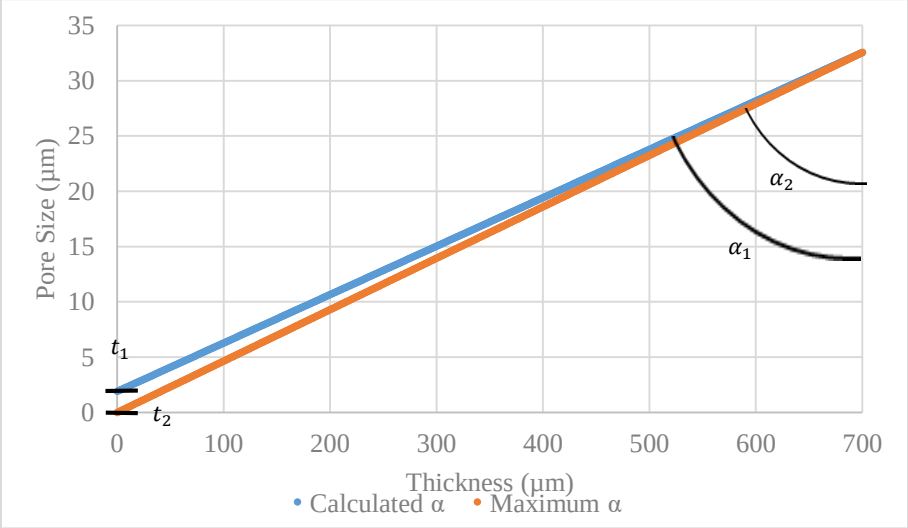

Figure 4.35- Variation of the pore size throughout thickness, for the calculated angle by the linear regression from top and bottom lapping results, α_1, and the maximum angle, α_2. t_i- top pore size.

4.2.1.4 Conclusion

Table 4.8- Study of angles, thickness and pore sizes using lapping results.

		Bottom		Top		Bottom and Top	
Angle (º)	**α_1**	88.4	0.3%	87.1	1.7%	88.7	-0.1%
	α_2	88.6		88.6		88.7	
Thickness (µm)	**th_1**	653	15.9%	383	97.7%	801	-5.4%
	th_m	757		757		757	
Pore Size Bottom (µm)	**b_1**	34	-	34	108.6%	33	-5.9%
	b_2	-		71		31	
Pore Size Top (µm)	**t_1**	0	-	0.5	-	2	-
	t_2	-		-		0	

Bottom results are more reliable than top results due to the error associated with top surface imaging analysis, as seen in section 4.1.2.1, as well as bottom pore sizes being calculated as an average of 5 photos, while top pore sizes were calculated based on an analysis of a single photo per sample.

The angle results of each method are similar, although bottom and top results present the lowest errors, while top results have the highest error due to the non-accurate results. It can be concluded that the angle of the pores is between 88 and 89°.

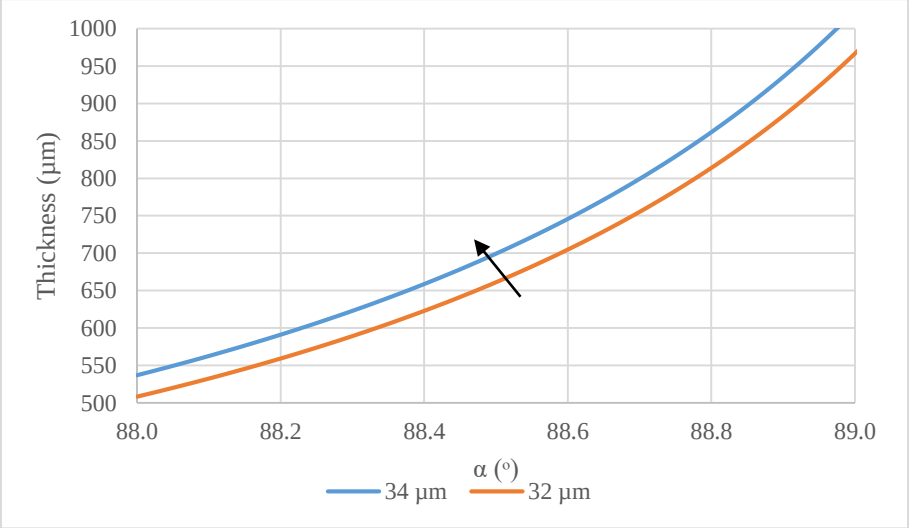

Figure 4.36- Variation of the angle α, with the thickness of the membranes for different bottom pore sizes.

Figure 4.36 shows that for the same angle, the higher the initial thickness, the bigger the bottom pore size. It is also possible to verify that small angle variations, for the same bottom pore size, lead to big thickness increments, which shows a big sensibility to this parameter in the calculations done.

4.2.2 Connectivity of the pores

In order to study if the pores connect with each other, Image Pro Premier measurements of the bottom lapping pictures were studied. Figure 4.37 shows that from 0 to 50µm of material removal pores are being opened, increasing their area. From 50µm forward pores are becoming smaller. At 50µm of material removal pores reach the highest area, however not all the pores are opened, as it's possible to observe in Figure 4.39 and from Figure C.1 to C.7, Appendix C.

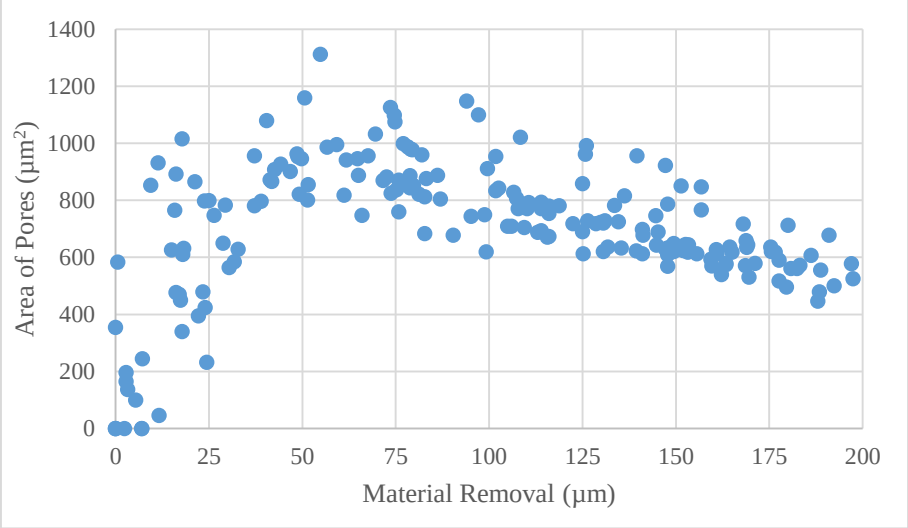

Figure 4.37- Variation of the area of pores with material removal.

The majority of the pores are opened at 125µm of material removal and therefore have the highest percentage of open pores. In Figure 4.35 is observed that the % of open pores increases from 0-125µm of material removal, and is stable from 125 to 200µm. The constant porosity is due to the decrease of the pores area and the increase of their number, Figure 4.39.

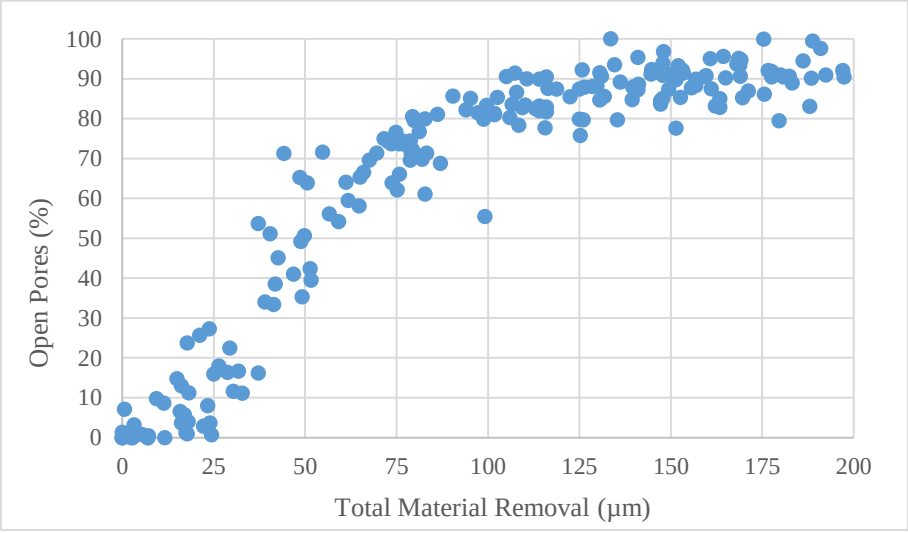

Figure 4.38- Variation of the % of open pores with material removal.

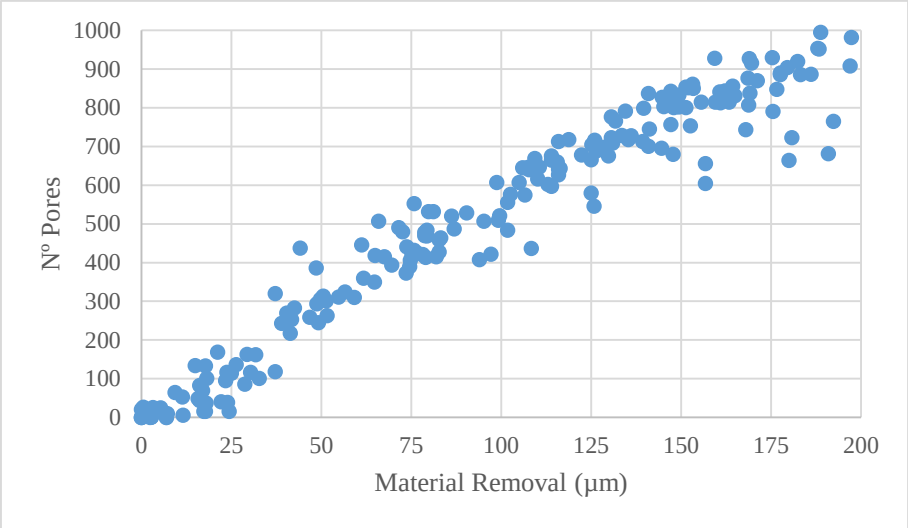

Figure 4.39- Variation of the number of pores with material removal.

In Figure 4.40 is possible to observe that pores are dividing at 96µm of material removal. It would be expected that these two pores, now separated, would be just one at lower material removal. It is also possible that the pores touching is an illusion due to the luminosity of the photo. In conclusion, either the pores are connected at a low material removal, or not every pore goes through the whole membrane and therefore are only opened at higher material removal. This last option contradicts with Figure 4.42, where is shown that material removal on the bottom surface does not affect the permeability. Although since permeability depends of several parameters is not possible to conclude anything. In order to verify the second option, pore sizes on both bottom and top surface and final membrane thickness had to be set, and would have to be observed an increase of the flux with material removal on the bottom.

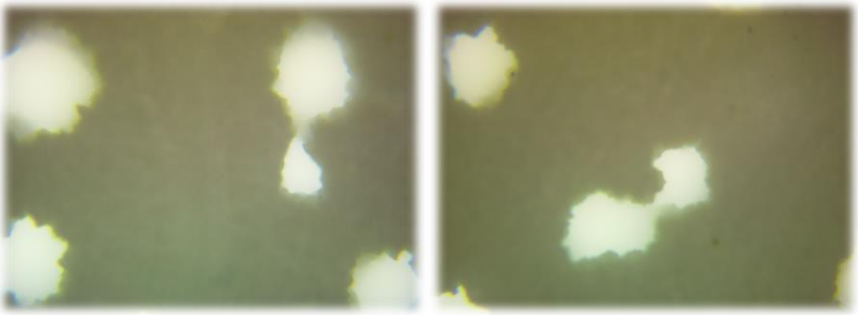

Figure 4.40- Pictures with 40x lens of bottom surface with 96µm of material removal.

4.2.3 Permeability tests

Permeation data for SSL membranes has been collected by Porometer as explained in section 3.2.5, and at the laboratory of the University of Surrey with the permeability rig designed by Smart Separations Ltd, explained in section 3.2.3. Gas permeation data using the two methods were then compared.

- **Porometer tests**

Figure 4.41 shows a plot of membrane permeation flux rates for the samples shown in Table 4.9.

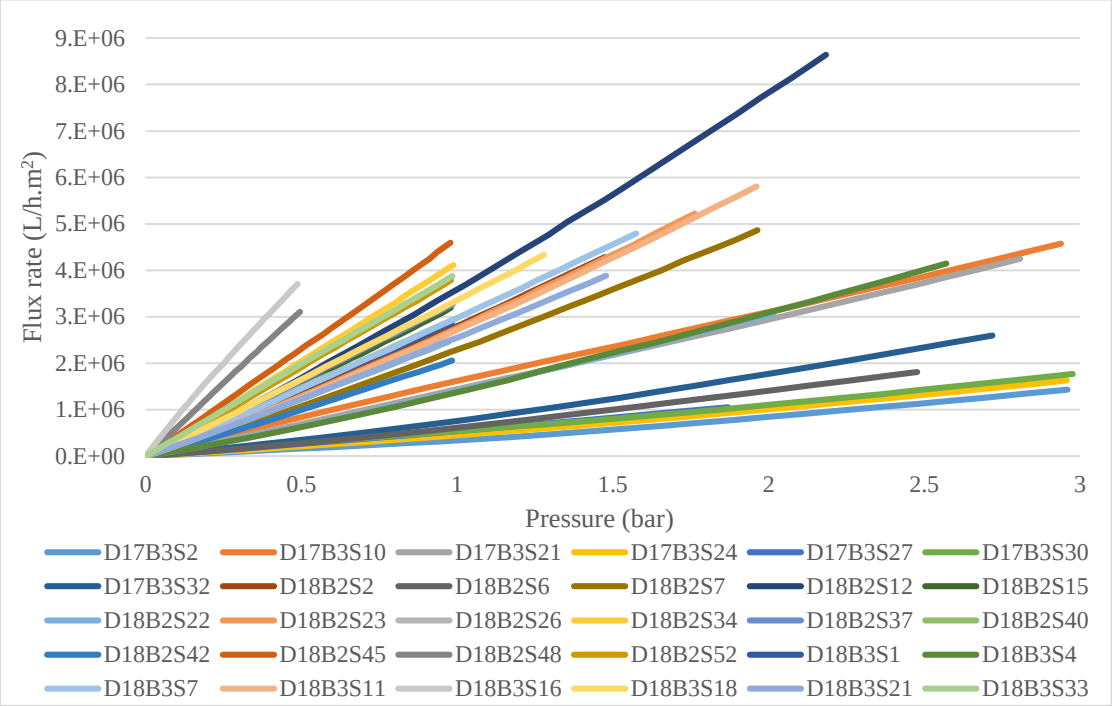

Figure 4.41- Flux rates of Smart Separations's membranes.

Table 4.9 shows the maximum flow rates achieved for all the samples tested and the corresponding lmh value at 1 bar.

Table 4.9- Flux data and properties of Smart Separations membranes.

	Max pressure (bar)	Maximum flow rate (L/h)	Maximum flux rate (L/h.m^2)	Permeability (L/h.m^2.bar)	Mean thickness	Pore Size (µm)
D17B3S2	2.96	406	1.4E+06	3.6E+05	576	-
D17B3S10	2.94	1298	4.6E+06	1.7E+06	604	1.60
D17B3S21	2.81	1207	4.2E+06	1.5E+06	562	0.82
D17B3S24	2.96	462	1.6E+06	4.7E+05	585	0.42
D17B3S27	1.87	299	1.1E+06	5.7E+05	569	0.59
D17B3S30	2.98	503	1.8E+06	5.6E+05	610	3.45
D17B3S32	2.72	738	2.6E+06	8.0E+05	563	0.35
D18B2S2	1.47	1217	4.3E+06	2.8E+06	570	1.42
D18B2S6	2.48	515	1.8E+06	6.9E+05	556	0.38
D18B2S7	1.97	1381	4.9E+06	2.5E+06	541	0.88
D18B2S12	2.19	2453	8.6E+06	3.7E+06	634	0.52
D18B2S15	0.98	908	3.2E+06	3.2E+06	592	1.61
D18B2S22	2.02	868	3.1E+06	1.4E+06	621	0.58
D18B2S23	1.76	1483	5.2E+06	2.9E+06	619	0.91
D18B2S26	0.97	822	2.9E+06	2.9E+06	591	1.56
D18B2S34	0.99	1168	4.1E+06	4.1E+06	570	1.80
D18B2S37	0.99	930	3.3E+06	3.3E+06	564	1.46
D18B2S40	0.97	700	2.5E+06	2.5E+06	579	1.34
D18B2S42	0.98	584	2.1E+06	2.1E+06	534	1.31
D18B2S45	0.98	1305	4.6E+06	4.6E+06	571	1.83
D18B2S48	0.50	881	3.1E+06	-	607	3.45
D18B2S52	0.98	1076	3.8E+06	3.8E+06	588	1.35
D18B3S1	0.98	813	2.9E+06	2.9E+06	632	1.50
D18B3S4	2.57	1178	4.1E+06	1.4E+06	657	0.32
D18B3S7	1.58	1362	4.8E+06	3.0E+06	616	2.00
D18B3S11	1.96	1650	5.8E+06	2.7E+06	628	0.66
D18B3S16	0.49	1052	3.7E+06	-	584	6.20
D18B3S18	1.28	1231	4.3E+06	3.4E+06	665	1.59
D18B3S21	1.48	1103	3.9E+06	2.6E+06	631	0.95
D18B3S33	0.99	1102	3.9E+06	3.9E+06	511	2.20

Samples from two different batches were used. In the denomination of the samples D represents the batch number, B the membrane sheet, and S the sample number. It can be seen that there is a large variation between the flux rates for the different samples, as expected, since each sample has been lapped to a different extent and therefore has a different thickness and pore size. At the maximum pressure for each sample, the maximum and minimum flux are 4.6E+6 L/h.m^2.bar and 3.6E+5 L/h.m^2.bar respectively. As explained and shown by SEM

pictures in section 4.1.2.1 due to number of open pores per area and presence of air bubbles, big pore sizes not always correspond to better fluxes, or vice versa.

Figure 4.42 shows membrane flux versus a selection of membrane properties, including pore size determined by Porometer and optical microscopy/image analysis, bottom and top material removal and mean thickness of samples. Plots of flux versus different membrane properties failed to produce correlations. However, as pore size, material removal, and membrane thickness have not been varied systematically, the flux is a product of multiple variables and will not produce a correlation with individual membrane properties. However, it is possible to observe that the flux increases with top material removal and consequently pore size, as expected.

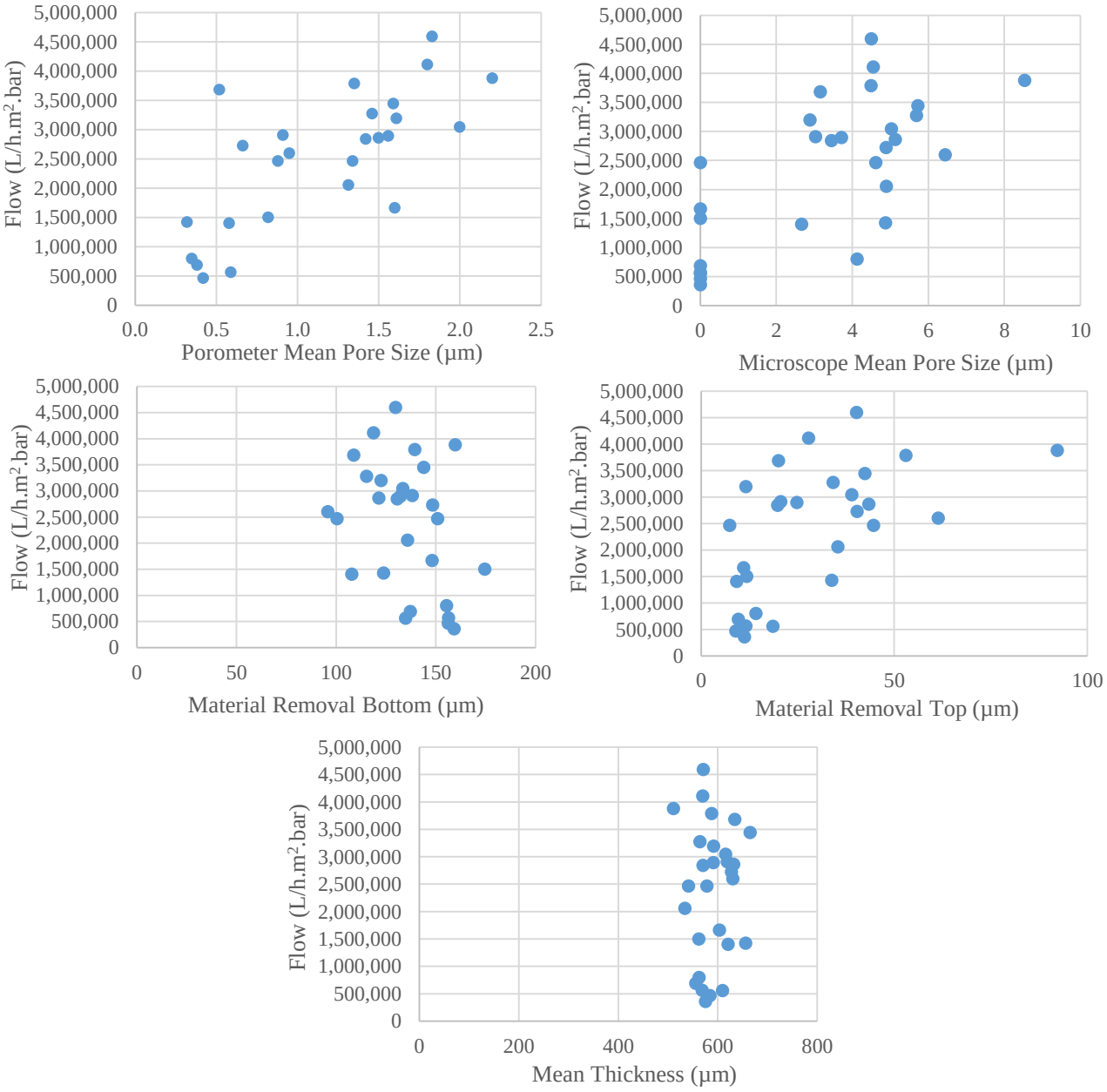

Figure 4.42- Flux vs. Smart Separations membrane properties.

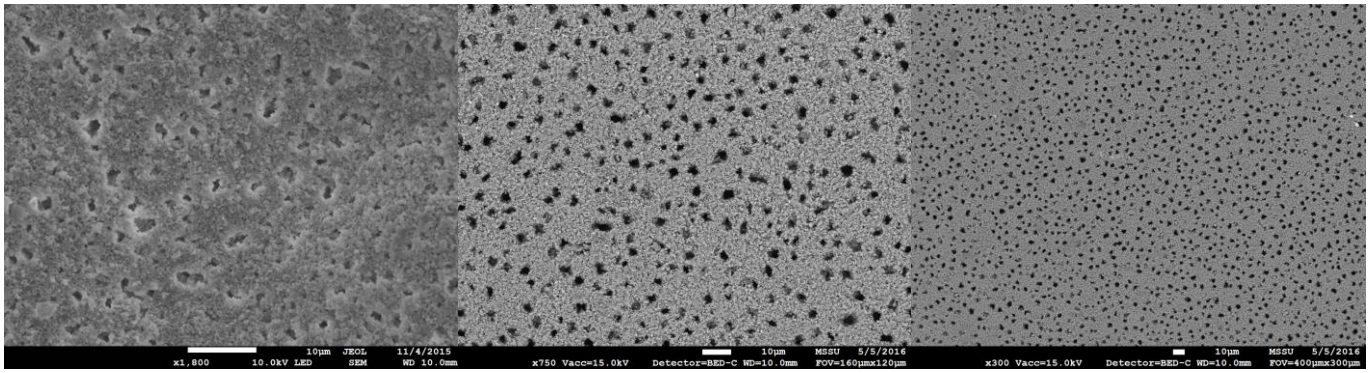

Figure 4.43- Smart Separations membranes with blocked pores.

SEM pictures of samples sent to Porometer, Figure 4.43, show that some pores were apparently blocked with small particles of alumina removed from the membranes surface during lapping. This might have caused lower flow rates and consequently smaller pore sizes. In order to solve this problem a new ultrasonic bath and three detergents were purchased, Figure 4.44. The new ultrasonic bath has three operating modes and allows a bath temperature of up to 80°C. During membrane cleaning it was observed that membranes would move to the corners of the bath and sometimes even overlap each other, which affected the effectiveness of the cleaning. Therefore, a support to maintain membranes in the same place in a diagonal position was designed, Figure 4.45.

Figure 4.44- Flux vs. Smart Separations membrane properties.

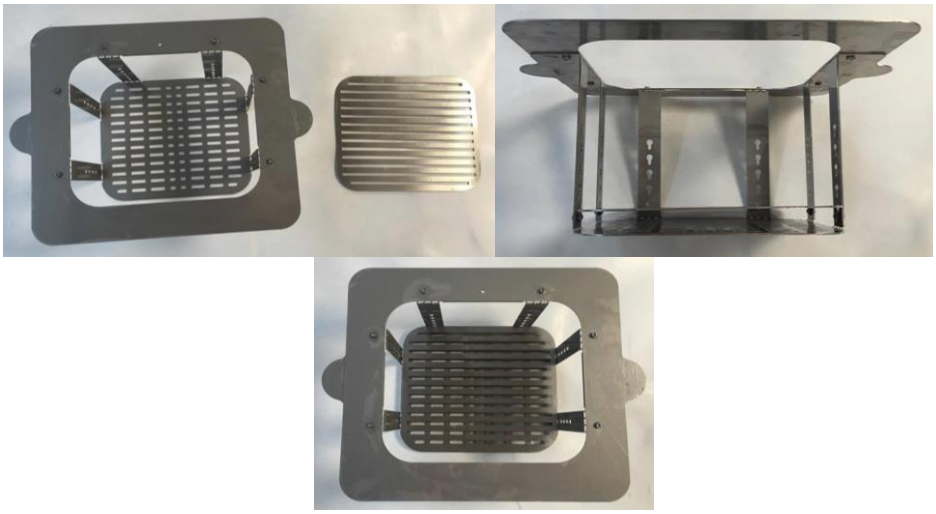

Figure 4.45- Ultrasonic bath support.

Two water based diamond slurries were also purchased, Figure 4.46, to study if it would facilitate the cleaning of the membranes. Further tests have to be done in order to determine the best cleaning method for lapped membranes, using all these new tools.

Figure 4.46- Water based diamond slurries.

- **Permeability rig tests**

Permeability tests were conducted using the method explained in section 3.2.3. in order to validate the method, Figure 4.47.

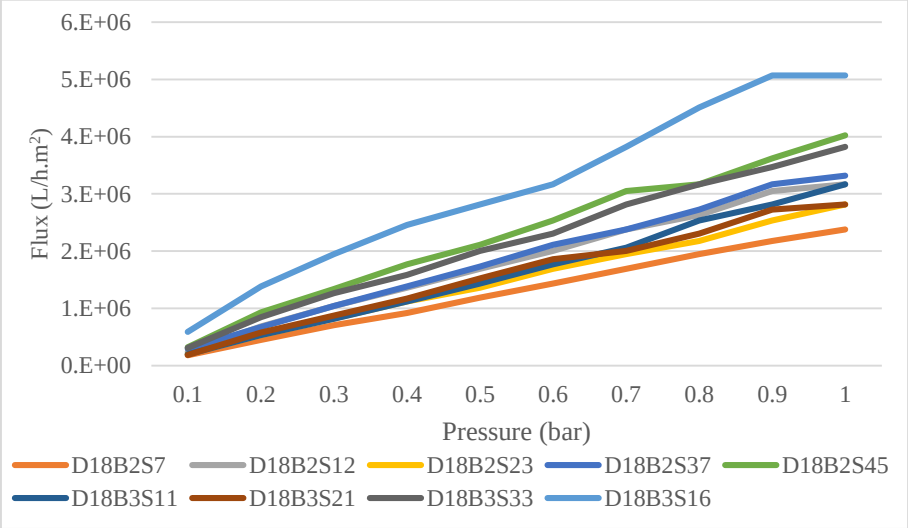

Figure 4.47- Flux data using SS permeability rig.

Table 4.10 shows flow data of both methods at 0.5 bar of pressure and the correspondent error for each sample.

Table 4.10- Flux data at 0.5bar of two methods.

	Permeability rig Flux (L/h.m^2)	Porometer Flux (L/h.m^2)	Error (%)
D18B2S7	1.2E+06	9.9E+05	20
D18B2S12	1.7E+06	1.6E+06	6
D18B2S23	1.4E+06	1.2E+06	9
D18B2S37	1.7E+06	1.8E+06	2
D18B2S45	2.1E+06	2.4E+06	13
D18B3S11	1.4E+06	1.1E+06	35
D18B3S21	1.5E+06	1.1E+06	41
D18B3S33	2.0E+06	2.0E+06	2
D18B3S16	2.8E+06	4.1E+06	31

According to Table 4.10 data from both methods is similar since only 3 samples have an error superior to 20%, and sample D18B3S11 broke during the permeability test using SS permeability rig, justifying the difference between the results. Even with the errors associated with the "in-house" method, it is possible to validate it and its results.

4.2.4 Dust-load test

Smart Separations commissioned to Particle Technology the characterisation of our filters through dust challenge tests and comparing them with a commercially available filter, in order to test their effectiveness to reject different sized particles. A photograph of the SS composite filter is represented in Figure 4.48, composed by 30x 11.56cm^2 individual filters with 5µm pores contained within an acrylic structure, designed by the company.

Figure 4.48- Photograph of the composite filter contained within the test housing.

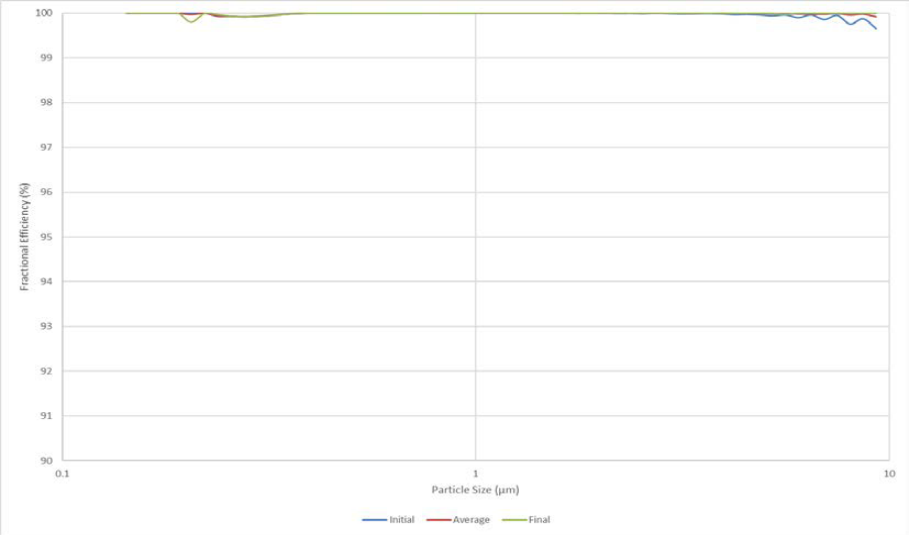

Figure 4.49- Fractional efficiency profiles of the Sterlitech filter.

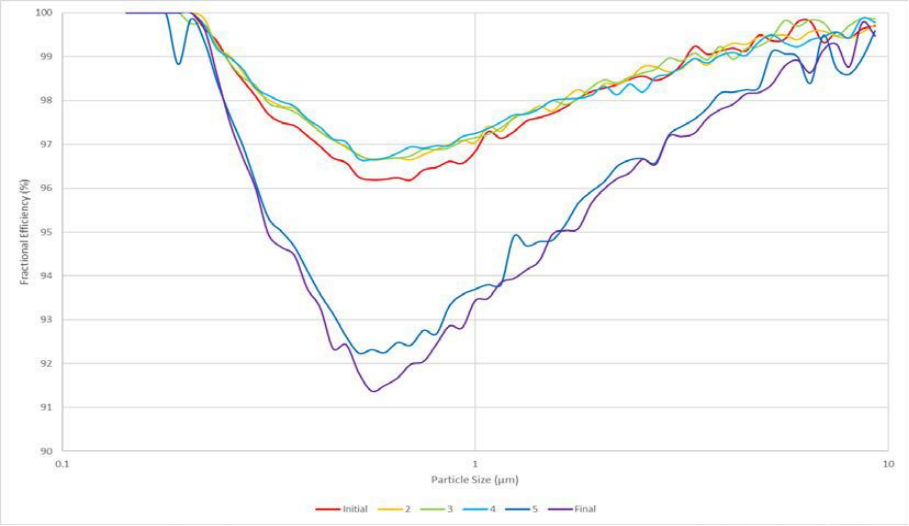

Figure 4.50- Fractional efficiency profiles of the Smart Separation filter.

The Sterlitech filter exhibited a consistently high performance over the test duration, Figure 4.49, while Smart Separations's filter exhibits two trends, Figure 4.50. The first consists of the initial four measurements taken, which show the expected trend of a filter becoming more efficient as the filter cake builds up. The two final fractional efficiency results are significantly lower than the previous four, displaying clear signs of structural failure of Smart Separations filters. Due to the electrostatic charge of the particles, the ones smaller than 0.8µm adhere to the filter surfaces, explaining the higher efficiency for these particles. The test also shows that Smart Separations filters are less efficient with particles smaller than 1µm, which would be expected since pores are 5µm in size, according to the imaging analysis, while Sterlitech have 0.8µm. However, prior to failure, Smart Separations filter displayed signs of blocking faster than the Sterlitech filter, while being comparatively less efficient.

5
CONCLUSIONS

This thesis took on as its goal the optimisation of the manufacturing process of flat ceramic membranes produced by Smart Separations Ltd. This work focused primarily on lapping, the last and most important production stage of these membranes, which allow the opening of the pores and the control of their size, and thus their applications.

During bottom lapping, several lapping runs were performed on the same membranes for different time periods, studying the effect of time on material removal, where it was concluded that short time intervals remove material faster than longer ones. This is due to the accumulation of removed material between the membranes and the lapping plate, and therefore by cleaning the membranes, fixtures and lapping plate after each lapping run, material is removed faster.

During top surface lapping, the effect of cut thickness was studied, having performed a lapping run on each membrane with different durations and a cut thickness of 25 or 50µm. It was then possible to conclude that higher cut thicknesses lead to faster material removal, and that the cut thickness controls the amount of material to be removed. Therefore, there is faster material removal when part of the membrane is above the alignment of the fixture's ceramic ring, and slower when they are aligned or below.

With these experiments it was also possible to establish an SOP. It contains the lapping conditions in order to obtain the maximum percentage of open pores with the least material removal possible, and thus, optimising the membranes' flux and their physical strength. It was then concluded that is necessary to remove 125µm, by performing lapping nine times for 10s or once for 600s with a cut thickness of 125µm to obtain 89% of open pores.

Since filtration occurs in the top surface, it was necessary to determine the lapping conditions to obtain a certain pore size within the microfiltration range. Despite the bottom surfaces' calibration having been performed in such a way as to minimise the errors concerning the membrane roughness and cut thickness, a higher precision is required than the currently available, making it difficult to achieve the purpose of this experiment due to variance of the results obtained. In order to produce more reliable results, regarding membrane thickness, pore sizes and pore size distribution, the accuracy of the fixtures and its micrometers should be

improved, which is currently 25µm. Since current lapping techniques are manually performed, which result in higher potential for errors, the implementation of an automatic lapping machine and a slurry dispenser could overcome some of the challenges concerning the accuracy and procedure reproducibility, which then express themselves in the results, as shown in this study.

After lapping, membranes' pore sizes were characterised by imaging analysis using an optical microscope, SEM and bubble point method, having obtained different pore size results with different techniques. The obtained results through the bubble point method are notably inferior to the rest, due to the employed method and area of analysis. It can then be concluded that for a more accurate characterisation based on imaging analysis, several photos of the same membrane must be analysed in order to increase the analysed area, as well as an improvement of the microscope's resolution to produce better quality images, and thus more accurate results.

Smart Separations membranes' microstructure, more specifically the pores' angle, led to the conclusion that these present a conical structure with an angle between 88 and 89º. In this study, thickness, material removal and pore sizes calculated through optical microscope imaging analysis were used, which confirmed that the pores on the top surface are smaller than the ones calculated using this method.

By comparing permeability results from a subcontractor company and the in-house tests, it was possible to verify the reliability of the latter, due to the similarity of results. However, it wasn´t possible to conclude which is the dominant factor contributing to flux, since the parameters were not systematically and individually varied during lapping.

For the same reason, nothing can be concluded regarding the pores' connectivity even though the images indicate their proximity.

After the permeability tests, membranes were observed under SEM, and it was possible to verify the blockage of the pores with removed material and possibly diamond slurry. In order to decrease this, a new cleaning method must be studied and implemented using the new ultrasonic bath and detergents.

Dust rejection tests showed that SSL membranes are above 96% efficient for all particle sizes tested, although it has to be improved: comparing the SSL membrane to a commercially available membrane, the former presents a significantly lower efficiency. This efficiency should be improved by a better control of the pore sizes, as well as its distribution. During the test some membranes even broke, showing that the membranes' strength should also be improved to resist higher pressures during filtration.

Despite the identified limitations, and a few others, this study allowed for a better understanding of the lapping process, having identified its weak spots as well as the membranes' microstructure and effectiveness concerning both permeability and dust rejection.

Future work

- Perform some experiments in order to test the new lapping machine design, since it controls the removal of material through the pressure applied to the membranes, and possibly modify it, if necessary.
- Conduct tests to determine the frequency and amount of slurry to be applied on the plate in order to implement an automated diamond slurry dispenser.
- A study on the influence of the several lapping parameters, namely, diamond particle size, rotation speed and time, would be interesting in order to obtain better understanding of lapping and its fine control.
- Study the best cleaning method considering time, temperature, operation mode and detergent. As well as studying if the water-based diamond slurry facilitates the cleaning.
- Perform lapping experiments where the individual membrane properties, such as top and bottom material removal, final thickness and pore size are systematically changed in order to study their effects on the flux, in order to optimize it, and make conclusions concerning the pores' connectivity.
- It would also be interesting to perform rejection tests in order to characterise the membranes' efficiency with different pore sizes for different sized particles.
- Study ways to improve membranes' mechanical strength, in order to resist high filtration pressures.

REFERENCES

"How to use a polishing machine: basic principles." Retrieved 30/01/2016, from http://www.astrosurf.com/gap47/T400/Machine/Utilisation_machines/utlisation_machines_eng.htm.

Almandoz, M. C., et al. (2015). "Composite ceramic membranes from natural aluminosilicates for microfiltration applications." Ceramics International **41**(4): 5621-5633.

American water works association (2005). Microfiltration and ultrafiltration membranes for drinking water.

Basile, A. (2013). Handbook of membrane reactors, Woodhead publishing series in energy.

Belibi, P. B., et al. (2015). "Microfiltration ceramic membranes from local Cameroonian clay applicable to water treatment." Ceramics International **41**(2, Part B): 2752-2759.

Chan, R. and V. Chen (2004). "Characterization of protein fouling on membranes: opportunities and challenges." Journal of Membrane Science **242**(1–2): 169-188.

Charcosset, C. (2012). 1 - Principles on membrane and membrane processes. Membrane Processes in Biotechnology and Pharmaceutics. C. Charcosset. Amsterdam, Elsevier**:** 1-41.

Chemistry Explained (2015). "Chemistry Explained." Retrieved 23/09/2015, from http://www.chemistryexplained.com/Bo-Ce/Ceramics.html.

Engis Corporation (2016). Retrieved 01/02/2016, from http://www.engis.com/lapping-plate-care.php.

Falco, M. D., et al. (2011). Nuclear Power - Deployment, Operation and Sustainability.

Foley, G. (2013). Membrane Filtration. Dublin City University, Cambridge University Press.

Ghouil, B., et al. (2015). "Development and characterization of tubular composite ceramic membranes using natural alumino-silicates for microfiltration applications." Materials Characterization **103**: 18-27.

Glover, D. P. "Petrophysics MSc Course Notes." Retrieved 21/10/2015, from http://homepages.see.leeds.ac.uk/~earpwjg/PG_EN/CD%20Contents/GGL-66565%20Petrophysics%20English/Chapter%203.PDF.

Government digital service (2015). "Environmental management." Retrieved 13/10/2015, from https://www.gov.uk/topic/environmental-management.

Irvin, M. (2011). Diamond lapping and lapping plate control, Gardner Publications, Inc.**:** 26.

Irvin, M. (2011). Diamond lapping and polishing: flat lapping is often the process of choice when finishing a ceramic surface to precise dimensions, BNP Media**:** 24.

Jaffrin, M. (2015). Membrane Filtration Processes.

Kallioinen, M. and M. Nystro¨m (2008). Advanced Membrane Technology and Applications, John Wiley & Sons, Hoboken.

Koch Membrane Systems (2015). "About Microfiltration." Retrieved 20/09/2015, from http://www.kochmembrane.com/Learning-Center/Technologies/What-is-Microfiltration.aspx.

Kumar, R. V., et al. (2015). "Elaboration of novel tubular ceramic membrane from inexpensive raw materials by extrusion method and its performance in microfiltration of synthetic oily wastewater treatment." Journal of Membrane Science **490**: 92-102.

Laitinen, N. (2002). Development of a ceramic membrane filtration equipment and its applicability for different wastewaters, Lappeenranta University od Technology. **Doctor of Science**.

Lenntech. "Membrane Technology." Retrieved 19/09/2015, from http://www.lenntech.com/membrane-technology.htm#ixzz3n8465u4q.

Li, K. (2007). Ceramic Membranes for Separation and Reaction. Department of Chemical Engineering and Chemical Technology, Imperial College London, UK, WILEY.

Lieven, G., et al. (2005). Pressure driven separations of liquid feeds, Google Patents.

Lorente-Ayza, M. M., et al. (2015). "Comparison of extruded and pressed low cost ceramic supports for microfiltration membranes." Journal of the European Ceramic Society **35**(13): 3681-3691.

Lorente-Ayza, M. M., et al. (2015). "Influence of starch content on the properties of low-cost microfiltration ceramic membranes." Ceramics International **41**(10, Part A): 13064-13073.

Macedo, H., *Apparatus and Methods*, GB Patent number GB2519734, May 2015

Macedo, H., *Ceramic Filter,* GB Patent number GB2526173, August 2016.

Macedo, H., Drinkwater, R., *Apparatus and Methods*, GB Patent number GB2534130, July 2016.

Marshall, T. J., et al. (1996). Soil Physics, Cambridge University Press.

Momeni, S. M. and M. Pakizeh (2013). "Preparation, characterization and gas permeation study of PSf/MgO nanocomposite membrane." Brazilian Journal of Chemical Engineering **30**: 589-597.

Mulder, M. (1996). Basic Principles of Membrane Technology, Kluwer Academic Publishers.

Noble, R. D. and S. A. Stern (1995). Membrane Separation Technology Principles and Applications. Membrane Science and Technology Series, 2, Elsevier.

Parma, S. (2013). Preparation and characterization of ceramic microfiltration membrane using red mud as cost effective resource. Department of chemical engineering, National Institute of Technology Rourkela. **Master**

Polytechnic of Turin. "Field emisison SEM." Retrieved 15/10/2015, from http://areeweb.polito.it/ricerca/carbongroup/fac_fesem.html.

Reingruber, H., et al. (2011). "Quantitative characterization of microfiltration membranes by 3D reconstruction." Journal of Membrane Science **372**(1–2): 66-74.

Schneider, G. J. (2002). "CHAPTER 18 Lapping And Honing." T & P: Tooling & Production **68**(6): 28.

Somasundaran, P. (2006). Encyclopedia of Surface and Colloid Science. A. T. Hubbard, Taylor & Francis Group. **2**.

Staszak, K., et al. (2013). "Comparison of polymeric and ceramic membranes performance in the process of micellar enhanced ultrafiltration of cadmium(II) ions from aqueous solutions." Chemical Papers **67**(4): 380-388.

Sterlitech, C. (2015). "Choosing the Appropriate Membrane." Retrieved 22/09/2015, from http://www.sterlitech.com/choosing-the-appropriate-membrane/].

Sterlitech, C. (2015). "Principles of Filtration." 22/09/2015, from http://www.sterlitech.com/principles-of-filtration.

Sutherland, K. (2008). Filters and Filtration Handbook, Elsevier Ltd.

Synder Filtration (2015). "Membrane Material: Organic vs. Inorganic." Retrieved 2/10/2015, from http://synderfiltration.com/learning-center/articles/introduction-to-membranes/membrane-materials-organic-inorganic/.

Synder Filtration (2015). "Microfiltration Membrane Manufacturing." 29/09/2015, from http://synderfiltration.com/microfiltration/membrane-manufacturing/.

U.S. Environmental Protection Agency (2005). Membrane Filtration Guidance Manual.

University of Edinburgh (2010). "Confocal laser scanning microscope- tutorial." Confocal and advanced light microscopy facility. Retrieved 15/10/2015, from http://www.calm.ed.ac.uk/CALM%20UoE-CLSM%20tutorial%2001.html.

APPENDICES

Appendix A

- **Bottom lapping graphs**

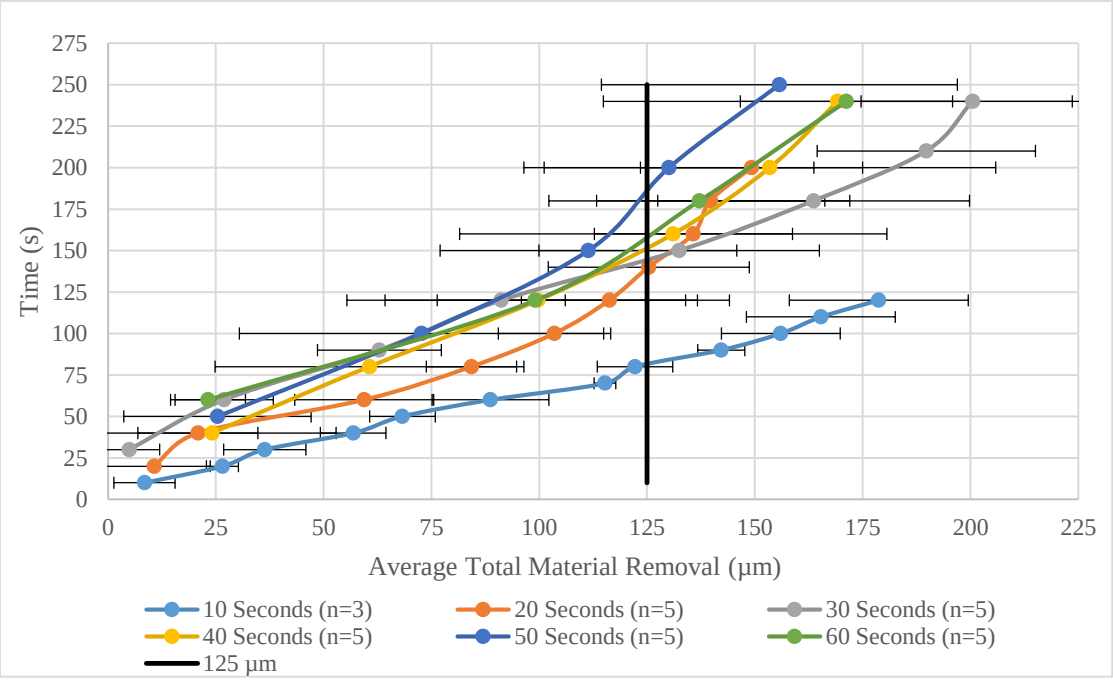

Figure A.1 - Different time intervals to remove 125µm from the bottom surface.

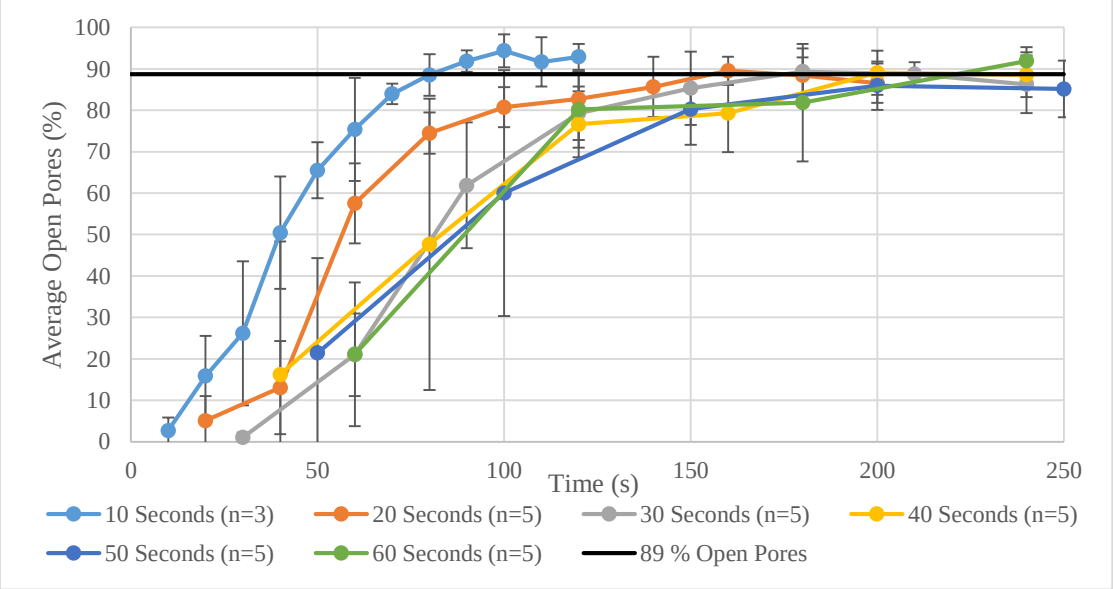

Figure A.2 - Different time intervals to obtain 89% open pores.

Appendix B

- **Lapping Plate error**

The calibration gauge covers all the diameter of the plate, measuring the flatness of the whole plate. Two flatness measurements were taken, and the difference between the plate flatness and the zero point calculated.

The flatness gauge did negative readings during both top and bottom lapping, which means that the plate presented a concave shape. As more lapping was done, more concave the plate became. The plate was being most used on the inner part of it. The error associated with the lapping plate reached a maximum of 5µm per sample, as seen in Table B.1.

Table B.1 – Flatness gauge readings during bottom lapping and lapping plate error.

Bottom Lapping Plate Flatness			
Calibration Point	**Plate Flatness 1**	**Plate Flatness 2**	**Difference**
1	95.5	95.5	55
1	95	95	60
1	93.5	93	77.5
1	94.5	94	67.5
1	94	93.5	72.5
1	95	94	65
1	93.5	93.5	75
Plate Diameter (cm)		38	
Samples Diameter (cm)		2.3	
Plate Error (µm)		5	

Before top lapping the plate was conditioned, therefore the plate had a maximum error of 2µm per sample, as represented in Table B.2.

Table B.2 – Flatness gauge readings during top lapping and lapping plate error.

Top Lapping Plate Flatness			
Calibration Point	**Plate Flatness 1**	**Plate Flatness 2**	**Difference**
1	0	0	10
1	0	0	10
1	99	99	20
1	98	98	30
1	99	98	25
1	98	99	25
1	98	99	25
Plate Diameter (cm)		38	
Samples Diameter (cm)		2.3	
Plate Error (µm)		2	

- **Smart Separations's Fixtures error**

The depth micrometer was used to measure the depth of the ceramic surface of each SS's fixture. There were taken 4 measurements of the depth of the ceramic surface for each fixture.

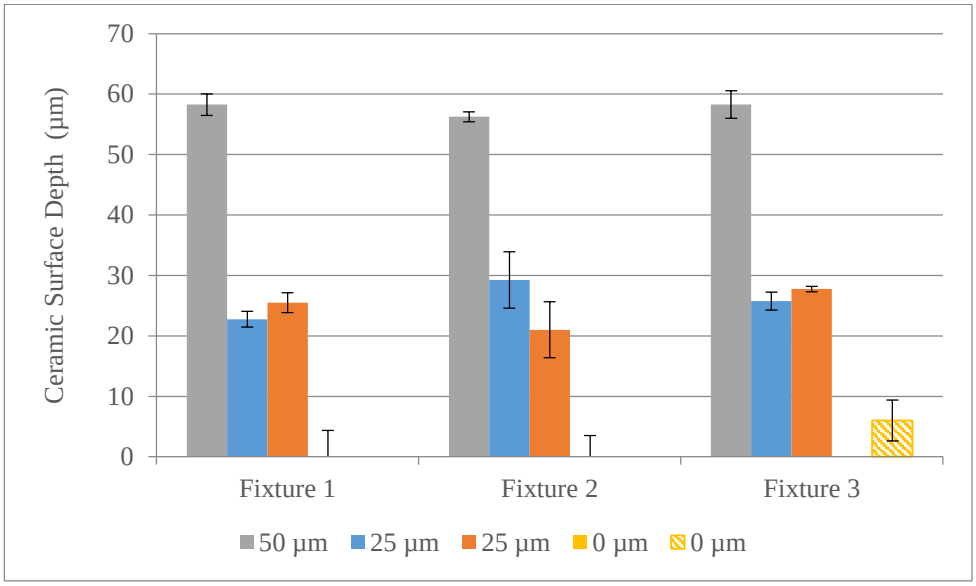

Figure B.1 – Depth measurements of the three SS fixtures.

The different colours of the columns distinguish different depths of the ceramic surface. The strip bar means that is it a negative value. The errors bars show the standard deviations of the 4 depth measurements. Fixture 2 is the less accurate fixture with a maximum error of around 5µm associated to the depth of the ceramic surface.

Appendix C

- **Sequence of photo during bottom lapping**

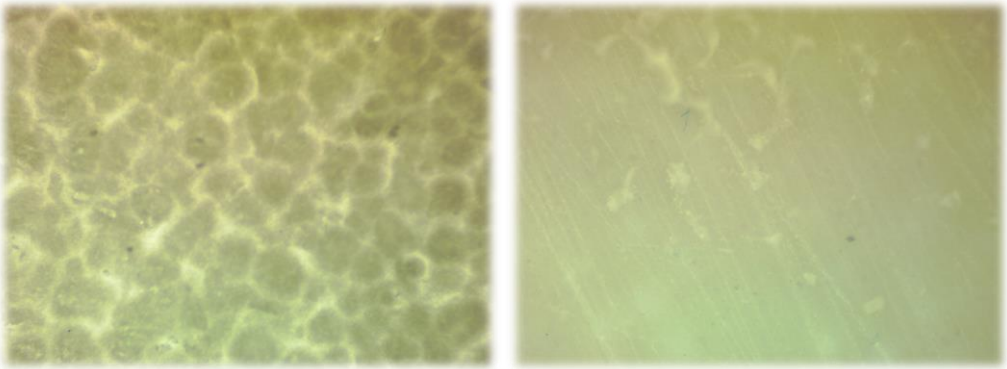

Figure C.1 - Pictures with 10x lens of bottom surface with 0 and 7µm of material removal.

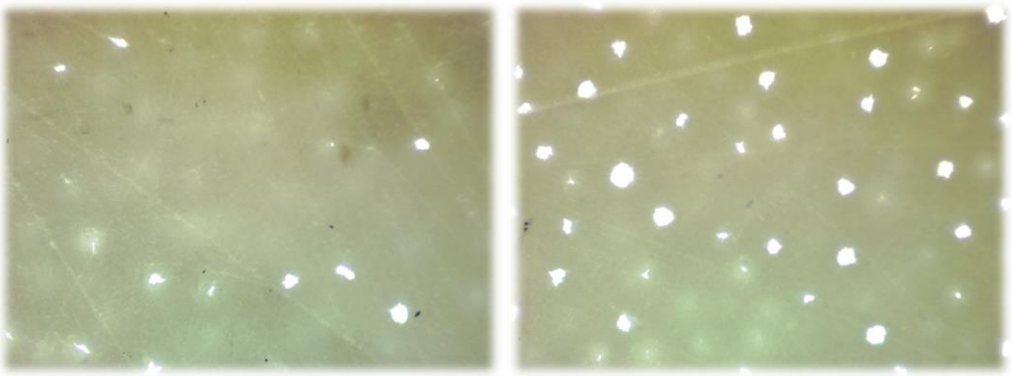

Figure C.2- Pictures with 10x lens of bottom surface with 18 and 32µm of material removal.

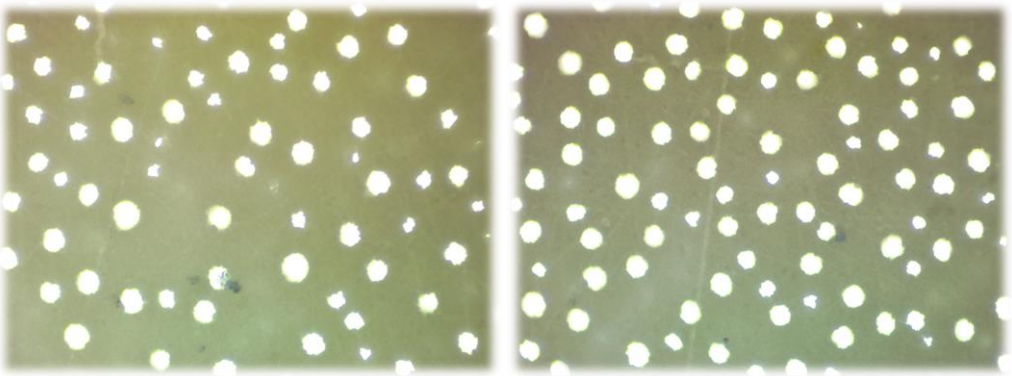

Figure C.3- Pictures with 10x lens of bottom surface with 50 and 68µm of material removal.

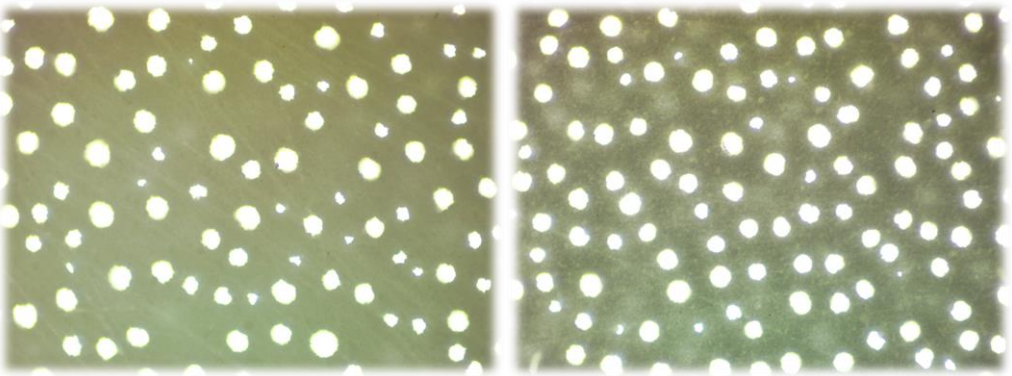

Figure C.4- Pictures with 10x lens of bottom surface with 79 and 107µm of material removal.

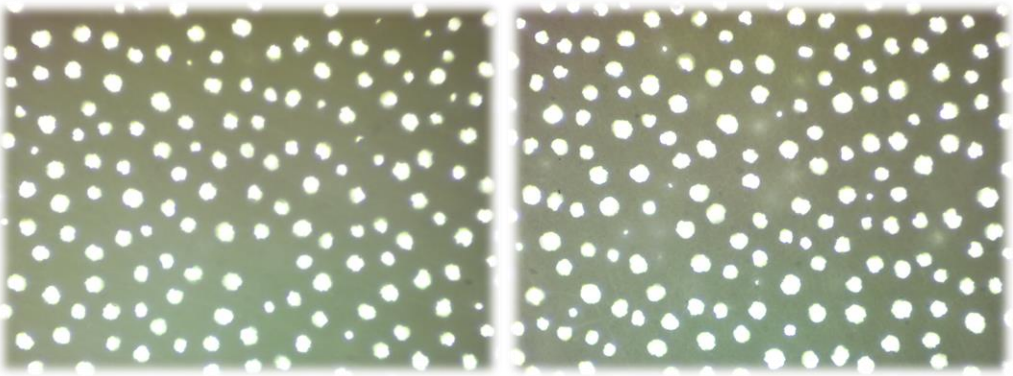

Figure C.5- Pictures with 10x lens of bottom surface with 114 and 116µm of material removal.

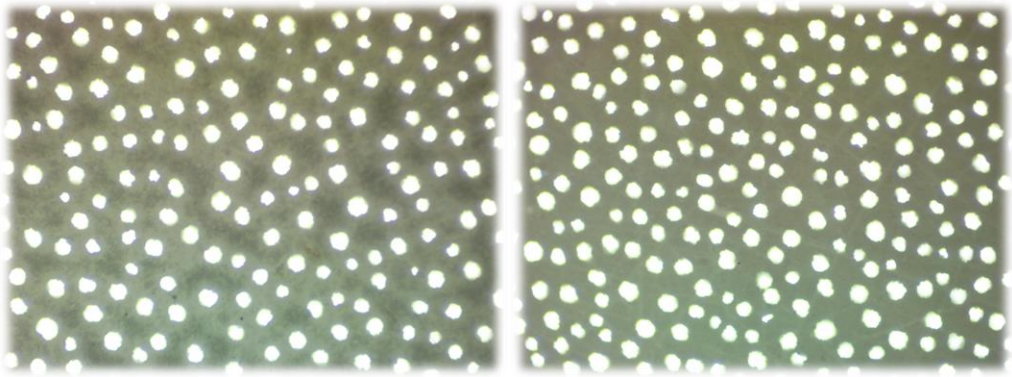

Figure C.6- Pictures with 10x lens of bottom surface with 149 and 175µm of material removal.

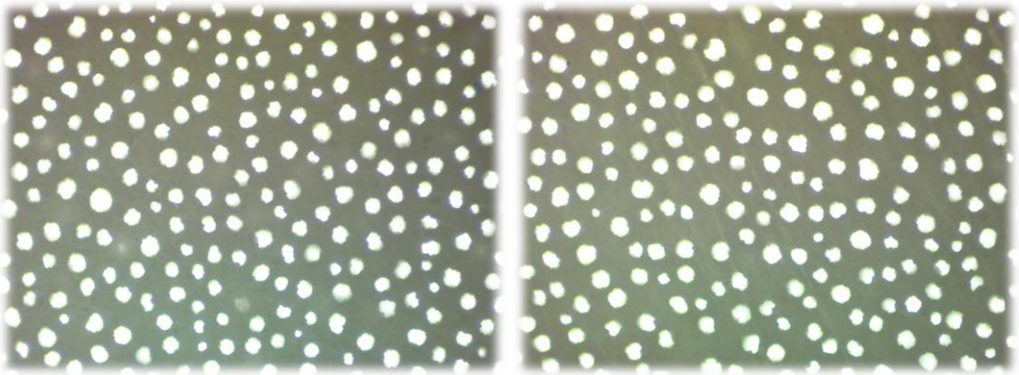

Figure C.7- Pictures with 10x lens of bottom surface with 189 and 208µm of material removal.

Appendix D

- **Pore Geometry using thickness values of the bottom surface lapping**

Lapping was performed on the bottom surface of several membranes with a mean initial thickness of 757µm. In order to analyse pores' geometry, the results of the bottom lapping experiments, specifically thickness values (492-700µm) and corresponding pore sizes, represented in Figure D.1, were studied. Only thickness values under 700µm were considered, because for higher thickness not all the pores are opened and didn't reach their maximum pore size.

In Figure D.1 the relation between mean pore size and thickness, as well as the corresponding linear regression is shown It is concluded that between 492-700 µm of thickness the pores present a conic structure.

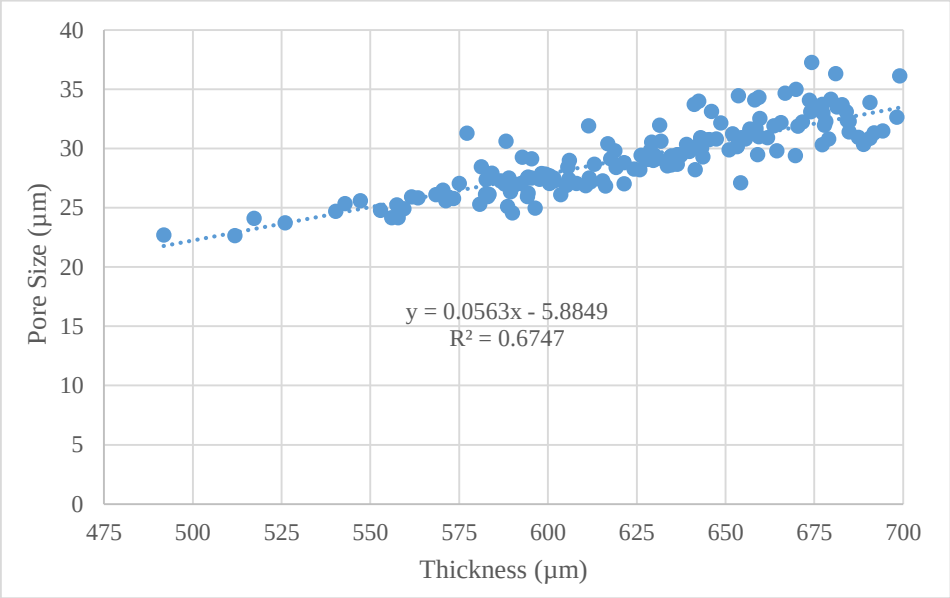

Figure D.1 - Variation of the pore size of the bottom surface with the thickness.

Using the linear regression from the Figure D.1, two points, (700,34) and (492,22), were considered in order to obtain the angle of the pores (Figure D.2A). The obtained result is $\alpha_1 = 88.4^{o}$ shown in Table 4.4., case A. Assuming top pore size of 0µm, the following analyses, outlined in Figure 4.14, will be done.

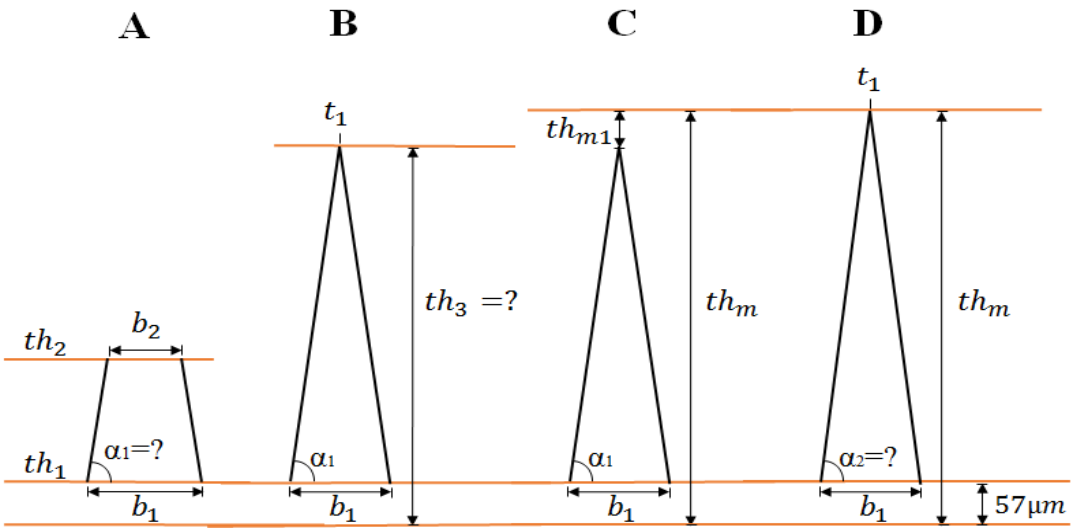

Figure D.2- Pores measurements using bottom lapping results α_i- angles; t_1-top pore size; b_1-bottom pore size th_i-calculated membrane thickness; th_m- mean membrane thickness; th_{m1}- difference between mean membrane thickness and calculated membrane thickness.

The results from Table D.1 show that according to the linear regression the bottom surface has a pore size of 34µm (case A). Assuming bottom pore size of 34µm, according to the linear regression the thickness of the membrane is 652µm (case B). The thickness of the membranes should correspond to the mean value of the membrane, 757µm, representing a 13.8% increase. Which means that the pores close 104µm from the top surface of the mean

membrane thickness (Figure 4.10C). In section 4.2.1.2 is shown, at 104µm from the top surface the pores are already opened. This means that the angle should be higher than the one calculated by the linear regression, which will now be calculated.

According to the linear regression for the mean thickness of the membrane, 757µm, the bottom pore size is 34µm for these parameters the angle should be 88.6º, corresponding to an increment of 0.3%, case D.

Table D.1 - Result of membranes measurements evaluation using bottom lapping results.

		A	B	C	D	Error (%)
Angle (º)	**α_1**	88.4	88.4	88.4	-	0.3
	α_2	-	-	-	88.6	
Thickness (µm)	**th_1**	700	-	-	-	-
	th_2	492	-	-	-	-
	th_3	-	652			13.8
	th_m	-	-	757	757	
	th_{m1}	-	-	104	-	-
Pore Size (µm)	**b_1**	34	34	34	34	-
	b_2	22	-	-	-	-
	t_1	-	0	-	0	-

Figure D.3 shows the variation of pore size in relation to the thickness, considering the 2 obtained angles.

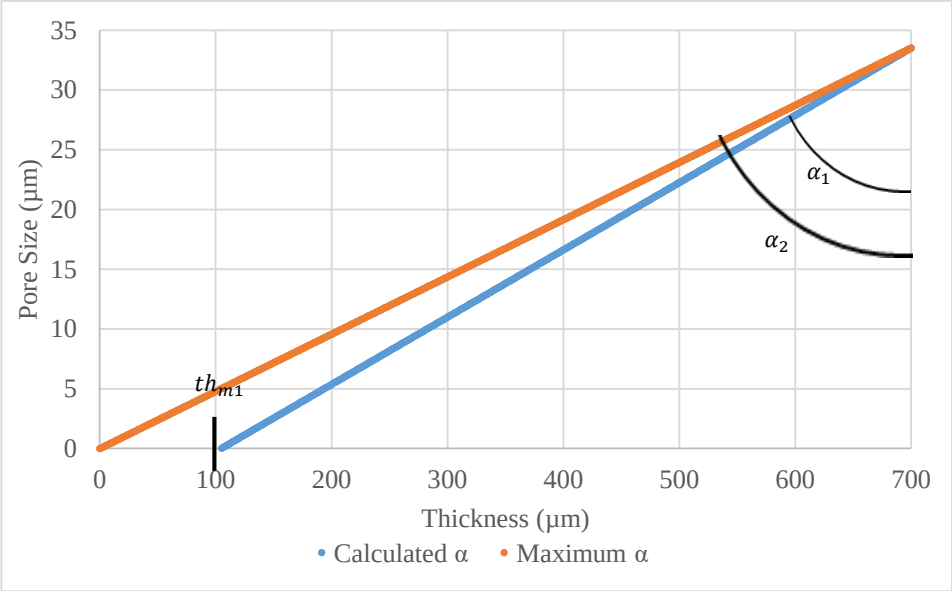

Figure D.3- Variation of pore size throughout thickness, for the calculated angle by the linear regression from bottom lapping results, α_1, and the maximum angle, α_2. th_{m1}-difference between membranes' mean thickness and the calculated thickness.